Eur. Phys. J. C (2024) 84:78
https://doi.org/10.1140/epjc/s10052-023-12130-5

THE EUROPEAN PHYSICAL JOURNAL C

Regular Article - Experimental Physics

Measurement of the $H \to \gamma\gamma$ and $H \to ZZ^* \to 4\ell$ cross-sections in pp collisions at $\sqrt{s} = 13.6$ TeV with the ATLAS detector

ATLAS Collaboration[*]

CERN, 1211 Geneva 23, Switzerland

Received: 21 June 2023 / Accepted: 4 October 2023 / Published online: 24 January 2024

Abstract The inclusive Higgs boson production cross-section is measured in the di-photon and the $ZZ^* \to 4\ell$ decay channels using 31.4 and 29.0 fb^{-1} of pp collision data respectively, collected with the ATLAS detector at a centre-of-mass energy of $\sqrt{s} = 13.6$ TeV. To reduce the model dependence, the measurement in each channel is restricted to a particle-level phase space that closely matches the channel's detector-level kinematic selection, and it is corrected for detector effects. These measured fiducial cross-sections are $\sigma_{\text{fid},\gamma\gamma} = 76^{+14}_{-13}$ fb, and $\sigma_{\text{fid},4\ell} = 2.80 \pm 0.74$ fb, in agreement with the corresponding Standard Model predictions of 67.6 ± 3.7 fb and 3.67 ± 0.19 fb. Assuming Standard Model acceptances and branching fractions for the two channels, the fiducial measurements are extrapolated to the full phase space yielding total cross-sections of $\sigma(pp \to H) = 67^{+12}_{-11}$ pb and 46 ± 12 pb at 13.6 TeV from the di-photon and $ZZ^* \to 4\ell$ measurements respectively. The two measurements are combined into a total cross-section measurement of $\sigma(pp \to H) = 58.2 \pm 8.7$ pb, to be compared with the Standard Model prediction of $\sigma(pp \to H)_{\text{SM}} = 59.9 \pm 2.6$ pb.

Contents

1 Introduction

Since the discovery of the Higgs boson (denoted by H in this paper) by the ATLAS and CMS collaborations [1,2] at the Large Hadron Collider (LHC) [3], a major goal of the physics programme of the LHC experiments has been to measure its properties and determine whether they correspond to those predicted by the Standard Model (SM) of particle physics or involve new phenomena beyond those described by this theory.

[*] e-mail: atlas.publications@cern.ch

Despite the small branching ratios of Higgs boson decays into two photons and four leptons ($ZZ^* \to 4\ell$, with $\ell =$ e or μ), these decay channels are particularly interesting for this purpose given the excellent mass reconstruction and photon and lepton identification efficiencies of the ATLAS detector.

In 2022 the LHC increased the centre-of-mass energy of the proton–proton (pp) collisions to the new world-record value of 13.6 TeV. In the analysis described in this paper, 31.4 and 29.0 fb^{-1} of pp collision data recorded with the ATLAS detector are used to derive the first ATLAS measurements of the $H \to \gamma\gamma$ and $H \to ZZ^* \to 4\ell$ cross-sections at this new energy. The cross-sections are measured inclusively in the production modes. They are derived via a fit to the reconstructed invariant mass spectra. To reduce the model dependence, the measurements are restricted to a kinematic phase space of the Higgs boson decay products defined at particle level that closely matches the selection criteria applied at the detector level, and they are corrected for detector effects (unfolding). This approach is usually referred to as a 'fiducial cross-section' measurement. The fiducial cross-sections of the two decay channels are also extrapolated to the full phase space, corrected for the predicted SM decay branching ratios and combined. The ATLAS and CMS experiments have previously published fiducial cross-section measurements for the $H \to \gamma\gamma$ and $H \to ZZ^* \to 4\ell$ processes at different centre-of-mass energies up to 13 TeV [4–12]. These results do not show any significant deviation from the SM predictions.

All results reported in this paper assume a value of the Higgs boson mass of 125.09 ± 0.24 GeV [13].

2 ATLAS detector

The ATLAS experiment [14,15] at the LHC is a multipurpose particle detector with a forward–backward symmetric cylindrical geometry and a near 4π coverage in solid angle.[1] It consists of an inner tracking detector surrounded by a thin superconducting solenoid providing a 2 T axial magnetic field, electromagnetic and hadron calorimeters, and a muon spectrometer (MS). The inner tracking detector (ID) covers the pseudorapidity range $|\eta| < 2.5$. It consists of silicon pixel, silicon microstrip, and transition radiation tracking detectors. Lead/liquid-argon (LAr) sampling calorimeters provide electromagnetic (EM) energy measurements with high granularity. A steel/scintillator-tile hadron calorimeter covers the central pseudorapidity range of ($|\eta| < 1.7$). The endcap and forward regions are instrumented with LAr calorimeters for both the EM and hadronic energy measurements up to $|\eta| = 4.9$. The MS surrounds the calorimeters and is based on three large superconducting air-core toroidal magnets with eight coils each. The field integral of the toroids ranges between 2.0 and 6.0 Tm across most of the detector. The MS includes a system of precision tracking chambers and fast detectors for triggering. A two-level trigger system is used to select events. The first-level trigger is implemented in hardware and uses a subset of the detector information to accept events at a rate below 100 kHz. This is followed by a software-based trigger that reduces the accepted event rate to 3 kHz on average, depending on the data-taking conditions. An extensive software suite [16] is used in data simulation, in the reconstruction and analysis of real and simulated data, in detector operations, and in the trigger and data acquisition systems of the experiment.

3 Data and simulated event samples

The data and simulated event samples are summarised in the following.

3.1 Data

The measurement presented in this paper is based on pp collision data recorded by the ATLAS detector during the year 2022. Data are selected only if all the detector components relevant for each channel were known to be in good operating condition. The data samples correspond to an integrated luminosity of 31.4 fb^{-1} for the $H \to \gamma\gamma$ channel and of 29.0 fb^{-1} for $H \to ZZ^* \to 4\ell$ channel. The difference between the sizes of the two data samples is due to additional requirements to remove data-taking periods with lower muon trigger efficiency applied only to the $H \to ZZ^* \to 4\ell$ channel. The uncertainty in the integrated luminosity for data recorded in 2022 is 2.2% [17], following the methodology discussed in Ref. [18], using the LUCID-2 detector [19] for the primary luminosity measurements, complemented by measurements using the ID and calorimeters. The mean number of interactions per bunch crossing, called pile-up, averaged over all colliding bunch pairs is about 40.

Only events that satisfied single- or di-photon triggers [20] are used in the $H \to \gamma\gamma$ measurement. The single-photon trigger required the presence of a photon candidate with at least 140 GeV of transverse energy (E_{T}) in the event. This photon candidate is also required to satisfy *loose* [20] identification selections, as determined by properties of shower shapes in the calorimeters. The di-photon trigger required the presence of two photon candidates with E_{T} of at least 25

[1] ATLAS uses a right-handed coordinate system with its origin at the nominal interaction point (IP) in the centre of the detector and the z-axis along the beam pipe. The x-axis points from the IP to the centre of the LHC ring, and the y-axis points upwards. Polar coordinates (r, ϕ) are used in the transverse plane, ϕ being the azimuthal angle around the z-axis. The pseudorapidity is defined in terms of the polar angle θ as $\eta = -\ln\tan(\theta/2)$. Angular distance is measured in units of $\Delta R \equiv \sqrt{(\Delta\eta)^2 + (\Delta\phi)^2}$.

and 35 GeV, and satisfying analogous *medium* [20] identification requirements. On average, these trigger requirements are 99.4% efficient for the events that satisfy the analysis selection requirements outlined in Sect. 4.1. The efficiency is predominantly determined by the di-photon trigger; the single-photon trigger adds less than 0.1% of events of interest.

A total of 12 different single-lepton, dilepton, and trilepton triggers [20,21] were employed for the $H \to ZZ^* \to 4\ell$ measurement. The single-lepton trigger thresholds used in 2022 were 24 and 26 GeV for the muon and electron signatures, respectively. The ensemble of the lepton triggers ensures a signal selection efficiency of 98.2% for the events that satisfy the analysis selection requirements outlined in Sect. 5.1.

3.2 Simulated event samples

At the LHC, Higgs bosons are primarily produced through gluon–gluon fusion (ggF), vector-boson fusion (VBF, where $V = W, Z$), and associated production with a vector boson (VH) and top- or bottom-quark pairs ($t\bar{t}H$, $b\bar{b}H$). These signal processes were simulated using the POWHEG BOX v2 [22–26] Monte Carlo (MC) generator. Next-to-leading-order (NLO) accuracy was achieved for the ggF and VH processes with up to one extra parton by following the MINLO [27–29] approach, while the $gg \to ZH$ process was only computed at leading order (LO) in quantum chromodynamics (QCD). The VBF and $t\bar{t}H$ processes were simulated at NLO accuracy in QCD. The $b\bar{b}H$ process was not simulated. Instead, since the acceptance of ggF events is similar to that of $b\bar{b}H$ events, the ggF cross-section is scaled to account for this contribution. The $b\bar{b}H$ contribution accounts for approximately 1% of the total ggF + $b\bar{b}H$ production.

The samples are normalised to the state-of-the-art cross-section predictions [30] interpolated to the new LHC centre-of-mass energy of 13.6 TeV. The interpolation is based on cross-section values available at various centre-of-mass energies ranging from 6 to 15 TeV in 0.5 TeV steps [31]. The ggF sample is normalised to a next-to-next-to-next-to-leading-order (N^{3}LO) QCD calculation with NLO electroweak (EW) corrections [32–43] for the ggF process summed with a $b\bar{b}H$ contribution. The $b\bar{b}H$ contribution is normalised to a calculation that combines the complete NLO contributions that are present in the 4-flavour scheme calculation, including finite b-quark mass effects and top-loop induced top-to-bottom Yukawa-coupling interference contributions, with the resummation of collinear logarithms of m_b/m_H as present in the 5-flavour scheme calculation up to next-to-next-to-leading-order (NNLO) [44–47]. No EW corrections are included for $b\bar{b}H$. The VBF sample is normalised to an approximate NNLO QCD cross-section with NLO EW corrections [48–50]. The VH samples are normalised to cross-sections calculated at NNLO in QCD with NLO EW corrections for $q\bar{q}/qg \to VH$ and at NLO and next-to-leading-logarithm accuracy in QCD for $gg \to ZH$ [51–58]. The $t\bar{t}H$ cross-section is taken from a calculation accurate to NLO in QCD with NLO EW corrections [59–62]. Summing up all the production modes,[2] the total predicted SM Higgs boson cross-section at 13.6 TeV is $\sigma(pp \to H)_{\text{SM}} = 59.9 \pm 2.6$ pb.

All Higgs boson signal samples used the PDF4LHC 21 set [63] of parton distribution functions (PDFs) in all matrix element (ME) calculations. The samples were interfaced to PYTHIA 8.2 [64] (PYTHIA 8.3 [65]) to simulate $H \to \gamma\gamma$ ($H \to ZZ^* \to 4\ell$) decays and to model the effects of parton showering (PS), hadronisation and the underlying event (UE), with parameter values determined by the A14 set of tuned parameters (tune) [66]. The SM $H \to ZZ^* \to 4\ell$ ($\ell = e, \mu$) branching-ratio prediction is taken from PROPHECY4F [67,68] and includes the full NLO EW corrections, as well as interference effects that result in a branching ratio that is 10% higher for same-flavour final states (4μ and $4e$) than for different-flavour states ($2e2\mu$ and $2\mu2e$). The samples were generated with a Higgs boson mass of 125.0 GeV[3] and a Higgs boson width of 4.07 MeV. The predicted SM branching ratio is $(2.27 \pm 0.07) \times 10^{-3}$ for the $H \to \gamma\gamma$ decay [30] and $(1.25 \pm 0.03) \times 10^{-4}$ for the $H \to ZZ^* \to 4\ell$ ($\ell = e, \mu$) decay, for a Higgs boson mass of 125.09 GeV.

Background simulated event samples for the $H \to \gamma\gamma$ measurement, consisting of non-resonant prompt di-photon production ($\gamma\gamma$) within a di-photon mass range of $90 < m_{\gamma\gamma} < 175$ GeV, were generated with MADGRAPH5_AMC@NLO [69] at an accuracy of NLO for MEs with up to two partons. The NNPDF 3.0 NLO PDF set [70] was used. As with the Higgs boson signal samples, PS, hadronisation and UE were modelled in PYTHIA 8.2 with the A14 tune. The merging of ME and PS was performed following the FxFx merging scheme [71].

For the $H \to ZZ^* \to 4\ell$ measurement, the largest background contribution is from the $(Z^{(*)}/\gamma^*)(Z^{(*)}/\gamma^*)$ continuum background, jointly called non-resonant or continuum ZZ^*. The ZZ^* continuum background from quark–antiquark annihilation ($qq \to ZZ^*$) was modelled using SHERPA 2.2.12 [72–74], which provides a ME calculation accurate to NLO in QCD for 0- and 1-jet final states, and LO accuracy for 2- and 3-jet final states. The merging with the SHERPA PS [75] was performed using the ME+PS@NLO prescription [76]. Theoretical uncertainties in the $m_{4\ell}$ shape are evaluated by using Run 2 samples (generated at a centre-of-mass energy of 13 TeV) and comparing the baseline

[2] When computing the total cross-section, the small contribution from tH production (0.1 pb) is also included.

[3] A 90 MeV shift is applied to the signal parameterisation used in the fit to the data.

Table 1 Simulated signal and background event samples. The last column shows the total cross-sections used to normalise the signal samples for $m_H = 125.09$ GeV. The uncertainties on the cross-sections are based on the theoretical papers cited in the text and include several components as described in Ref. [30] (missing higher order QCD and EW corrections, PDF, strong coupling constant, quark mass effects, etc.)

Process	Generator	Showering	PDF set	σ [pb] $\sqrt{s}$ = 13.6 TeV
ggF + $b\bar{b}H$	POWHEG BOX v2 + MINLO	PYTHIA 8.2/8.3	PDF4LHC21	52.7 ± 2.6
VBF	POWHEG BOX v2	PYTHIA 8.2/8.3	PDF4LHC21	$4.075^{+0.088}_{-0.089}$
WH	POWHEG BOX v2 + MINLO	PYTHIA 8.2/8.3	PDF4LHC21	$1.453^{+0.029}_{-0.028}$
$q\bar{q} \to ZH$	POWHEG BOX v2 + MINLO	PYTHIA 8.2/8.3	PDF4LHC21	$0.806^{+0.033}_{-0.029}$
$gg \to ZH$	POWHEG BOX v2	PYTHIA 8.2/8.3	PDF4LHC21	$0.136^{+0.034}_{-0.026}$
$t\bar{t}H$	POWHEG BOX v2	PYTHIA 8.2/8.3	PDF4LHC21	$0.569^{+0.040}_{-0.057}$
$\gamma\gamma$, $m_{\gamma\gamma} \in$ 90–175 GeV	MADGRAPH5_AMC@NLO	PYTHIA 8.2	NNPDF 3.0 NLO	–
$qq \to ZZ^*$	SHERPA 2.2.12	SHERPA 2.2.12	NNPDF 3.0 NNLO	–
VV, VVV	SHERPA 2.2.12	SHERPA 2.2.12	NNPDF 3.0 NNLO	–
Z + jets	SHERPA 2.2.12	SHERPA 2.2.12	NNPDF 3.0 NLO	–
$t\bar{t}$	POWHEG BOX v2	PYTHIA 8.3	NNPDF 3.0 NLO	–
$t\bar{t}W$, $t\bar{t}Z$	SHERPA 2.2.12	SHERPA 2.2.12	NNPDF 3.0 NNLO	–

SHERPA 2.2.2 sample with a MADGRAPH5_AMC@NLO sample that uses FXFX merging at NLO for 0- and 1-jet final states, interfaced to PYTHIA 8 for PS.

The gluon-induced ZZ^* production is taken into account by scaling the expected ZZ^* continuum background from quark–antiquark annihilation to the expected cross-section for the sum of the two processes. This scaling is derived using Run 2 simulated event samples (generated at a centre-of-mass energy of 13 TeV) with SHERPA 2.2.2 and also takes into account the slightly different mass shapes of the two processes. Since the total normalisation of the ZZ^* sample is derived from the fit to the data (as described in the following), only the relative normalisation, used to determine the invariant mass shape, is relevant to this study. The higher-order QCD effects for the $gg \to ZZ^*$ continuum production are calculated for massless quark loops [77–79] in the heavy top-quark approximation [80], including the $gg \to H^* \to ZZ^*$ process [81,82]. The $gg \to ZZ^*$ LO cross-section was scaled by a K-factor of 1.7 ± 1.0, defined as the ratio of the higher-order to leading-order cross-section predictions. Production of ZZ^* via vector-boson scattering was simulated at LO in QCD with the SHERPA 2.2.2 generator.

The WZ background was modelled using the SHERPA 2.2.12 generator using the same set-up as for the $qq \to ZZ^*$ sample. The triboson backgrounds ZZZ, WZZ, and WWZ with four or more prompt leptons were modelled using SHERPA 2.2.12. Other sub-dominant backgrounds like the production of vector bosons in association with a top-quark pair ($t\bar{t}W/Z$) were simulated using the SHERPA 2.2.12 generator.

Events containing Z bosons with associated jets (Z+jets) were simulated using the SHERPA 2.2.12 generator. MEs were calculated for up to two partons at NLO and four partons at LO using COMIX [73] and OPENLOOPS [74], and merged with the SHERPA PS [75] using the ME+PS@NLO prescription [76]. The NNPDF3.0 NNLO PDF set was used in conjunction with a dedicated set of tuned PS parameters.

The $t\bar{t}$ background was modelled using POWHEG BOX v2 interfaced to PYTHIA 8.3 for PS, hadronisation, and the UE, and to EVTGEN v2.1.1 for heavy-flavour hadron decays [24–26,83]. For this sample, the A14 tune [84] and NNPDF3.0 NLO PDFs were used. Simulated Z+jets and $t\bar{t}$ background event samples are normalised to the data-driven estimates described in Sect. 5.3.

All generated signal and background events were passed through a simulation of the ATLAS detector using GEANT4 [85,86]. Scale factors are applied to the simulation to match the performance of the different physics objects to those measured in the data.

A summary of the simulated event samples used in this measurement together with the total cross-section values used for the normalisation of signal processes in the full phase space is provided in Table 1. All the background processes reported in this table (except the small irreducible VVV and $t\bar{t}W/Z$) are directly normalised to the data or derived from data control regions.

The effect of multiple interactions from the same or neighbouring bunch crossings was modelled through the overlay [87] of the hard-scatter signal and background events with a set of simulated inelastic pp events generated by EPOS 2.0.1.4 [88] and PYTHIA 8.2. Events with at least one high transverse-momentum (p_T) jet, isolated photon, or lepton from the decay of a b-hadron were simulated using PYTHIA 8.2. All other events were simulated using EPOS; a veto on EPOS events with such a high transverse-momentum signa-

ture ensured orthogonality with the PYTHIA 8.2 sample. The EPOS LHC tune was used to set the parameters of the EPOS generation, while the PYTHIA 8.2 parameters were set using the A3 tune [89]. The NNPDF2.3 LO set of PDFs [90] was used. Dedicated weights were used to ensure that the mean number of interactions per bunch crossing observed in the 2022 data is adequately described in these samples.

4 The $H \to \gamma\gamma$ measurement

4.1 Event reconstruction and selection

The events used in the $H \to \gamma\gamma$ measurement are selected using a multi-step procedure. Reconstructed photon candidates are first required to satisfy a set of preselection requirements. Subsequently, they are ranked according to their transverse energy and the two highest-E_{T} candidates are used to build a di-photon system and determine the primary vertex of the event. A final set of requirements is then applied to the di-photon system.

4.1.1 Photon reconstruction, identification and preselection

Photon reconstruction is performed using a dynamic clustering algorithm [91,92] in which variable-sized topological clusters [93] are built from signals significantly above the noise level in EM-calorimeter cells. Additional clusters consistent with energy deposits from the products of photon conversion are added to the original cluster if relevant. Tracks reconstructed in the ID are evaluated based on the quality of their matching to the reconstructed calorimeter-energy cluster. Photon candidates with no matching track are labelled unconverted photons while photon candidates with a matching track with no innermost pixel-layer hits or with two matching tracks are classified as converted photons. All photon candidates are required to be within the acceptance region of the finely segmented first layer of the EM calorimeter, $|\eta| < 2.37$, and outside of the area that falls between the barrel and endcap calorimeters, $1.37 < |\eta| < 1.52$. Their energy measurement is calibrated using the method described in Ref. [92].

The procedure described above is effective at reconstructing not only prompt photons but also other similar objects, such as di-photon decays of neutral hadrons inside jets. These other objects are rejected using an identification algorithm based on calorimeter shower-shape information [94]. The *loose* [92] working point serves as the initial preselection requirement. It is based on the shape of the shower in the second layer of the EM calorimeter and on the amount of energy deposited in the hadronic calorimeter, and has a nominal prompt-photon efficiency of above 98% for prompt photons with transverse momentum greater than 30 GeV.

An additional preselection requirement retains events with at least two photon candidates, each with $E_{\mathrm{T}} > 25$ GeV, and a di-photon system is built. In events where more than two photon candidates satisfy these preselection requirements, the two highest-E_{T} candidates are used to construct the di-photon system.[4]

4.1.2 Primary vertex selection

The primary vertex of the event is selected using a neural-network algorithm [95] trained to distinguish between the hard-scatter vertex of ggF events and vertices from pile-up interactions. The algorithm makes use of information about all reconstructed vertices in the event[5] and about the kinematic properties of the two photons forming the di-photon system, as measured in the calorimeter and complemented, in the case of converted photons, by kinematics of matching ID tracks. The use of this neural network provides a vertex selection efficiency of 71.4% for the most abundant ggF process, to be compared with an efficiency of 52.2% when the primary vertex is selected solely based on the sum of the p_{T}-squared of its associated tracks, which is generally the default in ATLAS. This efficiency is estimated by using MC simulation, requiring a distance along the z-axis between the particle-level primary vertex and the reconstructed one of less than 0.3 mm. Agreement between data and simulation is validated in the Run 3 data sample using $Z \to ee$ events, treating the electrons as unconverted photon candidates (i.e., ignoring their track information). A weak dependence of the performance on pile-up levels is observed, but it is well-modelled by the simulation.

Once the primary vertex is selected, the direction of the two photon candidates is re-computed. This has the benefit of improving the E_{T} measurement of the photon candidates through its dependence on the photon candidate's direction in η. It also improves the di-photon invariant mass resolution by about 8%.

4.1.3 Event selection

The event selection is completed by a set of requirements on the two photon candidates that constitute the di-photon system.

First, a matching requirement is applied between the selected photon candidates and the corresponding photons at trigger level, as described in Sect. 3.1. Either one of the photon candidates must be matched to the single-photon trigger, or both photon candidates must be matched to the di-photon

[4] The two highest-E_{T} candidates match the Higgs boson decay products in over 99% of simulated signal events.

[5] Reconstructed vertices are required to have at least two associated ID tracks of transverse momentum $p_{\mathrm{T}} > 500$ MeV.

Table 2 Summary of the event selection requirements that define the fiducial phase space for the $H \to \gamma\gamma$ cross-section measurement

Photons	
Leading (sub-leading) p_{T}^{γ}	$p_{\mathrm{T}}^{\gamma}/m_{\gamma\gamma} > 0.35$ (0.25)
Pseudorapidity	$\lvert\eta\rvert < 2.37$ and outside $1.37 < \lvert\eta\rvert < 1.52$
Isolation ($\Delta R = 0.2$)	$E_{\mathrm{T}}^{\mathrm{iso}}/E_{\mathrm{T}}^{\gamma} < 0.05$
Di-photon system	
Mass window	105 GeV $< m_{\gamma\gamma} <$ 160 GeV

trigger. The leading E_{T} and sub-leading E_{T} photon candidates are additionally required to have $E_T/m_{\gamma\gamma} > 0.35$ and > 0.25 respectively.

At this stage, a more stringent *tight* [96] working point requirement is applied. The efficiency of the *tight* working point requirement varies with the E_{T} of the photon, ranging from 84% (85%) at $E_{\mathrm{T}} = 25$ GeV to 94% (98%) at $E_{\mathrm{T}} = 100$ GeV for unconverted (converted) photons. This working point makes use of the same information as the *loose* working point used for the preselection, albeit with more stringent requirements, and adds information from the finely segmented first layer of the EM calorimeter.

To further reject hadronic background, surviving photon candidates are required to be isolated from other significant activity in the ID or the calorimeters. Track-based isolation is determined by the scalar sum of the p_{T} of all tracks of at least 1 GeV that are within a cone of $\Delta R = 0.2$ of the photon candidate and are compatible with originating from the selected primary vertex. Track isolation requirements are satisfied if this p_{T}-sum is less than 5% of the photon candidate's E_{T}. Calorimeter-based isolation, on the other hand, is defined as the scalar sum of the E_{T} of all positive-energy topological clusters within the same $\Delta R = 0.2$ cone, excluding the energy of the photon candidate itself. For calorimeter-based isolation, an additional subtraction is performed to remove pile-up and UE contributions. This uses an ambient energy correction based on the low-p_{T} jets of the event [91,97]. Calorimeter isolation requirements are satisfied if the resulting E_{T}-sum is less than 6.5% of the photon candidate's E_{T}. Both the track and calorimeter isolation requirements must be satisfied.

The last requirement restricts the invariant mass $m_{\gamma\gamma}$ of the two photon candidates to be within the range 105–160 GeV.

The number of selected events in the 2022 Run 3 data sample is 307 996. The selection efficiency, relative to the full phase space, is estimated from simulated events to be 36%.

4.1.4 Fiducial region

The fiducial region considered in this measurement is designed to closely match the selection requirements outlined above to minimise model dependence due to acceptance extrapolations. The di-photon fiducial region is defined by the presence of two prompt photons with transverse momentum greater than 0.35 and 0.25 times the di-photon invariant mass. The photons are required to be in the range of $\lvert\eta\rvert < 2.37$ but outside of the region $1.37 < \lvert\eta\rvert < 1.52$. They are also required to be isolated, based on a particle-level isolation criterion defined as the transverse energy obtained from the vectorial sum of the momenta of all the stable charged particles (mean lifetime $c\tau > 10$ mm) with p_{T} greater than 1 GeV and within a cone of $\Delta R = 0.2$ around the photon's direction. This quantity must be less than 5% of the photon's E_{T}. The invariant mass of the di-photon system is required to be within the range 105–160 GeV. These requirements are summarised in Table 2.

The signal acceptance of this di-photon fiducial region is 50% relative to the full phase space. In total, 2117 signal events are expected in the fiducial region assuming SM values for the production cross-section, the acceptance and the di-photon branching fraction. About 1.9% of the events that satisfy the detector-level event selection fail to satisfy the fiducial selection.

4.2 Fit procedure

The methodology used to extract the $pp \to H \to \gamma\gamma$ fiducial cross-section closely follows that of a previous ATLAS measurement [6]. The cross-section is measured via an analytic fit to the di-photon mass spectrum. The analytic function used to model the signal distribution is derived mainly from simulation, after applying the relevant calibrations, while the parameters of the analytic function used to model the background distribution are determined from a fit to the data. For this inclusive measurement, the measured signal yields are corrected to particle level using a single correction factor derived from MC simulation. This correction factor takes into account detector effects and out-of-acceptance signal contributions.

The fiducial cross-section is extracted via an unbinned maximum-likelihood fit to the reconstructed di-photon invariant mass spectrum in the range 105–160 GeV. Confidence intervals are based on the profile-likelihood-ratio test statistic [98]. The systematic uncertainties listed in Sect. 4.5 are

implemented in the fit as nuisance parameters constrained by additional Gaussian or log-normal likelihood terms. The probability density functions for the signal and background are described by analytic functions detailed in Sects. 4.3 and 4.4. In the likelihood, the signal yield N_S is parameterised in terms of the fiducial cross-section as

$$N_S = \sigma_{\text{fid}} \times \mathcal{L} \times C_{\mathcal{F}}, \tag{1}$$

where σ_{fid} is the fiducial cross-section, the parameter of interest of the fit, and is defined as the product of the total production cross-section σ_{tot}, the di-photon branching ratio $\mathcal{B}_{\gamma\gamma}$ and the acceptance $\mathcal{A}$:

$$\sigma_{\text{fid}} = \sigma_{\text{tot}} \times \mathcal{B}_{\gamma\gamma} \times \mathcal{A}. \tag{2}$$

The signal acceptance $\mathcal{A}$ is the fraction of signal events that passes the particle-level fiducial selection described in Sect. 4.1. The other terms of Eq. (1) are $\mathcal{L}$, the integrated luminosity, and $C_{\mathcal{F}}$, the correction factor, defined as the ratio of the number of signal events selected at detector level to the number of signal events selected at particle level after applying the selection criteria described in Sect. 4.1. The correction factor is computed inclusively assuming that the ratio of the different Higgs boson production modes is as in the SM. The value of $C_{\mathcal{F}}$, derived from the signal simulated event samples, is 71.6%. The dependence on the production mode is very weak and ranges from 71.5% for ggF to 72.4% for VBF.[6]

4.3 Signal modelling

The signal mass shape is modelled with a double-sided Crystal Ball function, detailed in Ref. [99]. This function is characterised by a Gaussian component that describes the central part of the mass spectrum and two independent power-law tails. In total the signal function is described by six shape parameters and one overall-normalisation parameter. Among the shape parameters are the position of the signal peak, linked to the Higgs boson mass, and the experimental resolution. They can be mapped to the mean μ_{CB} and the width σ_{CB} of the central Gaussian component. Another four parameters determine the shape of the power-law tails. These six Crystal Ball shape parameters are determined from a fit to the signal simulated event samples and are kept fixed in the fit to the data within the associated systematic uncertainties described in Sect. 4.5.1. Lastly, the overall normalisation is expressed by the parameter N_S previously defined. It is determined in the fit to the data. The validity of the signal parameterisation is checked by a 'closure test' performed with a fit to a simulated data sample obtained by injecting known signal yields on top of a background template.

Since the signal samples are generated at a Higgs boson mass of 125.0 GeV, the mean value of the central Gaussian component used in the signal parameterisation is shifted by 90 MeV to emulate a signal at 125.09 GeV [13].

Contributions from the different Higgs boson production modes are added together according to the yield fractions predicted by the SM. No significant differences are found between the signal shapes of the different production modes, indicating that the signal parameterisation is not sensitive to assumptions on their relative normalisation.

Several sources of systematic uncertainty associated with the signal modelling are taken into account. They are described in Sect. 4.5.

4.4 Background modelling

Analytic models are also used to describe the various background contributions. The functional form chosen for the background model is assessed using background templates built using MC simulation and data control regions. These templates are also used for the estimation of related systematic uncertainties.

4.4.1 Background templates

The main sources of background are the non-resonant production of prompt and isolated di-photons ($\gamma\gamma$) and the γj[7] and jj processes where one or two hadronic jets j are misidentified as photons. The relative contribution of each background component is measured in data using a two-dimensional double-sideband method [100]. With this method the fraction of the three components is measured to be $73.0 \pm 1.9\%$ for the $\gamma\gamma$, $23.6 \pm 1.5\%$ for the γj, and $3.4 \pm 0.4\%$ for the jj process.

A background template of the di-photon invariant mass is built by summing the $\gamma\gamma$, γj and jj components according to the measured fractions. The $\gamma\gamma$ component is directly derived from the simulated background event sample after applying the event selection described in Sect. 4.1. The shape of the sum of the γj and jj components is derived from data control samples defined by inverting the identification and/or isolation requirements of one or both photons. Since the ratio of the $m_{\gamma\gamma}$ distribution of the γj and jj components to that of the simulated $\gamma\gamma$ event sample is found to be described by a simple linear function in $m_{\gamma\gamma}$, a linear fit to the ratio of these distributions is used to provide an $m_{\gamma\gamma}$-dependent weight that is applied to the $\gamma\gamma$ sample to obtain a template that accounts for both the γj and jj components.

[6] A larger value of 75% for the correction factor is obtained for the $gg \to ZH$ process, but in the SM this process only accounts for 0.3% of the selected signal yield.

[7] The γj estimate includes both cases where either the leading E_{T} or the sub-leading E_{T} photon are from misidentified jets.

To get a better description of the background, a second-order polynomial in $m_{\gamma\gamma}$ is fitted to the ratio of the template to the data in the sidebands (i.e., excluding the 120–130 GeV mass region) and is used to correct the background template shape.

A second, alternative template used for background modelling studies is created through the implementation of a normalising flow (NF) method [101] that uses a generative machine-learning model based on MADE [102] and MAF [103], developed to emulate the detector response to photons and applied to particle-level simulated $\gamma\gamma$ events. This method is much faster than the standard full GEANT4 simulation, and can be applied to very large samples. The alternative template is produced using the equivalent of about 3.5 ab^{-1} of integrated luminosity, compared to the 1.3 ab^{-1} of the GEANT4-based sample. To correct for the photon identification and isolation efficiencies, which are not part of the learning procedure, a parameterised photon efficiency derived as a function of the photon transverse energy and pseudorapidity from the full simulation is applied to the NF simulated events. The prompt di-photon background component obtained with the NF approach is then corrected to take into account the non-prompt photon contributions using a procedure identical to the one described above for the GEANT4-based sample, including the reweighting of the simulated mass spectrum with a second-order polynomial to the data sidebands.

4.4.2 Functional form

The $m_{\gamma\gamma}$ background distribution is characterised by a smoothly falling spectrum. It can be parameterised by an empirical function selected using the background templates described above. The parameters of this function are fitted to data, but the functional form itself is chosen following a procedure, used in a previous publication [6], which aims to minimise the statistical and systematic uncertainties in the measured signal while still ensuring a good description of the background $m_{\gamma\gamma}$ spectrum.

Three families of functions are studied for this empirical component: power-law functions, Bernstein polynomials and exponential functions of polynomials. The criteria used to select the background function from among these families and to determine the associated systematic uncertainty, referred to as the spurious signal (SS) [1], are described in the following. The procedure begins by considering functions of lowest order; the order is increased until a function satisfying the criteria is found.

As a first requirement, only functions able to fit the data mass sidebands with a χ^2 probability greater than 1% are considered. For all functions that satisfy this criterion, a spurious-signal test is performed. The SS yields are defined as the measured signal obtained in signal-plus-background fits to the background-only templates. They are determined not only for a signal mass of 125 GeV, but for all values of m_H between 123 and 127 GeV in steps of 0.5 GeV. The maximum absolute value of the SS yield in this mass range is taken to be the background modelling uncertainty. Only functions with an absolute value of the SS yield below 20% of the statistical error of the expected fitted signal yield or below 10% of the expected SM signal yield are considered. Among the functions that satisfy this requirement, those with the smallest number of degrees of freedom are selected to minimise the statistical uncertainty that dominates this measurement. If more than one function passes this final selection, the one with the smallest SS is selected. As a conservative approach, the SS is computed using the two background templates (GEANT4- and NF-based) described in Sect. 4.4.1 and the largest value is selected. The function selected by this procedure is an exponential function of a second-order polynomial in $m_{\gamma\gamma}$, with an associated SS uncertainty corresponding to 6.2% of the expected SM signal yield.

To test the robustness of the background modelling choice, the procedure described above is repeated on different background templates. These additional templates are obtained using only the prompt-photon simulation reweighted to the data sidebands, either from the full-simulation samples or from the particle-level samples corrected for detector effects with the NF approach. For these additional templates, the procedure still selects the same function and the values of the SS are smaller than those of the original templates described in Sect. 4.4.1, hence no additional uncertainty is associated with this test.

4.5 Systematic uncertainties

The measurement of the fiducial $H \to \gamma\gamma$ cross-section is affected by several sources of uncertainty, which can be broken down into three categories: those that affect the shape of the $m_{\gamma\gamma}$ signal distribution, those that affect the background modelling, and those that impact the detector and fiducial corrections to the measured signal yields and thus the correction factor $C_{\mathcal{F}}$. The uncertainty in the luminosity measurement also affects the fiducial cross-section measurement, as illustrated by the relation in Eq. (1). This uncertainty, described in Sect. 3.1, is evaluated to be 2.2%.

4.5.1 Systematic uncertainties in the $m_{\gamma\gamma}$ signal modelling

Since the fiducial cross-section is measured from a fit to the $m_{\gamma\gamma}$ spectrum, any sources of uncertainty that affect the peak position or the width of the signal peak will have an impact on the cross-section measurement. Uncertainties in the photon-energy scale result in a shift of the position of the signal peak, while uncertainties in the photon-energy resolution result in the broadening or narrowing of this peak. These uncertainties

are evaluated as described in Refs. [92,104] using Run 2 data and simulation. Additional uncertainties are included to take into account the change in conditions between Run 2 and Run 3, and changes to the MC simulation. The uncertainty arising from differences in the photon-energy scale between data and simulation has a modest impact of under 0.25% on the position of the peak; an additional 0.4% uncertainty accounts for changes in the detector simulation between Run 2 and Run 3. The photon-energy resolution uncertainty is the single largest contributor to the signal shape uncertainty, with a total error of about 10% in the width of the peak.

The peak position is also affected by the uncertainty in the Higgs boson mass, taken as 0.24 GeV from the combination of the Higgs boson mass measurements performed by the ATLAS and CMS collaborations during the first run of the LHC [13]. This uncertainty has an impact on the cross-section measurement of 0.1%.

4.5.2 *Systematic uncertainties in the $m_{\gamma\gamma}$ background modelling*

The choice of the analytic function used to model the background $m_{\gamma\gamma}$ distribution can affect the measured cross-section, and the associated impact is quantified through the spurious signal yield described in Sect. 4.4.

4.5.3 *Systematic uncertainties in the $C_{\mathcal{F}}$ correction factor*

Both experimental and theoretical uncertainties can affect the correction factor $C_{\mathcal{F}}$, and in the case of theoretical uncertainties, introduce a slight model dependence into the measurement. These sources of uncertainty also have an impact on the fiducial acceptance, and they are relevant when extrapolating the fiducial cross-section measurement results to the full phase space.

Several experimental uncertainties impact the $C_{\mathcal{F}}$ correction factor. These include uncertainties related to the efficiency of the photon trigger, identification and isolation selections, to the impact of the di-photon vertex selection, and to the estimation of the photon-energy scale and resolution.

The efficiency of the di-photon trigger is estimated with an uncertainty of about 2% for Run 3 data based on the bootstrap method [20,105]. The single photon trigger contributes only to 0.1% of the selected signal events and its uncertainty is therefore neglected. All other photon-related uncertainties are assessed using Run 2 data and additional uncertainties take into account effects from the change in conditions between Run 2 and Run 3, and changes to the MC simulation.

The photon identification efficiency in simulated events is corrected to match the efficiency observed in data as detailed in Ref. [92]. The uncertainty in the simulation-to-data correction is estimated to have an impact of about 5% on $C_{\mathcal{F}}$. The uncertainty in the photon isolation efficiency is derived from a similar methodology to that of the photon identification as detailed in Ref. [92]. The photon isolation efficiency uncertainty is estimated to have a 1.6% impact on $C_{\mathcal{F}}$. The efficiency of the vertex selection algorithm is computed both in data and in simulation. As described in Sect. 4.1, the difference between the two is evaluated using $Z \to ee$ events. The resulting impact on $C_{\mathcal{F}}$ from this efficiency uncertainty amounts to below 0.03%.

Changes to the photon-energy scale and resolution result in the migration of events into and out of the fiducial region, with a maximal impact on $C_{\mathcal{F}}$ below 0.1%.

The uncertainty in the modelling of pile-up is evaluated by varying by ±9% the value of the visible inelastic cross-section used to reweight the pile-up distribution in the simulation to that observed in the data [106]. The uncertainty in the modelling of pile-up is estimated to have an impact of about 1.2% on $C_{\mathcal{F}}$.

Several sources of theoretical uncertainty are also considered. The correction factor $C_{\mathcal{F}}$ is computed by combining all production modes of the Higgs boson assuming SM cross-sections. Values of $C_{\mathcal{F}}$ that are different between production modes introduce a model dependence through the SM cross-section assumption. A signal composition uncertainty is therefore derived by varying the cross-section of each production mode within its measured uncertainty as determined in Ref. [107]. The impact of this uncertainty on $C_{\mathcal{F}}$ is 0.02%. Uncertainties in $C_{\mathcal{F}}$ due to the ME generator, scale and PDF set choice, and the modelling of the PS, UE and hadronisation, are all small and neglected in the fit model.

Additional uncertainties are considered when extrapolating the fiducial cross-section to the full phase space to derive the total cross-section. They include uncertainties in the acceptance that are derived following the same procedure as in Refs. [6,108], mainly originating from missing higher-order terms in the perturbative QCD calculations, the modelling of PS, the PDFs and the value of α_s, for a total amount of 1.4%. An uncertainty in the $H \to \gamma\gamma$ branching ratio of 2.9% [30] is also included.

4.6 Results

The invariant mass spectrum, superimposed with the background and signal functions obtained from the fit to the data, is shown in Fig. 1.

The value of the fiducial cross-section, extracted from the fit to this $m_{\gamma\gamma}$ spectrum, is measured to be $\sigma_{\text{fid}} = 76 \pm 11\,(\text{stat.})\,^{+9}_{-7}\,(\text{syst.})$ fb and is in agreement with the SM prediction of $\sigma_{\text{fid,SM}} = 67.6 \pm 3.7$ fb. The SM prediction is derived using the cross-section calculations described in Sect. 3.2 and corrected for acceptance effects, assessed using the simulated event samples.

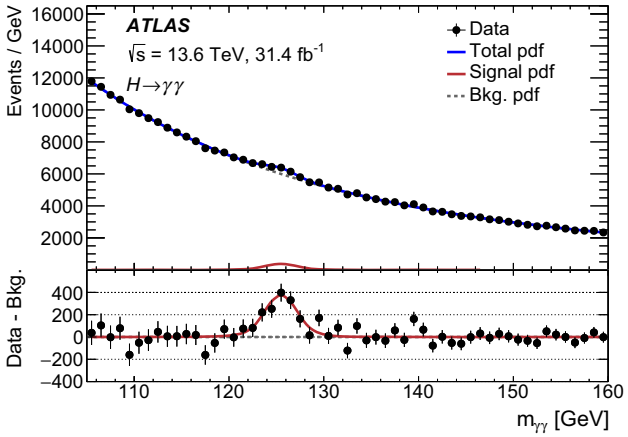

Fig. 1 Di-photon invariant mass spectrum within the $H \to \gamma\gamma$ fiducial region, as observed in data. The signal, background and total probability density functions (pdf) derived from the fit to data in the window $105 \leq m_{\gamma\gamma} \leq 160$ GeV are also shown

The breakdown of the total uncertainty into its different components is detailed in Table 3. The statistical component is obtained by fixing all the nuisance parameters associated with systematic uncertainties to their best-fit values. The grouped squared systematic uncertainties are obtained by subtracting the squared values of the uncertainties obtained from two fits, one performed with the corresponding nuisance parameters fixed to their best-fit value and the other with them free floating in the fit.

5 The $H \to ZZ^* \to 4\ell$ measurement

5.1 Event reconstruction and selection

The selection of events for the $H \to ZZ^* \to 4\ell$ measurement relies on the reconstruction and identification of lepton (electron and muon) candidates, used to build a quadruplet that defines the Higgs boson candidate. It closely follows the analyses reported in Refs. [5,109]. A brief description is provided below.

5.1.1 Electron and muon reconstruction, identification and preselection

Electron reconstruction is performed using energy clusters in the EM calorimeter built with a dynamical, topological cell-based approach [91,92] similar to the one described for photons in Sect. 4.1.1. These clusters are required to be matched to reconstructed ID tracks. A Gaussian-sum filter algorithm [110] is used to compensate for radiative energy losses in the ID for the track reconstruction. Electron identification is based on a likelihood discriminant that combines the properties and transition radiation response of the track,

Table 3 Breakdown of the relative uncertainties in the inclusive di-photon fiducial cross-section measurement

Source	Uncertainty (%)
Statistical uncertainty	14.0
Systematic uncertainty	10.3
Background modelling (spurious signal)	6.0
Photon trigger and selection efficiency	5.8
Photon energy scale & resolution	5.5
Luminosity	2.2
Pile-up modelling	1.2
Higgs boson mass	0.1
Theoretical (signal) modelling	< 0.1
Total	17.4

the EM shower shape of the energy cluster and the quality of the track-to-cluster matching. A *loose* likelihood working point selection [92], applied in combination with track hit requirements, serves as a preselection requirement and provides an electron reconstruction and identification efficiency of at least 90% for isolated electrons with $p_{\mathrm{T}} > 30$ GeV and within the range of 85–90% for isolated electrons with $p_{\mathrm{T}} < 30$ GeV [92].[8] The energy of electron candidates is calibrated as described in Ref. [92]. All electron candidates are required to have $E_{\mathrm{T}} > 7$ GeV and be within the acceptance of the ID, $|\eta| < 2.47$.

Muon reconstruction [111] in the range of $|\eta| < 2.5$ is primarily performed through a global fit to fully reconstructed tracks in the ID and the MS. Muon candidates are identified using a *loose* [111] identification criterion and required to have $p_{\mathrm{T}} > 5$ GeV. The identification criterion has an efficiency of 98% for isolated muons with $p_{\mathrm{T}} = 5$ GeV, and rises to 99% for muons with higher p_{T}. At the centre of the detector ($0 < |\eta| < 0.1$), where the MS geometrical coverage is reduced, muon candidates are also identified through the matching of a fully reconstructed ID track to either an MS track segment or a calorimeter energy deposit consistent with a minimum ionising particle (calorimeter-tagged muons). In these two cases, the muon candidate's momentum is measured using only the ID track. For calorimeter-tagged muon candidates, the p_{T} requirement is raised to $p_{\mathrm{T}} > 15$ GeV. No more than one calorimeter-tagged muon is allowed per event. The momentum of muon candidates is calibrated using the procedure described in Ref. [111].

[8] Electron efficiency values are taken from Run 2, and additional systematic uncertainties are included to take into account the change in conditions between Run 2 and Run 3, and changes to the MC simulation.

Table 4 Summary of the event selection requirements for leptons and Higgs boson candidates outlined in Sect. 5.1. SFOC lepton pairs are same-flavour opposite-charge lepton pairs. For the mass requirement of the subleading lepton pair, $m_{\text{threshold}}$ is 12 GeV for $m_{4\ell} < 140$ GeV, and rises linearly to 50 GeV for $m_{4\ell} = 190$ GeV

Leptons	
Muons	$p_{\text{T}} > 5$ GeV, $\lvert\eta\rvert < 2.5$
Electrons	$E_{\text{T}} > 7$ GeV, $\lvert\eta\rvert < 2.47$
Lepton selection and pairing	
Lepton kinematics	$p_{\text{T}} > 20, 15, 10$ GeV
Leading pair (m_{12})	SFOC lepton pair with smallest $\lvert m_Z - m_{\ell\ell}\rvert$
Subleading pair (m_{34})	Remaining SFOC lepton pair with smallest $\lvert m_Z - m_{\ell\ell}\rvert$
Event selection (at most one Higgs boson candidate per channel)	
Mass requirements	50 GeV $< m_{12} <$ 106 GeV and $m_{\text{threshold}} < m_{34} <$ 115 GeV
Lepton separation	$\Delta R(\ell_i, \ell_j) > 0.1$
J/ψ veto	$m(\ell_i, \ell_j) > 5$ GeV for all SFOC lepton pairs
Impact parameter	$\lvert d_0\rvert/\sigma(d_0)$ <5 (3) for electrons (muons)
Mass window	105 GeV $< m_{4\ell} <$ 160 GeV
Vertex selection	$\chi^2/N_{\text{dof}} < 6$ (9) for 4μ (other channels)
If extra lepton with $p_{\text{T}} > 12$ GeV	Quadruplet with largest matrix element value

5.1.2 Primary vertex selection

The events used in the $H \to ZZ^* \to 4\ell$ measurement are required to have at least one reconstructed vertex with at least two associated ID tracks of transverse momentum $p_{\text{T}} >$ 500 MeV. If more than one reconstructed vertex is found, the vertex with the largest $\sum p_{\text{T}}^2$ (counting all of its associated tracks) is selected as the primary interaction vertex.

The impact parameters of electron and muon candidates are computed relative to the primary interaction vertex.[9] Muon candidates with transverse impact parameter d_0 greater than 1 mm are rejected. Both muon and electron candidates are required to have a longitudinal impact parameter $\lvert z_0 \sin\theta\rvert$ less than 0.5 mm.

5.1.3 Event selection

The rest of the event selection is focused on the selection of a Higgs boson candidate using four lepton candidates. It is first required that the selected leptons can be matched to at least one of the leptons that triggered the event as described in Sect. 3.1.

Same-flavour opposite-charge (SFOC) lepton candidate pairs are first selected using all electron and muon candidates in the event that satisfy the preselection. The SFOC pair with mass closest to the Z boson mass ($m_Z = 91.188$ GeV) is called the leading pair and its mass is labelled m_{12}, while the other becomes the subleading pair, with mass m_{34}. If multiple combinations of SFOC pairs can be formed, a Higgs boson candidate is chosen based on the combination resulting in a leading pair mass m_{12} closest to the Z boson mass. If there is more than one type of quadruplet (4μ, $2e2\mu$, $2\mu2e$ or $4e$) satisfying these selection criteria in the event, the quadruplet from the channel with highest selection efficiency is chosen as the Higgs boson candidate.

At this stage, the three leading lepton candidates of each Higgs boson candidate are required to satisfy $p_{\text{T}} > 20$, 15 and 10 GeV respectively. Higgs boson candidate events are subjected to further selection requirements on the SFOC pair masses, the lepton candidate separation, a J/ψ mass veto, the impact parameter significance ($d_0/\sigma(d_0)$) of the lepton candidates, and the quality of the vertex of the event, as outlined in Table 4.

In addition, track- and calorimeter-based isolation requirements are imposed on the lepton candidates to suppress contributions from the $t\bar{t}$ and Z + jets reducible backgrounds. A track-based isolation requirement is defined using the scalar p_{T} sum of all tracks with $p_{\text{T}} > 500$ MeV that lie within a cone of $\Delta R = 0.3$ around the muon or electron candidate and that either originate from the primary vertex or have $\lvert z_0 \sin\theta\rvert < 3$ mm. For lepton candidates with $p_{\text{T}} > 33$ GeV, the size of this cone falls linearly as a function of p_{T} to a minimum cone size of 0.2 at 50 GeV. Similarly, a calorimeter-based isolation requirement based on the scalar E_{T} sum is calculated from the positive-energy topological clusters that are not associated with the lepton candidate's track within a cone of $\Delta R = 0.2$ around the lepton candidate. This

[9] The transverse impact parameter d_0 of a charged-particle track is defined in the transverse plane as the distance from the primary vertex to the track's point of closest approach. The longitudinal impact parameter z_0 is the distance in the z direction between this point and the primary vertex.

Table 5 Summary of the event selection requirements that define the fiducial phase space for the $H \to ZZ^* \to 4\ell$ cross-section measurement. SFOC lepton pairs are same-flavour opposite-charge lepton pairs

Leptons	
Leptons	$p_{\mathrm{T}} > 5$ GeV, $\lvert\eta\rvert < 2.7$
Lepton selection and pairing	
Lepton kinematics	$p_{\mathrm{T}} > 20, 15, 10$ GeV
Leading pair (m_{12})	SFOC lepton pair with smallest $\lvert m_Z - m_{\ell\ell}\rvert$
Subleading pair (m_{34})	Remaining SFOC lepton pair with smallest $\lvert m_Z - m_{\ell\ell}\rvert$
Event selection (at most one quadruplet per event)	
Mass requirements	50 GeV $< m_{12} <$ 106 GeV and 12 GeV $< m_{34} <$ 115 GeV
Lepton separation	$\Delta R(\ell_i, \ell_j) > 0.1$
J/ψ veto	$m(\ell_i, \ell_j) > 5$ GeV for all SFOC lepton pairs
Mass window	105 GeV $< m_{4\ell} <$ 160 GeV
If extra lepton with $p_{\mathrm{T}} > 12$ GeV	Quadruplet with largest matrix element value

calorimeter-based isolation is corrected for electron shower leakage, and pile-up and UE contributions. Both the track- and calorimeter-based isolation are corrected for track and topological-cluster contributions from the other lepton candidates. For muons, the sum of the track isolation and 0.4 times the value of the calorimeter isolation is required to be less than 16% of the lepton candidate's p_{T}. For electrons, the sum of the track isolation is required to be less than 15% of the lepton candidate's p_{T} and the calorimeter isolation is required to be less than 20% of the lepton candidate's p_{T}.

If an extra prompt lepton candidate with $p_{\mathrm{T}} > 12$ GeV and passing all identification and isolation requirements detailed above is present in the event, the quadruplet of lepton candidates selected as the Higgs boson candidate is chosen using a method based on the ME. The ME for the Higgs boson decay is calculated at LO using MadGraph5_aMC@NLO for each quadruplet in the event, and the quadruplet with the highest ME value is chosen, with the reconstructed lepton momentum vectors used as inputs to the calculation. This procedure increases the probability of selecting the correct Higgs boson candidate in cases where the extra lepton comes from the decay of a vector boson or top quark in VH-leptonic or $t\bar{t}H/tH$ production.

The quadruplet defined at this stage of the selection is determined to be the final Higgs boson candidate.

The four-lepton mass resolution (in particular the long radiative mass tail) is improved by accounting for reconstructed final-state radiation (FSR) photons originating from the Z boson decay products, as described in Refs. [5,109]. The Higgs boson candidate is required to have a four-lepton mass of $105 < m_{4\ell} < 160$ GeV.

The selection efficiency, relative to the full phase space, is estimated from simulated events to be 27%, 23%, 14% and 13% for the 4μ, $2e2\mu$, $2\mu2e$ and $4e$ final states, respectively.

5.1.4 Fiducial region

The fiducial region is defined using simulation at particle level and the selection requirements outlined in Table 5. To minimise model-dependent acceptance extrapolations, these are chosen to closely match the selection requirements outlined in Sects. 5.1.1–5.1.3.

The fiducial selection is applied to final-state electrons and muons that do not originate from hadrons or τ-lepton decays, after 'dressing', where the four-momenta of photons within a cone of size $\Delta R = 0.1$ around the lepton are added to the lepton's four-momentum. Photons that originate from hadron decays are excluded from this procedure.

The quadruplet selection using the selected dressed leptons follows the same procedure as in Sect. 5.1.3. In the case of VH or $t\bar{t}H$ production, additional leptons not originating from a Higgs boson decay can induce a 'lepton mispairing' when assigning them to the leading and subleading Z bosons. To improve the lepton pairing efficiency, the ME-based pairing method described in Sect. 5.1.3 is employed.

The acceptance of the fiducial selection, defined as the ratio of the number of events passing the particle-level selection to the number of events generated in a given final state (relative to the full phase space of $H \to ZZ^* \to 2\ell2\ell'$, where $\ell, \ell' = e$ or μ), is about 49% for each final state. About 1.4% of the events that satisfy the detector-level selection fail to satisfy the particle-level selection. This is mostly due to resolution effects.

5.2 Fit procedure

The $pp \to H \to ZZ^* \to 4\ell$ fiducial cross-section is extracted using a procedure analogous to the one presented in Sect. 4.2 for the $H \to \gamma\gamma$ measurement. The signal yield

N_S is parameterised as in Eqs. (1) and (2), with the fiducial cross-section similarly defined as the product of the total cross-section, the $H \to ZZ^* \to 4\ell$ branching ratio and the fiducial acceptance determined by the selection of Sect. 5.1.4. The correction factor $C_{\mathcal{F}}$, derived from the signal simulated event samples, has values of 55%, 47%, 30% and 26% for the 4μ, $2e2\mu$, $2\mu2e$ and $4e$ final states respectively. The value of $C_{\mathcal{F}}$ for the different production modes ranges from 43% for VBF to 29% for $t\bar{t}H$, and has value of 39% for the dominant production mode ggF. When averaging the four final states and assuming a relative composition of production modes as in the SM, the value of $C_{\mathcal{F}}$ is 40%.

To extract the number of signal events in each decay final state, invariant mass templates for the Higgs boson signal process and for the background processes are fitted to a $m_{4\ell}$ binned distribution in data. The signal and ZZ^* templates are constructed using the simulated event samples presented in Sect. 3.2. The normalisations of the signal and non-resonant ZZ^* background are freely floated in a simultaneous fit to the $m_{4\ell}$ spectrum within the range of 105–160 GeV. One single common ZZ^* normalisation factor is used to normalise this background in the 4μ, $2e2\mu$, $2\mu2e$ and $4e$ final states. Reducible backgrounds, mainly consisting of the Z + jets, $t\bar{t}$ and WZ processes, are estimated by using dedicated control regions described in more detail in Sect. 5.3 below.

The systematic uncertainties detailed in Sect. 5.4 are included in the fit and implemented as nuisance parameters. They include, among other things, variations of the signal and background template shapes, and variations of the reducible background normalisation.

5.3 Reducible background estimation

Background contributions from processes such as Z + jets, $t\bar{t}$ and WZ can satisfy the event selection due to the presence of at least one jet, one photon or one lepton from a hadron decay that is misidentified as a prompt lepton. These reducible backgrounds are significantly smaller than the non-resonant ZZ^* background and are estimated by using data where possible with different approaches as described in Refs. [5,109] and outlined below. Due to the comparatively higher rate of misidentification at lower momentum, the data driven approaches are split into $\ell\ell + \mu\mu$ and $\ell\ell + ee$ final states, which refer to the channels where the sub-leading lepton pair consists of muons or electrons respectively. All the control regions directly used to estimate the reducible backgrounds are mutually exclusive to each other and to the signal regions.

In the $\ell\ell+\mu\mu$ final states, the normalisations of the Z+jets and $t\bar{t}$ backgrounds are determined by performing fits to the invariant mass spectrum of the leading lepton pair in dedicated independent control regions that target each of the two background processes for each final state. Depending on the background process being targeted, the control regions are formed by relaxing the χ^2 requirement on the four-lepton vertex fit, and by inverting or relaxing isolation and/or impact-parameter requirements on the subleading muon candidate pair. Additional control regions ($e\mu\mu\mu$ and $\ell\ell + \mu^{\pm}\mu^{\pm}$) are used to improve the background yield estimate by reducing the statistical uncertainty in the fitted normalisation. Transfer factors to extrapolate from the control regions to the signal region are obtained separately for $t\bar{t}$ and Z + jets using simulation. The $m_{4\ell}$ shape for the two processes in each final state is obtained from simulation.

For the $\ell\ell+ee$ final states, an $\ell\ell+ee$ control region selection requires the electrons in the subleading lepton candidate pair to have the same charge, and relaxes the identification, impact parameter and isolation requirements on the electron candidate with the lowest E_{T}. This electron candidate, denoted by X, can be a light-flavour jet, an electron from a photon conversion or an electron from a heavy-flavour hadron decay. The heavy-flavour background, which accounts for about 35% of the reducible background in these channels, is determined from simulation, whereas the light-flavour and photon-conversion backgrounds are obtained using the sPlot method [112]. This method is based on a fit to the number of hits in the innermost ID layer, performed in the data control region. Transfer factors to extrapolate from the $\ell\ell+ee$ control region to the signal region for the light-flavour jets and converted photons are obtained from simulated event samples, and are corrected using a $Z+X$ data control region. The $m_{4\ell}$ shape is taken from the control region for the light-flavour jets and converted-photons components and from simulation for the heavy-flavour background. The agreement between simulation and data of the reducible background mass shape is checked in a region where the selection criteria on the d_0 and isolation are relaxed [5,109] and no significant discrepancies are found.

Additional contributions from rare processes, such as $t\bar{t}Z$, $t\bar{t}W$ and VVV are estimated from simulation.

5.4 Systematic uncertainties

The $H \to ZZ^* \to 4\ell$ fiducial cross-section measurement is affected by both experimental and theoretical uncertainties. Experimental uncertainties include uncertainties in the efficiency of electron and muon reconstruction, identification, isolation and trigger selections, and in electron and muon energy calibration. Theoretical uncertainties include the modelling of the signal and background processes.

5.4.1 Experimental uncertainties

Uncertainties in the electron (muon) reconstruction, identification, energy-momentum scale and resolution, and isolation efficiency have an impact on the expected signal yield

and on the shape of the signal and ZZ^* background. These uncertainties have an impact of approximately 6.3% (3.8%) on the measurement. The electron (muon) uncertainties are assessed using Run 2 (Run 3) data and simulation with methods described in Refs. [92,104,111]. For electrons, additional uncertainties are included to take into account the change in conditions between Run 2 and Run 3, and changes to the MC simulation. Lepton trigger efficiency uncertainties have a negligible impact.

The impact of the precision of the Higgs boson mass measurement of $m_H = 125.09 \pm 0.24$ GeV [13] is also negligible.

The uncertainty in the predicted yields due to uncertainties related to the pile-up modelling is below 1%.

The uncertainty in the luminosity measurement impacts the expected yields of both the signal and background contributions, except for background estimates in which the data-driven methods can reduce its impact. As discussed in Sect. 3.1, the luminosity uncertainty is 2.2%.

For the data-driven measurement of the reducible background, three sources of uncertainty are considered following the strategy described in Ref. [5]: a statistical uncertainty, an overall normalisation systematic uncertainty for each of $\ell\ell+\mu\mu$ and $\ell\ell+ee$, and a shape systematic uncertainty that varies for each final state. The joint impact of these sources of uncertainty on the cross-section measurement is below 1%.

5.4.2 *Theoretical uncertainties*

Sources of theoretical uncertainty include the effects of missing higher-order corrections, PS and UE modelling, and PDF plus α_s uncertainties. They affect the modelling of both signal and background processes.

For the signal, the sources of theoretical uncertainty are the same as those described in Sect. 4.5 for the $H \to \gamma\gamma$ measurement. For the fiducial cross-section measurement, they impact the expected signal yield through their effect on the correction factor $C_{\mathcal{F}}$, which includes the effects of the selection efficiency and of out-of-acceptance corrections.

Uncertainties due to missing higher-order QCD effects for the signal are estimated by using the same scheme as in Refs. [113,114]. These uncertainties have a negligible impact on the fiducial cross-section measurement.

The effects of PS and UE modelling uncertainties are estimated by using tune eigenvector variations and comparisons between acceptances calculated with PYTHIA 8 and HERWIG 7 PS algorithms. This uncertainty has a negligible impact on the fiducial cross-section measurement.

The impact of the PDF uncertainty is estimated by using the 30 eigenvector variations of the PDF4LHC_NLO_30 Hessian PDF set calculated at NLO, following the PDF4LHC recommendations [115]. This uncertainty has a negligible impact on the fiducial cross-section measurement.

Finally, additional uncertainties in $C_{\mathcal{F}}$ arise from uncertainties in the relative production mode composition, which can introduce a bias in the unfolding method. The size of the uncertainty is assessed by varying the production cross-sections within their measured uncertainties, as taken from Ref. [116], with a resulting impact of less than 1%.

When extrapolating to the full phase space to derive the total cross-section measurement the impact of these sources of uncertainty on the acceptance is also included, alongside an uncertainty in the $H \to ZZ^* \to 4\ell$ decay branching ratio of 2.2% [67,117]. At this stage the PS and UE modelling uncertainties are no longer negligible, and have an impact of 1.4%.

The ZZ^* process normalisation is derived from a simultaneous fit to the signal region and to sideband regions, hence the theoretical uncertainties in the ZZ^* normalisation such as from missing higher-order effects in QCD, PDF uncertainties and PS modelling do not have any impact on this measurement. In addition, the $m_{4\ell}$ shape obtained from SHERPA is compared with that obtained from MADGRAPH5_AMC@NLO, and the difference is taken as an additional source of systematic uncertainty. The difference between SHERPA and MADGRAPH5_AMC@NLO on the predicted $m_{4\ell}$ shape varies linearly from approximately $\mp 3\%$ at low $m_{4\ell}$ to $\pm 3\%$ at high $m_{4\ell}$. These sources of uncertainty have an impact of about 1% on the cross-section measurement.

The uncertainty in the gluon-induced ZZ^* process is taken into account by changing the relative composition of the quark-initiated and gluon-initiated ZZ^* components according to the theoretical uncertainty in their respective predicted cross-sections. This uncertainty has a negligible impact on the fiducial cross-section measurement.

5.5 Results

The observed number of events in each of the four decay final states (4μ, $2e2\mu$, $2\mu2e$ and $4e$), and the expected signal and background yields after the fit to the data (post-fit), are presented in Table 6. For illustrative purposes, the events shown in this table are selected in a narrower mass window ($115 < m_{4\ell} < 130$ GeV) relative to that used in the fit to the data.

Figure 2 shows the expected (post-fit) and observed (data) four-lepton invariant mass distribution.

The value of the fiducial cross-section, extracted from the $m_{4\ell}$ template fit described in Sect. 5.2, is measured to be $\sigma_{\text{fid}} = 2.80 \pm 0.70$ (stat.) ± 0.21 (syst.) fb and is in agreement with the SM prediction of $\sigma_{\text{fid,SM}} = 3.67 \pm 0.19$ fb. The breakdown of the total uncertainty into its different components, derived with the procedure described in Sect. 4.6, is detailed in Table 7.

Table 6 Predicted SM signal (pre-fit), expected (post-fit) and observed numbers of events in the four decay final states after the event selection, in the mass range 115 GeV $< m_{4\ell} <$ 130 GeV. The sum of the post-fit Higgs boson events and the estimated background yields (reported as Total) are compared with the data. Combined statistical and systematic uncertainties are included for the predictions (see Sect. 5.4)

Final state	Signal SM (pre-fit)	Signal (post-fit)	ZZ^*background	Other backgrounds	Total	Observed
4μ	14.8 ± 1.0	11.3 ± 0.8	8.3 ± 0.6	1.0 ± 0.3	20.6 ± 1.0	23
$2e2\mu$	11.1 ± 0.8	8.5 ± 0.6	6.5 ± 0.4	1.0 ± 0.3	16.0 ± 0.8	13
$2\mu 2e$	7.0 ± 1.3	5.4 ± 1.0	3.2 ± 0.6	0.9 ± 0.1	9.4 ± 1.2	12
$4e$	7.4 ± 1.5	5.7 ± 1.1	3.1 ± 0.7	0.8 ± 0.2	9.6 ± 1.4	9
Total	40.3 ± 3.8	30.9 ± 2.9	21.1 ± 2.0	3.6 ± 0.7	55.6 ± 4.4	57

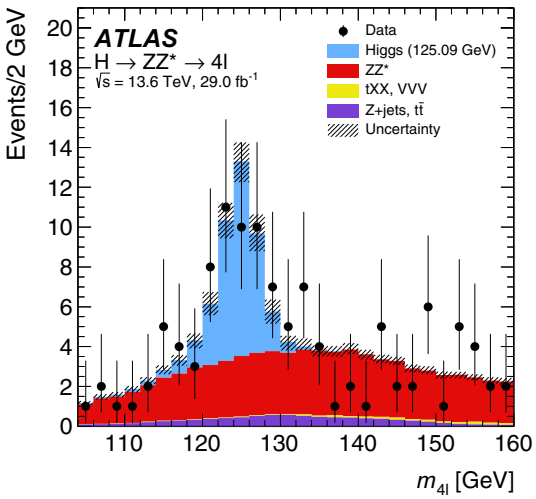

Fig. 2 The observed and expected (post-fit) inclusive four-lepton invariant mass distribution for the selected Higgs boson candidates, shown for an integrated luminosity of 29.0 fb^{-1} at $\sqrt{s} = 13.6$ TeV. The uncertainty in the prediction is shown by the hatched band, and includes the theoretical uncertainties in the SM cross-section for the signal and the main background processes. The tXX label indicates the sum of the $t\bar{t}W$ and $t\bar{t}Z$ processes

Table 7 Breakdown of the relative uncertainties in the fiducial $H \to ZZ^* \to 4\ell$ cross-section measurement

Source	Uncertainty (%)
Statistical uncertainty	25.1
Systematic uncertainty	7.9
Electron uncertainties	6.3
Muon uncertainties	3.8
Luminosity	2.2
ZZ^* theoretical uncertainties	0.7
Reducible background estimation	0.6
Other uncertainties	< 1.0
Total	26.4

6 Total cross-section measurements

Assuming SM values for the fiducial acceptances and for the branching fractions of the two channels, the fiducial measurements are extrapolated to the full phase space. When performing the extrapolation to the full phase space, additional uncertainties in the acceptance and in the branching fraction are considered (see Sects. 4.5, 5.4). The total Higgs boson production cross-section at 13.6 TeV is measured to be $\sigma(pp \to H) = 67^{+12}_{-11}$ pb using the $H \to \gamma\gamma$ channel and $\sigma(pp \to H) = 46 \pm 12$ pb using the $H \to 4\ell$ channel. The two measurements are compatible with a p-value of 20%.

A likelihood combination of the two decay channels is performed, following the method described in Ref. [118].

Experimental and theoretical uncertainties that affect both channels are correlated via common nuisance parameters. The correlated experimental uncertainties include the uncertainties in the integrated luminosity, in the description of pile-up in the simulation, in the common electron–photon energy scale, in the Higgs boson mass value, and in the relative contributions of the different Higgs boson production modes. Additionally, the common sources of theoretical uncertainty in the $H \to ZZ^* \to 4\ell$ and $H \to \gamma\gamma$ branching fractions (α_s, b- and c-quark masses, and partial decay widths into the main decay channels, such as two vector bosons, two gluons, or a $b\bar{b}$ pair) are also correlated. Finally, the theoretical uncertainties in the acceptance factor due to missing higher-order QCD effects, PDF variations, variations of the modelling of the PS, and signal composition are also correlated.

The asymptotic approximation [98] for the distribution of the profile likelihood ratio is assumed in the computation of uncertainties. The validity of this approximation was verified in previous analyses by performing pseudo-experiments.

The total Higgs boson production cross-section, obtained by combining the $H \to \gamma\gamma$ and $H \to ZZ^* \to 4\ell$ results, is $\sigma(pp \to H) = 58.2 \pm 8.7 = 58.2 \pm 7.5\,(\text{stat.}) \pm 4.5\,(\text{syst.})$ pb at 13.6 TeV. All three results ($H \to \gamma\gamma$, $H \to ZZ^* \to 4\ell$ and their combination) are in agreement with the SM prediction of $\sigma(pp \to H)_{\text{SM}} = 59.9 \pm 2.6$ pb.

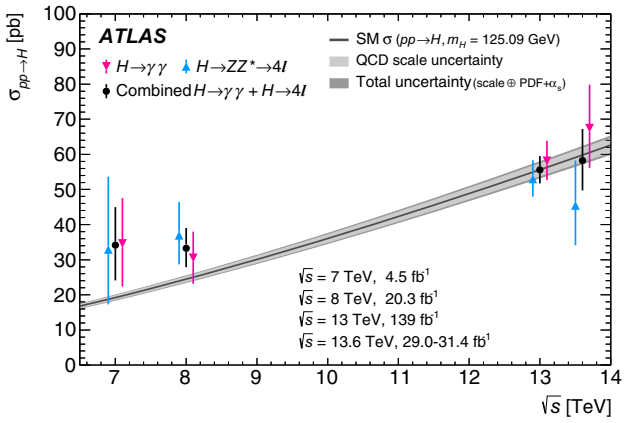

Fig. 3 Values of the $\sigma(pp \to H)$ measurements from this and previous [119,120] ATLAS publications as a function of the pp centre-of-mass energy. The SM predicted values and their uncertainties are shown by the shaded band. The individual channel results are offset along the x-axis for display purposes

The nuisance parameters associated with the position of the signal mass peak do not show any significant pull.

The values of the total cross-section determined from this analysis, and those from previously published ATLAS studies [119,120], are shown in Fig. 3 as a function of the pp centre-of-mass energy. The measurements at the new centre-of-mass energy of 13.6 TeV are in good agreement with the SM prediction.

7 Conclusion

The pp collision data recorded with the ATLAS detector at $\sqrt{s} = 13.6$ TeV are used to derive the first measurement of the $H \to \gamma\gamma$ and $H \to ZZ^* \to 4\ell$ cross-sections at this new LHC centre-of-mass energy, with corresponding integrated luminosities of 31.4 and 29.0 fb^{-1}, respectively. The cross-section measurements are restricted to kinematic phase spaces of the Higgs boson decay products that closely match the selection criteria applied at detector level, and are corrected for detector effects. The measured fiducial cross-sections are $\sigma_{\text{fid},\gamma\gamma} = 76^{+14}_{-13}$ fb for the $H \to \gamma\gamma$ channel and $\sigma_{\text{fid},4\ell} = 2.80 \pm 0.74$ fb for the $H \to ZZ^* \to 4\ell$ channels. They are in agreement with the corresponding Standard Model predictions of 67.6 ± 3.7 fb and 3.67 ± 0.19 fb.

Assuming SM values for the acceptances and the branching fractions of the two channels, the fiducial measurements are extrapolated to the full phase space, yielding total Higgs boson production cross-sections $\sigma(pp \to H) = 67^{+12}_{-11}$ pb and $\sigma(pp \to H) = 46 \pm 12$ pb at 13.6 TeV for the $H \to \gamma\gamma$ and $H \to ZZ^* \to 4\ell$ channels, respectively. These measurements are combined into a measurement of $\sigma(pp \to H) = 58.2 \pm 8.7$ pb, in agreement with the SM prediction of $\sigma(pp \to H)_{\text{SM}} = 59.9 \pm 2.6$ pb.

Acknowledgements We thank CERN for the very successful operation of the LHC, as well as the support staff from our institutions without whom ATLAS could not be operated efficiently. We acknowledge the support of ANPCyT, Argentina; YerPhI, Armenia; ARC, Australia; BMWFW and FWF, Austria; ANAS, Azerbaijan; CNPq and FAPESP, Brazil; NSERC, NRC and CFI, Canada; CERN; ANID, Chile; CAS, MOST and NSFC, China; Minciencias, Colombia; MEYS CR, Czech Republic; DNRF and DNSRC, Denmark; IN2P3-CNRS and CEA-DRF/IRFU, France; SRNSFG, Georgia; BMBF, HGF and MPG, Germany; GSRI, Greece; RGC and Hong Kong SAR, China; ISF and Benoziyo Center, Israel; INFN, Italy; MEXT and JSPS, Japan; CNRST, Morocco; NWO, Netherlands; RCN, Norway; MEiN, Poland; FCT, Portugal; MNE/IFA, Romania; MESTD, Serbia; MSSR, Slovakia; ARRS and MIZŠ, Slovenia; DSI/NRF, South Africa; MICINN, Spain; SRC and Wallenberg Foundation, Sweden; SERI, SNSF and Cantons of Bern and Geneva, Switzerland; MOST, Taiwan; TENMAK, Türkiye; STFC, United Kingdom; DOE and NSF, United States of America. In addition, individual groups and members have received support from BCKDF, CANARIE, Compute Canada and CRC, Canada; PRIMUS 21/SCI/017 and UNCE SCI/013, Czech Republic; COST, ERC, ERDF, Horizon 2020 and Marie Skłodowska-Curie Actions, European Union; Investissements d'Avenir Labex, Investissements d'Avenir Idex and ANR, France; DFG and AvH Foundation, Germany; Herakleitos, Thales and Aristeia programmes co-financed by EU-ESF and the Greek NSRF, Greece; BSF-NSF and MINERVA, Israel; Norwegian Financial Mechanism 2014–2021, Norway; NCN and NAWA, Poland; La Caixa Banking Foundation, CERCA Programme Generalitat de Catalunya and PROMETEO and GenT Programmes Generalitat Valenciana, Spain; Göran Gustafssons Stiftelse, Sweden; The Royal Society and Leverhulme Trust, United Kingdom. The crucial computing support from all WLCG partners is acknowledged gratefully, in particular from CERN, the ATLAS Tier-1 facilities at TRIUMF (Canada), NDGF (Denmark, Norway, Sweden), CC-IN2P3 (France), KIT/GridKA (Germany), INFN-CNAF (Italy), NL-T1 (Netherlands), PIC (Spain), ASGC (Taiwan), RAL (UK) and BNL (USA), the Tier-2 facilities worldwide and large non-WLCG resource providers. Major contributors of computing resources are listed in Ref. [121].

Data availability This manuscript has no associated data or the data will not be deposited. [Authors' comment: All ATLAS scientific output is published in journals, and preliminary results are made available in Conference Notes. All are openly available, without restriction on use by external parties beyond copyright law and the standard conditions agreed by CERN. Data associated with journal publications are also made available: tables and data from plots (e.g. cross section values, likelihood profiles, selection efficiencies, cross section limits, ...) are stored in appropriate repositories such as HEPDATA (http://hepdata.cedar.ac.uk/). ATLAS also strives to make additional material related to the paper available that allows a reinterpretation of the data in the context of new theoretical models. For example, an extended encapsulation of the analysis is often provided for measurements in the framework of RIVET (http://rivet.hepforge.org/). This information is taken from the ATLAS Data Access Policy, which is a public document that can be downloaded from http://opendata.cern.ch/record/413 [opendata.cern.ch]].

Funded by SCOAP[3].

References

1. ATLAS Collaboration, Observation of a new particle in the search for the Standard Model Higgs boson with the ATLAS detector at the LHC. Phys. Lett. B **716**, 1 (2012). https://doi.org/10.1016/j.physletb.2012.08.020. arXiv:1207.7214 [hep-ex]
2. CMS Collaboration, Observation of a new boson at a mass of 125 GeV with the CMS experiment at the LHC. Phys. Lett. B **716**, 30 (2012). https://doi.org/10.1016/j.physletb.2012.08.021. arXiv:1207.7235 [hep-ex]
3. L. Evans, P. Bryant, L.H.C. Machine, JINST **3**, S08001 (2008). https://doi.org/10.1088/1748-0221/3/08/S08001
4. ATLAS Collaboration, Measurements of fiducial and differential cross sections for Higgs boson production in the diphoton decay channel at $\sqrt{s} = 8$ TeV with ATLAS. JHEP **09**, 112 (2014). https://doi.org/10.1007/JHEP09(2014)112. arXiv:1407.4222 [hep-ex]
5. ATLAS Collaboration, Measurements of the Higgs boson inclusive and differential fiducial cross sections in the 4ℓ decay channel at $\sqrt{s} = 13$ TeV. Eur. Phys. J. C **80**, 942 (2020). https://doi.org/10.1140/epjc/s10052-020-8223-0. arXiv:2004.03969 [hep-ex]
6. ATLAS Collaboration, Measurements of the Higgs boson inclusive and differential fiducial cross-sections in the diphoton decay channel with pp collisions at $\sqrt{s} = 13$ TeV with the ATLAS detector. JHEP **08**, 027 (2022). https://doi.org/10.1007/JHEP08(2022)027. arXiv:2202.00487 [hep-ex]
7. ATLAS Collaboration, Fiducial and differential cross sections of Higgs boson production measured in the four-lepton decay channel in pp collisions at $\sqrt{s} = 8$ TeV with the ATLAS detector. Phys. Lett. B **738**, 234 (2014). https://doi.org/10.1016/j.physletb.2014.09.054. arXiv:1408.3226 [hep-ex]
8. CMS Collaboration, Measurement of differential cross sections for Higgs boson production in the diphoton decay channel in pp collisions at $\sqrt{s} = 8$ TeV. Eur. Phys. J. C **76**, 13 (2016). https://doi.org/10.1140/epjc/s10052-015-3853-3. arXiv:1508.07819 [hep-ex]
9. CMS Collaboration, Measurement of the Higgs boson inclusive and differential fiducial production cross sections in the diphoton decay channel with pp collisions at $\sqrt{s} = 13$ TeV (2022). arXiv:2208.12279 [hep-ex]
10. CMS Collaboration, Measurements of production cross sections of the Higgs boson in the four-lepton final state in proton-proton collisions at $\sqrt{s} = 13$ TeV. Eur. Phys. J. C **81**, 488 (2021). https://doi.org/10.1140/epjc/s10052-021-09200-x. arXiv:2103.04956 [hep-ex]
11. CMS Collaboration, Measurement of differential and integrated fiducial cross sections for Higgs boson production in the four-lepton decay channel in pp collisions at $\sqrt{s} = 7$ and 8 TeV. JHEP **04**, 005 (2016). https://doi.org/10.1007/JHEP04(2016)005. arXiv:1512.08377 [hep-ex]
12. CMS Collaboration, Measurements of inclusive and differential cross sections for the Higgs boson production and decay to four-leptons in proton-proton collisions at $\sqrt{s}$ = 13 TeV. JHEP **08**, 040 (2023). https://doi.org/10.1007/JHEP08(2023)040. arXiv:2305.07532 [hep-ex]
13. ATLAS and CMS Collaborations, Combined Measurement of the Higgs Boson Mass in pp Collisions at $\sqrt{s} = 7$ and 8 TeV with the ATLAS and CMS Experiments. Phys. Rev. Lett. **114**, 191803 (2015). https://doi.org/10.1103/PhysRevLett.114.191803. arXiv:1503.07589 [hep-ex]
14. ATLAS Collaboration, The ATLAS Experiment at the CERN Large Hadron Collider. JINST **3**, S08003 (2008). https://doi.org/10.1088/1748-0221/3/08/S08003
15. ATLAS Collaboration, The ATLAS Experiment at the CERN Large Hadron Collider: a description of the detector configuration for Run 3 (2023). arXiv:2305.16623 [physics.ins-det]
16. ATLAS Collaboration, The ATLAS Collaboration Software and Firmware, ATL-SOFT-PUB-2021-001, 2021. https://cds.cern.ch/record/2767187
17. ATLAS Collaboration, Preliminary analysis of the luminosity calibration of the ATLAS 13.6 TeV data recorded in 2022, ATL-DAPR-PUB-2023-001 (2023). https://cds.cern.ch/record/2853525
18. ATLAS Collaboration, Luminosity determination in pp collisions at $\sqrt{s} = 13$ TeV using the ATLAS detector at the LHC (2022). arXiv:2212.09379 [hep-ex]
19. G. Avoni et al., The new LUCID-2 detector for luminosity measurement and monitoring in ATLAS. JINST **13**, P07017 (2018). https://doi.org/10.1088/1748-0221/13/07/P07017
20. ATLAS Collaboration, Performance of electron and photon triggers in ATLAS during LHC Run 2. Eur. Phys. J. C **80**, 47 (2020). https://doi.org/10.1140/epjc/s10052-019-7500-2. arXiv:1909.00761 [hep-ex]
21. ATLAS Collaboration, Performance of the ATLAS muon triggers in Run 2. JINST **15**, P09015 (2020). https://doi.org/10.1088/1748-0221/15/09/p09015. arXiv:2004.13447 [hep-ex]
22. K. Hamilton, P. Nason, E. Re, G. Zanderighi, NNLOPS simulation of Higgs boson production. JHEP **10**, 222 (2013). https://doi.org/10.1007/JHEP10(2013)222. arXiv:1309.0017 [hep-ph]
23. K. Hamilton, P. Nason, G. Zanderighi, Finite quark-mass effects in the NNLOPS POWHEG+MiNLO Higgs generator. JHEP **05**, 140 (2015). https://doi.org/10.1007/JHEP05(2015)140. arXiv:1501.04637 [hep-ph]
24. S. Alioli, P. Nason, C. Oleari, E. Re, A general framework for implementing NLO calculations in shower Monte Carlo programs: the POWHEG BOX. JHEP **06**, 043 (2010). https://doi.org/10.1007/JHEP06(2010)043. arXiv:1002.2581 [hep-ph]
25. P. Nason, A new method for combining NLO QCD with shower Monte Carlo algorithms. JHEP **11**, 040 (2004). https://doi.org/10.1088/1126-6708/2004/11/040. arXiv:hep-ph/0409146
26. S. Frixione, P. Nason, C. Oleari, Matching NLO QCD computations with parton shower simulations: the POWHEG method. JHEP **11**, 070 (2007). https://doi.org/10.1088/1126-6708/2007/11/070. arXiv:0709.2092 [hep-ph]
27. K. Hamilton, P. Nason, G. Zanderighi, MINLO: multi-scale improved NLO. JHEP **10**, 155 (2012). https://doi.org/10.1007/JHEP10(2012)155. arXiv:1206.3572 [hep-ph]
28. J.M. Campbell et al., NLO Higgs boson production plus one and two jets using the POWHEG BOX, MadGraph4 and MCFM. JHEP **07**, 092 (2012). https://doi.org/10.1007/JHEP07(2012)092. arXiv:1202.5475 [hep-ph]
29. K. Hamilton, P. Nason, C. Oleari, G. Zanderighi, Merging H/W/Z + 0 and 1 jet at NLO with no merging scale: a path to parton shower + NNLO matching. JHEP **05**, 082 (2013). https://doi.org/10.1007/JHEP05(2013)082. arXiv:1212.4504 [hep-ph]
30. D. de Florian et al., Handbook of LHC Higgs Cross Sections: 4. Deciphering the Nature of the Higgs Sector (2016). arXiv:1610.07922 [hep-ph]
31. LHC Higgs Working Group, Ad Interim 13.6 TeV cross sections. https://twiki.cern.ch/twiki/bin/view/LHCPhysics/LHCHWG136TeVxsec_extrap
32. U. Aglietti, R. Bonciani, G. Degrassi, A. Vicini, Two-loop light fermion contribution to Higgs production and decays. Phys. Lett.

B **595**, 432 (2004). https://doi.org/10.1016/j.physletb.2004.06.063. arXiv:hep-ph/0404071
33. S. Actis, G. Passarino, C. Sturm, S. Uccirati, NLO electroweak corrections to Higgs boson production at hadron colliders. Phys. Lett. B **670**, 12 (2008). https://doi.org/10.1016/j.physletb.2008.10.018. arXiv:0809.1301 [hep-ph]
34. S. Actis, G. Passarino, C. Sturm, S. Uccirati, NNLO computational techniques: the cases $H \to \gamma\gamma$ and $H \to gg$. Nucl. Phys. B **811**, 182 (2009). https://doi.org/10.1016/j.nuclphysb.2008.11.024. arXiv:0809.3667 [hep-ph]
35. C. Anastasiou, R. Boughezal, F. Petriello, Mixed QCD-electroweak corrections to Higgs boson production in gluon fusion. JHEP **04**, 003 (2009). https://doi.org/10.1088/1126-6708/2009/04/003. arXiv:0811.3458 [hep-ph]
36. A. Pak, M. Rogal, M. Steinhauser, Finite top quark mass effects in NNLO Higgs boson production at LHC. JHEP **02**, 025 (2010). https://doi.org/10.1007/JHEP02(2010)025. arXiv:0911.4662 [hep-ph]
37. R.V. Harlander, K.J. Ozeren, Top mass effects in Higgs production at next-to-next-to-leading order QCD: Virtual corrections. Phys. Lett. B **679**, 467 (2009). https://doi.org/10.1016/j.physletb.2009.08.012. arXiv:0907.2997 [hep-ph]
38. R.V. Harlander, K.J. Ozeren, Finite top mass effects for hadronic Higgs production at next-to-next-to-leading order. JHEP **11**, 088 (2009). https://doi.org/10.1088/1126-6708/2009/11/088. arXiv:0909.3420 [hep-ph]
39. R.V. Harlander, H. Mantler, S. Marzani, K.J. Ozeren, Higgs production in gluon fusion at next-to-next-to-leading order QCD for finite top mass. Eur. Phys. J. C **66**, 359 (2010). https://doi.org/10.1140/epjc/s10052-010-1258-x. arXiv:0912.2104 [hep-ph]
40. C. Anastasiou, C. Duhr, F. Dulat, F. Herzog, B. Mistlberger, Higgs Boson gluon-fusion production in QCD at three loops. Phys. Rev. Lett. **114**, 212001 (2015). https://doi.org/10.1103/PhysRevLett.114.212001. arXiv:1503.06056 [hep-ph]
41. C. Anastasiou et al., High precision determination of the gluon fusion Higgs boson cross-section at the LHC. JHEP **05**, 058 (2016). https://doi.org/10.1007/JHEP05(2016)058. arXiv:1602.00695 [hep-ph]
42. F. Dulat, A. Lazopoulos, B. Mistlberger, iHixs 2-inclusive Higgs cross sections. Comput. Phys. Commun. **233**, 243 (2018). https://doi.org/10.1016/j.cpc.2018.06.025. arXiv:1802.00827 [hep-ph]
43. M. Bonetti, K. Melnikov, L. Tancredi, Higher order corrections to mixed QCD-EW contributions to Higgs boson production in gluon fusion. Phys. Rev. D **97**, 056017 (2018). https://doi.org/10.1103/PhysRevD.97.056017 (**Erratum**: Phys. Rev. D 97 (2018) 099906). arXiv:1801.10403 [hep-ph]
44. S. Forte, D. Napoletano, M. Ubiali, Higgs production in bottom-quark fusion in a matched scheme. Phys. Lett. B **751**, 331 (2015). https://doi.org/10.1016/j.physletb.2015.10.051. arXiv:1508.01529 [hep-ph]
45. S. Forte, D. Napoletano, M. Ubiali, Higgs production in bottom-quark fusion: matching beyond leading order. Phys. Lett. B **763**, 190 (2016). https://doi.org/10.1016/j.physletb.2016.10.040. arXiv:1607.00389 [hep-ph]
46. M. Bonvini, A.S. Papanastasiou, F.J. Tackmann, Resummation and matching of b-quark mass effects in $b\bar{b}H$ production. JHEP **11** (2015). https://doi.org/10.1007/jhep11(2015)196. arXiv:1508.03288 [hep-ph]
47. M. Bonvini, A.S. Papanastasiou, F.J. Tackmann, Matched predictions for the $b\bar{b}H$ cross section at the 13 TeV LHC. JHEP **10** (2016). https://doi.org/10.1007/jhep10(2016)053. arXiv:1605.01733 [hep-ph]
48. M. Ciccolini, A. Denner, S. Dittmaier, Strong and electroweak corrections to the production of a Higgs Boson + 2 Jets via weak interactions at the large hadron collider. Phys. Rev. Lett. **99**, 161803 (2007). https://doi.org/10.1103/PhysRevLett.99.161803. arXiv:0707.0381 [hep-ph]
49. M. Ciccolini, A. Denner, S. Dittmaier, Electroweak and QCD corrections to Higgs production via vector-boson fusion at the CERN LHC. Phys. Rev. D **77**, 013002 (2008). https://doi.org/10.1103/PhysRevD.77.013002. arXiv:0710.4749 [hep-ph]
50. P. Bolzoni, F. Maltoni, S.-O. Moch, M. Zaro, Higgs Boson production via vector-boson fusion at next-to-next-to-leading order in QCD. Phys. Rev. Lett. **105**, 011801 (2010). https://doi.org/10.1103/PhysRevLett.105.011801. arXiv:1003.4451 [hep-ph]
51. M.L. Ciccolini, S. Dittmaier, M. Krämer, Electroweak radiative corrections to associated WH and ZH production at hadron colliders. Phys. Rev. D **68**, 073003 (2003). https://doi.org/10.1103/PhysRevD.68.073003. arXiv:hep-ph/0306234
52. O. Brein, A. Djouadi, R. Harlander, NNLO QCD corrections to the Higgs-strahlung processes at hadron colliders. Phys. Lett. B **579**, 149 (2004). https://doi.org/10.1016/j.physletb.2003.10.112. arXiv:hep-ph/0307206
53. O. Brein, R.V. Harlander, M. Wiesemann, T. Zirke, Top-quark mediated effects in hadronic Higgs-Strahlung. Eur. Phys. J. C **72**, 1868 (2012). https://doi.org/10.1140/epjc/s10052-012-1868-6. arXiv:1111.0761 [hep-ph]
54. L. Altenkamp, S. Dittmaier, R.V. Harlander, H. Rzehak, T.J.E. Zirke, Gluon-induced Higgs-strahlung at next-to-leading order QCD. JHEP **02**, 078 (2013). https://doi.org/10.1007/JHEP02(2013)078. arXiv:1211.5015 [hep-ph]
55. A. Denner, S. Dittmaier, S. Kallweit, A. Mück, HAWK 2.0: A Monte Carlo program for Higgs production in vector-boson fusion and Higgs strahlung at hadron colliders. Comput. Phys. Commun. **195**, 161 (2015). https://doi.org/10.1016/j.cpc.2015.04.021. arXiv:1412.5390 [hep-ph]
56. O. Brein, R.V. Harlander, T.J.E. Zirke, vh@nnlo-Higgs Strahlung at hadron colliders. Comput. Phys. Commun. **184**, 998 (2013). https://doi.org/10.1016/j.cpc.2012.11.002. arXiv:1210.5347 [hep-ph]
57. R.V. Harlander, A. Kulesza, V. Theeuwes, T. Zirke, Soft gluon resummation for gluon-induced Higgs Strahlung. JHEP **11**, 082 (2014). https://doi.org/10.1007/JHEP11(2014)082. arXiv:1410.0217 [hep-ph]
58. R.V. Harlander, J. Klappert, S. Liebler, L. Simon, vh@nnlo-v2: new physics in Higgs Strahlung. JHEP **05**, 089 (2018). https://doi.org/10.1007/JHEP05(2018)089. arXiv:1802.04817 [hep-ph]
59. W. Beenakker et al., NLO QCD corrections to $t\bar{t}H$ production in hadron collisions. Nucl. Phys. B **653**, 151 (2003). https://doi.org/10.1016/S0550-3213(03)00044-0. arXiv:hep-ph/0211352
60. S. Dawson, C. Jackson, L.H. Orr, L. Reina, D. Wackeroth, Associated Higgs boson production with top quarks at the CERN Large Hadron Collider: NLO QCD corrections. Phys. Rev. D **68**, 034022 (2003). https://doi.org/10.1103/PhysRevD.68.034022. arXiv:hep-ph/0305087
61. Y. Zhang, W.-G. Ma, R.-Y. Zhang, C. Chen, L. Guo, QCD NLO and EW NLO corrections to $t\bar{t}H$ production with top quark decays at hadron collider. Phys. Lett. B **738**, 1 (2014). https://doi.org/10.1016/j.physletb.2014.09.022. arXiv:1407.1110 [hep-ph]
62. S. Frixione, V. Hirschi, D. Pagani, H.-S. Shao, M. Zaro, Electroweak and QCD corrections to top-pair hadroproduction in association with heavy bosons. JHEP **06**, 184 (2015). https://doi.org/10.1007/JHEP06(2015)184. arXiv:1504.03446 [hep-ph]
63. R. Ball et al., The PDF4LHC21 combination of global PDF fits for the LHC Run III. IOP Publ. **49**, 080501 (2022). https://doi.org/10.1088/1361-6471/ac7216. arXiv:2203.05506 [hep-ph]
64. T. Sjöstrand et al., An introduction to PYTHIA 8.2. Comput. Phys. Commun. **191**, 159 (2015). https://doi.org/10.1016/j.cpc.2015.01.024. arXiv:1410.3012 [hep-ph]
65. C. Bierlich et al., A comprehensive guide to the physics and usage of PYTHIA **8**, 3 (2022). arXiv:2203.11601 [hep-ph]

66. ATLAS Collaboration, ATLAS Pythia 8 tunes to 7 TeV data, ATL-PHYS-PUB-2014-021 (2014). https://cds.cern.ch/record/1966419
67. A. Bredenstein, A. Denner, S. Dittmaier, M.M. Weber, Precise predictions for the Higgs-boson decay $H \to WW/ZZ \to 4$ leptons. Phys. Rev. D **74**, 013004 (2006). https://doi.org/10.1103/PhysRevD.74.013004. arXiv:hep-ph/0604011
68. A. Bredenstein, A. Denner, S. Dittmaier, M.M. Weber, Precision calculations for the Higgs decays $H \to ZZ/WW \to 4$ leptons. Nucl. Phys. Proc. Suppl. **160**, 131 (2006). https://doi.org/10.1016/j.nuclphysbps.2006.09.104. arXiv:hep-ph/0607060
69. J. Alwall et al., The automated computation of tree-level and next-to-leading order differential cross sections, and their matching to parton shower simulations. JHEP **07**, 079 (2014). https://doi.org/10.1007/JHEP07(2014)079. arXiv:1405.0301 [hep-ph]
70. R.D. Ball et al., Parton distributions for the LHC run II. JHEP **04**, 040 (2015). https://doi.org/10.1007/JHEP04(2015)040. arXiv:1410.8849 [hep-ph]
71. R. Frederix, S. Frixione, Merging meets matching in MC@NLO. JHEP **12**, 061 (2012). https://doi.org/10.1007/JHEP12(2012)061. arXiv:1209.6215 [hep-ph]
72. T. Gleisberg et al., Event generation with SHERPA 1.1. JHEP **02**, 007 (2009). https://doi.org/10.1088/1126-6708/2009/02/007. arXiv:0811.4622 [hep-ph]
73. T. Gleisberg, S. Höche, Comix, a new matrix element generator. JHEP **12**, 039 (2008). https://doi.org/10.1088/1126-6708/2008/12/039. arXiv:0808.3674 [hep-ph]
74. F. Cascioli, P. Maierhöfer, S. Pozzorini, Scattering amplitudes with open loops. Phys. Rev. Lett. **108**, 111601 (2012). https://doi.org/10.1103/PhysRevLett.108.111601. arXiv:1111.5206 [hep-ph]
75. S. Schumann, F. Krauss, A parton shower algorithm based on Catani-Seymour dipole factorisation. JHEP **03**, 038 (2008). https://doi.org/10.1088/1126-6708/2008/03/038. arXiv:0709.1027 [hep-ph]
76. S. Höche, F. Krauss, M. Schönherr, F. Siegert, QCD matrix elements + parton showers. The NLO case. JHEP **04**, 027 (2013). https://doi.org/10.1007/JHEP04(2013)027. arXiv:1207.5030 [hep-ph]
77. F. Caola, K. Melnikov, R. Rontsch, L. Tancredi, QCD corrections to ZZ production in gluon fusion at the LHC. Phys. Rev. D **92**, 094028 (2015). https://doi.org/10.1103/PhysRevD.92.094028. arXiv:1509.06734 [hep-ph]
78. F. Caola, K. Melnikov, R. Röntsch, L. Tancredi, QCD corrections to W^+W^- production through gluon fusion. Phys. Lett. B **754**, 275 (2016). https://doi.org/10.1016/j.physletb.2016.01.046. arXiv:1511.08617 [hep-ph]
79. J.M. Campbell, R.K. Ellis, M. Czakon, S. Kirchner, Two loop correction to interference in $gg \to ZZ$. JHEP **08**, 011 (2016). https://doi.org/10.1007/JHEP08(2016)011. arXiv:1605.01380 [hep-ph]
80. K. Melnikov, M. Dowling, Production of two Z-bosons in gluon fusion in the heavy top quark approximation. Phys. Lett. B **744**, 43 (2015). https://doi.org/10.1016/j.physletb.2015.03.030. arXiv:1503.01274 [hep-ph]
81. M. Bonvini, F. Caola, S. Forte, K. Melnikov, G. Ridolfi, Signal-background interference effects for $gg \to H \to W^+W^-$ beyond leading order. Phys. Rev. D **88**, 034032 (2013). https://doi.org/10.1103/PhysRevD.88.034032. arXiv:1304.3053 [hep-ph]
82. C.S. Li, H.T. Li, D.Y. Shao, J. Wang, Soft gluon resummation in the signal-background interference process of gg($\to$ h*)$\to$ ZZ. JHEP **08**, 065 (2015). https://doi.org/10.1007/JHEP08(2015)065. arXiv:1504.02388 [hep-ph]
83. S. Frixione, G. Ridolfi, P. Nason, A positive-weight next-to-leading-order Monte Carlo for heavy flavour hadroproduction. JHEP **09**, 126 (2007). https://doi.org/10.1088/1126-6708/2007/09/126. arXiv:0707.3088 [hep-ph]
84. ATLAS Collaboration, Studies on top-quark Monte Carlo modelling for Top2016, ATL-PHYS-PUB-2016-020 (2016). https://cds.cern.ch/record/2216168
85. GEANT4 Collaboration, S. Agostinelli et al., GEANT4: a simulation toolkit. Nucl. Instrum. Methods A **506**, 250 (2003). https://doi.org/10.1016/S0168-9002(03)01368-8
86. ATLAS Collaboration, The ATLAS simulation infrastructure. Eur. Phys. J. C **70**, 823 (2010). https://doi.org/10.1140/epjc/s10052-010-1429-9. arXiv:1005.4568 [physics.ins-det]
87. ATLAS Collaboration, Emulating the impact of additional proton–proton interactions in the ATLAS simulation by presampling sets of inelastic Monte Carlo events. Comput. Softw. Big Sci **6**, 3 (2021). https://doi.org/10.1007/s41781-021-00062-2. arXiv:2102.09495 [hep-ex]
88. S. Porteboeuf, T. Pierog, K. Werner, Producing Hard Processes Regarding the Complete Event: the EPOS Event Generator, 45th Rencontres de Moriond on QCD and High Energy Interactions (Gioi Publishers, 2010), p. 135. arXiv:1006.2967 [hep-ph]
89. ATLAS Collaboration, The Pythia 8 A3 tune description of ATLAS minimum bias and inelastic measurements incorporating the Donnachie–Landshoff diffractive model, ATL-PHYS-PUB-2016-017 (2016). https://cds.cern.ch/record/2206965
90. R.D. Ball et al., Parton distributions with LHC data. Nucl. Phys. B **867**, 244 (2013). https://doi.org/10.1016/j.nuclphysb.2012.10.003. arXiv:1207.1303 [hep-ph]
91. ATLAS Collaboration, Electron and photon reconstruction and performance in ATLAS using a dynamical, topological cell clustering-based approach, ATL-PHYS-PUB-2017-022 (2017). https://cds.cern.ch/record/2298955
92. ATLAS Collaboration, Electron and photon performance measurements with the ATLAS detector using the 2015–2017 LHC proton–proton collision data. JINST **14**, P12006 (2019). https://doi.org/10.1088/1748-0221/14/12/P12006. arXiv:1908.00005 [hep-ex]
93. ATLAS Collaboration, Topological cell clustering in the ATLAS calorimeters and its performance in LHC Run 1. Eur. Phys. J. C **77**, 490 (2017). https://doi.org/10.1140/epjc/s10052-017-5004-5. arXiv:1603.02934 [hep-ex]
94. ATLAS Collaboration, Measurement of the photon identification efficiencies with the ATLAS detector using LHC Run-1 data. Eur. Phys. J. C **76**, 666 (2016). https://doi.org/10.1140/epjc/s10052-016-4507-9. arXiv:1606.01813 [hep-ex]
95. ATLAS Collaboration, Measurement of Higgs boson production in the diphoton decay channel in pp collisions at center-of-mass energies of 7 and 8 TeV with the ATLAS detector. Phys. Rev. D **90**, 112015 (2014). https://doi.org/10.1103/PhysRevD.90.112015. arXiv:1408.7084 [hep-ex]
96. ATLAS Collaboration, Measurement of the photon identification efficiencies with the ATLAS detector using LHC Run 2 data collected in 2015 and 2016. Eur. Phys. J. C **79**, 205 (2019). https://doi.org/10.1140/epjc/s10052-019-6650-6. arXiv:1810.05087 [hep-ex]
97. M. Cacciari, G.P. Salam, Pileup subtraction using jet areas. Phys. Lett. B **659**, 119 (2008). https://doi.org/10.1016/j.physletb.2007.09.077. arXiv:0707.1378 [hep-ph]
98. G. Cowan, K. Cranmer, E. Gross and O. Vitells, Asymptotic formulae for likelihood-based tests of new physics. Eur. Phys. J. C **71**, 1554 (2011). https://doi.org/10.1140/epjc/s10052-011-1554-0 (**Erratum: Eur. Phys. J. C 73 (2013) 2501**). arXiv:1007.1727 [physics.data-an]
99. ATLAS Collaboration, Measurements of Higgs boson properties in the diphoton decay channel with 36 fb^{-1} of pp collision data at $\sqrt{s} = 13$ TeV with the ATLAS detector. Phys. Rev. D **98**, 052005 (2018). https://doi.org/10.1103/PhysRevD.98.052005. arXiv:1802.04146 [hep-ex]

100. ATLAS Collaboration, Measurement of the isolated diphoton cross section in pp collisions at $\sqrt{s} = 7$ TeV with the ATLAS detector. Phys. Rev. D **85**, 012003 (2012). https://doi.org/10.1103/PhysRevD.85.012003. arXiv:1107.0581 [hep-ex]
101. A. Xu, S. Han, X. Ju, H. Wang, Generative machine learning for detector response modeling with a conditional normalizing flow (2023). arXiv:2303.10148 [hep-ex]
102. M. Germain, K. Gregor, I. Murray, H. Larochelle, MADE: masked autoencoder for distribution estimation, *Proceedings of the 32nd International Conference on Machine Learning*, vol. 37 (2015), p. 881. https://doi.org/10.48550/arXiv.1502.03509. arXiv:1502.03509 [cs.LG]
103. G. Papamakarios, T. Pavlakou, I. Murray, Masked autoregressive flow for density estimation (2017). arXiv:1705.07057 [cs.LG]
104. ATLAS Collaboration, Electron and photon energy calibration with the ATLAS detector using 2015–2016 LHC proton–proton collision data. JINST **14**, P03017 (2019). https://doi.org/10.1088/1748-0221/14/03/P03017. arXiv:1812.03848 [hep-ex]
105. ATLAS Collaboration, Performance of the ATLAS trigger system in 2015. Eur. Phys. J. C **77**, 317 (2017). https://doi.org/10.1140/epjc/s10052-017-4852-3. arXiv:1611.09661 [hep-ex]
106. ATLAS Collaboration, Measurement of the inelastic proton–proton cross section at $\sqrt{s} = 13$ TeV with the ATLAS detector at the LHC. Phys. Rev. Lett **117**, 182002 (2016). https://doi.org/10.1103/PhysRevLett.117.182002. arXiv:1606.02625 [hep-ex]
107. ATLAS Collaboration, A detailed map of Higgs boson interactions by the ATLAS experiment ten years after the discovery. Nature **607**, 52 (2022). https://doi.org/10.1038/s41586-022-04893-w. arXiv:2207.00092 [hep-ex]
108. ATLAS Collaboration, Measurement of the properties of Higgs boson production at $\sqrt{s} = 13$ TeV in the $H \to \gamma\gamma$ channel using 139 fb^{-1} of pp collision data with the ATLAS experiment (2022). arXiv:2207.00348 [hep-ex]
109. ATLAS Collaboration, Higgs boson production cross-section measurements and their EFT interpretation in the 4ℓ decay channel at $\sqrt{s} = 13$ TeV with the ATLAS detector. Eur. Phys. J. C **80**, 957 (2020). https://doi.org/10.1140/epjc/s10052-020-8227-9 (**Erratum: Eur. Phys. J. C 81 (2021) 29**). arXiv:2004.03447 [hep-ex]
110. ATLAS Collaboration, Improved electron reconstruction in ATLAS using the Gaussian Sum Filter-based model for bremsstrahlung, ATLAS-CONF-2012-047 (2012). https://cds.cern.ch/record/1449796
111. ATLAS Collaboration, Muon reconstruction performance of the ATLAS detector in proton–proton collision data at $\sqrt{s} = 13$ TeV. Eur. Phys. J. C **76**, 292 (2016). https://doi.org/10.1140/epjc/s10052-016-4120-y. arXiv:1603.05598 [hep-ex]
112. M. Pivk, F.R. Le Diberder, $_S$Plot: A statistical tool to unfold data distributions. Nucl. Instrum. Methods A **555**, 356 (2005). https://doi.org/10.1016/j.nima.2005.08.106. arXiv:physics/0402083
113. J. Bendavid et al., Les Houches 2017: physics at TeV Colliders Standard Model Working Group Report (2018). arXiv:1803.07977 [hep-ph]
114. ATLAS Collaboration, Test of CP-invariance of the Higgs boson in vector-boson fusion production and its decay into four leptons (2023). arXiv:2304.09612 [hep-ex]
115. J. Butterworth et al., PDF4LHC recommendations for LHC Run II. J. Phys. G **43**, 023001 (2016). https://doi.org/10.1088/0954-3899/43/2/023001. arXiv:1510.03865 [hep-ph]
116. ATLAS Collaboration, Measurement of the Higgs boson coupling properties in the $H \to ZZ^* \to 4\ell$ decay channel at $\sqrt{s} = 13$ TeV with the ATLAS detector. JHEP **03**, 095 (2018). https://doi.org/10.1007/JHEP03(2018)095. arXiv:1712.02304 [hep-ex]
117. A. Bredenstein, A. Denner, S. Dittmaier, M.M. Weber, Radiative corrections to the semileptonic and hadronic Higgs-boson decays $H \to WW/ZZ \to 4$ fermions. JHEP **02**, 080 (2007). https://doi.org/10.1088/1126-6708/2007/02/080. arXiv:hep-ph/0611234
118. ATLAS Collaboration, Combined measurement of differential and total cross sections in the $H \to \gamma\gamma$ and the $H \to ZZ^* \to 4\ell$ decay channels at $\sqrt{s} = 13$ TeV with the ATLAS detector. Phys. Lett. B **786**, 114 (2018). https://doi.org/10.1016/j.physletb.2018.09.019. arXiv:1805.10197 [hep-ex]
119. ATLAS Collaboration, Measurements of the total and differential Higgs Boson production cross sections combining the $H \to \gamma\gamma$ and $H \to ZZ^* \to 4\ell$ decay channels at $\sqrt{s} = 8$ TeV with the ATLAS detector. Phys. Rev. Lett **115**, 091801 (2015). https://doi.org/10.1103/PhysRevLett.115.091801. arXiv:1504.05833 [hep-ex]
120. ATLAS Collaboration, Measurement of the total and differential Higgs boson production cross-sections at $\sqrt{s} = 13$ TeV with the ATLAS detector by combining the $H \to ZZ^* \to 4\ell$ and $H \to \gamma\gamma$ decay channels. JHEP **05**, 028 (2023). https://doi.org/10.48550/arXiv.2207.08615. arXiv:2207.08615 [hep-ex]
121. ATLAS Collaboration, ATLAS Computing Acknowledgements, ATL-SOFT-PUB-2021-003 (2021). https://cds.cern.ch/record/2776662

ATLAS Collaboration[⋆]

G. Aad[102], B. Abbott[120], K. Abeling[55], N. J. Abicht[49], S. H. Abidi[29], A. Aboulhorma[35e], H. Abramowicz[151], H. Abreu[150], Y. Abulaiti[117], B. S. Acharya[69a,69b,m], C. Adam Bourdarios[4], L. Adamczyk[86a], L. Adamek[155], S. V. Addepalli[26], M. J. Addison[101], J. Adelman[115], A. Adiguzel[21c], T. Adye[134], A. A. Affolder[136], Y. Afik[36], M. N. Agaras[13], J. Agarwala[73a,73b], A. Aggarwal[100], C. Agheorghiesei[27c], A. Ahmad[36], F. Ahmadov[38,y], W. S. Ahmed[104], S. Ahuja[95], X. Ai[62a], G. Aielli[76a,76b], A. Aikot[163], M. Ait Tamlihat[35e], B. Aitbenchikh[35a], I. Aizenberg[169], M. Akbiyik[100], T. P. A. Åkesson[98], A. V. Akimov[37], D. Akiyama[168], N. N. Akolkar[24], K. Al Khoury[41], G. L. Alberghi[23b], J. Albert[165], P. Albicocco[53], G. L. Albouy[60], S. Alderweireldt[52], M. Aleksa[36], I. N. Aleksandrov[38], C. Alexa[27b], T. Alexopoulos[10], F. Alfonsi[23b], M. Algren[56], M. Alhroob[120], B. Ali[132], H. M. J. Ali[91], S. Ali[148], S. W. Alibocus[92], M. Aliev[145], G. Alimonti[71a], W. Alkakhi[55], C. Allaire[66], B. M. M. Allbrooke[146], J. F. Allen[52], C. A. Allendes Flores[137f], P. P. Allport[20], A. Aloisio[72a,72b], F. Alonso[90], C. Alpigiani[138], M. Alvarez Estevez[99], A. Alvarez Fernandez[100], M. Alves Cardoso[56], M. G. Alviggi[72a,72b], M. Aly[101], Y. Amaral Coutinho[83b], A. Ambler[104], C. Amelung[36], M. Amerl[101], C. G. Ames[109], D. Amidei[106], S. P. Amor Dos Santos[130a], K. R. Amos[163], V. Ananiev[125], C. Anastopoulos[139], T. Andeen[11], J. K. Anders[36], S. Y. Andrean[47a,47b], A. Andreazza[71a,71b], S. Angelidakis[9], A. Angerami[41,ab], A. V. Anisenkov[37], A. Annovi[74a], C. Antel[56], M. T. Anthony[139], E. Antipov[145], M. Antonelli[53], F. Anulli[75a], M. Aoki[84], T. Aoki[153], J. A. Aparisi Pozo[163], M. A. Aparo[146], L. Aperio Bella[48], C. Appelt[18], A. Apyan[26], N. Aranzabal[36], C. Arcangeletti[53], A. T. H. Arce[51], E. Arena[92], J.-F. Arguin[108], S. Argyropoulos[54], J.-H. Arling[48], O. Arnaez[4], H. Arnold[114], G. Artoni[75a,75b], H. Asada[111], K. Asai[118], S. Asai[153], N. A. Asbah[61], J. Assahsah[35d], K. Assamagan[29], R. Astalos[28a], S. Atashi[160], R. J. Atkin[33a], M. Atkinson[162], H. Atmani[35f], P. A. Atmasiddha[106], K. Augsten[132], S. Auricchio[72a,72b], A. D. Auriol[20], V. A. Austrup[101], G. Avolio[36], K. Axiotis[56], G. Azuelos[108,ag], D. Babal[28b], H. Bachacou[135], K. Bachas[152,p], A. Bachiu[34], F. Backman[47a,47b], A. Badea[61], P. Bagnaia[75a,75b], M. Bahmani[18], A. J. Bailey[163], V. R. Bailey[162], J. T. Baines[134], L. Baines[94], C. Bakalis[10], O. K. Baker[172], E. Bakos[15], D. Bakshi Gupta[8], V. Balakrishnan[120], R. Balasubramanian[114], E. M. Baldin[37], P. Balek[86a], E. Ballabene[23a,23b], F. Balli[135], L. M. Baltes[63a], W. K. Balunas[32], J. Balz[100], E. Banas[87], M. Bandieramonte[129], A. Bandyopadhyay[24], S. Bansal[24], L. Barak[151], M. Barakat[48], E. L. Barberio[105], D. Barberis[57a,57b], M. Barbero[102], M. Z. Barel[114], K. N. Barends[33a], T. Barillari[110], M.-S. Barisits[36], T. Barklow[143], P. Baron[122], D. A. Baron Moreno[101], A. Baroncelli[62a], G. Barone[29], A. J. Barr[126], J. D. Barr[96], L. Barranco Navarro[47a,47b], F. Barreiro[99], J. Barreiro Guimarães da Costa[14a], U. Barron[151], M. G. Barros Teixeira[130a], S. Barsov[37], F. Bartels[63a], R. Bartoldus[143], A. E. Barton[91], P. Bartos[28a], A. Basan[100], M. Baselga[49], A. Bassalat[66,b], M. J. Basso[156a], C. R. Basson[101], R. L. Bates[59], S. Batlamous[35e], J. R. Batley[32], B. Batool[141], M. Battaglia[136], D. Battulga[18], M. Bauce[75a,75b], M. Bauer[36], P. Bauer[24], L. T. Bazzano Hurrell[30], J. B. Beacham[51], T. Beau[127], P. H. Beauchemin[158], F. Becherer[54], P. Bechtle[24], H. P. Beck[19,o], K. Becker[167], A. J. Beddall[82], V. A. Bednyakov[38], C. P. Bee[145], L. J. Beemster[15], T. A. Beermann[36], M. Begalli[83d], M. Begel[29], A. Behera[145], J. K. Behr[48], J. F. Beirer[55], F. Beisiegel[24], M. Belfkir[159], G. Bella[151], L. Bellagamba[23b], A. Bellerive[34], P. Bellos[20], K. Beloborodov[37], D. Benchekroun[35a], F. Bendebba[35a], Y. Benhammou[151], M. Benoit[29], J. R. Bensinger[26], S. Bentvelsen[114], L. Beresford[48], M. Beretta[53], E. Bergeaas Kuutmann[161], N. Berger[4], B. Bergmann[132], J. Beringer[17a], G. Bernardi[5], C. Bernius[143], F. U. Bernlochner[24], F. Bernon[36,102], T. Berry[95], P. Berta[133], A. Berthold[50], I. A. Bertram[91], S. Bethke[110], A. Betti[75a,75b], A. J. Bevan[94], N. K. Bhalla[54], M. Bhamjee[33c], S. Bhatta[145], D. S. Bhattacharya[166], P. Bhattarai[143], V. S. Bhopatkar[121], R. Bi[29,aj], R. M. Bianchi[129], G. Bianco[23a,23b], O. Biebel[109], R. Bielski[123], M. Biglietti[77a], M. Bindi[55], A. Bingul[21b], C. Bini[75a,75b], A. Biondini[92], C. J. Birch-sykes[101], G. A. Bird[20,134], M. Birman[169], M. Biros[133], S. Biryukov[146], T. Bisanz[49], E. Bisceglie[43a,43b], J. P. Biswal[134], D. Biswas[141], A. Bitadze[101], K. Bjørke[125], I. Bloch[48], C. Blocker[26], A. Blue[59], U. Blumenschein[94], J. Blumenthal[100], G. J. Bobbink[114], V. S. Bobrovnikov[37], M. Boehler[54], B. Boehm[166], D. Bogavac[36], A. G. Bogdanchikov[37], C. Bohm[47a], V. Boisvert[95], P. Bokan[48], T. Bold[86a], M. Bomben[5], M. Bona[94], M. Boonekamp[135], C. D. Booth[95], A. G. Borbély[59], I. S. Bordulev[37], H. M. Borecka-Bielska[108], G. Borissov[91], D. Bortoletto[126], D. Boscherini[23b], M. Bosman[13], J. D. Bossio Sola[36], K. Bouaouda[35a], N. Bouchhar[163], J. Boudreau[129], E. V. Bouhova-Thacker[91], D. Boumediene[40], R. Bouquet[5], A. Boveia[119], J. Boyd[36], D. Boye[29], I. R. Boyko[38], J. Bracinik[20], N. Brahimi[62d], G. Brandt[171], O. Brandt[32], F. Braren[48], B. Brau[103],

J. E. Brau[123], R. Brener[169], L. Brenner[114], R. Brenner[161], S. Bressler[169], D. Britton[59], D. Britzger[110], I. Brock[24], G. Brooijmans[41], W. K. Brooks[137f], E. Brost[29], L. M. Brown[165], L. E. Bruce[61], T. L. Bruckler[126], P. A. Bruckman de Renstrom[87], B. Brüers[48], A. Bruni[23b], G. Bruni[23b], M. Bruschi[23b], N. Bruscino[75a,75b], T. Buanes[16], Q. Buat[138], D. Buchin[110], A. G. Buckley[59], O. Bulekov[37], B. A. Bullard[143], S. Burdin[92], C. D. Burgard[49], A. M. Burger[40], B. Burghgrave[8], O. Burlayenko[54], J. T. P. Burr[32], C. D. Burton[11], J. C. Burzynski[142], E. L. Busch[41], V. Büscher[100], P. J. Bussey[59], J. M. Butler[25], C. M. Buttar[59], J. M. Butterworth[96], W. Buttinger[134], C. J. Buxo Vazquez[107], A. R. Buzykaev[37], S. Cabrera Urbán[163], L. Cadamuro[66], D. Caforio[58], H. Cai[129], Y. Cai[14a,14e], V. M. M. Cairo[36], O. Cakir[3a], N. Calace[36], P. Calafiura[17a], G. Calderini[127], P. Calfayan[68], G. Callea[59], L. P. Caloba[83b], D. Calvet[40], S. Calvet[40], T. P. Calvet[102], M. Calvetti[74a,74b], R. Camacho Toro[127], S. Camarda[36], D. Camarero Munoz[26], P. Camarri[76a,76b], M. T. Camerlingo[72a,72b], D. Cameron[36], C. Camincher[165], M. Campanelli[96], A. Camplani[42], V. Canale[72a,72b], A. Canesse[104], J. Cantero[163], Y. Cao[162], F. Capocasa[26], M. Capua[43a,43b], A. Carbone[71a,71b], R. Cardarelli[76a], J. C. J. Cardenas[8], F. Cardillo[163], T. Carli[36], G. Carlino[72a], J. I. Carlotto[13], B. T. Carlson[129,q], E. M. Carlson[165,156a], L. Carminati[71a,71b], A. Carnelli[135], M. Carnesale[75a,75b], S. Caron[113], E. Carquin[137f], S. Carrá[71a,71b], G. Carratta[23a,23b], F. Carrio Argos[33g], J. W. S. Carter[155], T. M. Carter[52], M. P. Casado[13,i], M. Caspar[48], E. G. Castiglia[172], F. L. Castillo[4], L. Castillo Garcia[13], V. Castillo Gimenez[163], N. F. Castro[130a,130e], A. Catinaccio[36], J. R. Catmore[125], V. Cavaliere[29], N. Cavalli[23a,23b], V. Cavasinni[74a,74b], Y. C. Cekmecelioglu[48], E. Celebi[21a], F. Celli[126], M. S. Centonze[70a,70b], V. Cepaitis[56], K. Cerny[122], A. S. Cerqueira[83a], A. Cerri[146], L. Cerrito[76a,76b], F. Cerutti[17a], B. Cervato[141], A. Cervelli[23b], G. Cesarini[53], S. A. Cetin[82], Z. Chadi[35a], D. Chakraborty[115], J. Chan[170], W. Y. Chan[153], J. D. Chapman[32], E. Chapon[135], B. Chargeishvili[149b], D. G. Charlton[20], T. P. Charman[94], M. Chatterjee[19], C. Chauhan[133], S. Chekanov[6], S. V. Chekulaev[156a], G. A. Chelkov[38,a], A. Chen[106], B. Chen[151], B. Chen[165], H. Chen[14c], H. Chen[29], J. Chen[62c], J. Chen[142], M. Chen[126], S. Chen[153], S. J. Chen[14c], X. Chen[62c,135], X. Chen[14b,af], Y. Chen[62a], C. L. Cheng[170], H. C. Cheng[64a], S. Cheong[143], A. Cheplakov[38], E. Cheremushkina[48], E. Cherepanova[114], R. Cherkaoui El Moursli[35e], E. Cheu[7], K. Cheung[65], L. Chevalier[135], V. Chiarella[53], G. Chiarelli[74a], N. Chiedde[102], G. Chiodini[70a], A. S. Chisholm[20], A. Chitan[27b], M. Chitishvili[163], M. V. Chizhov[38], K. Choi[11], A. R. Chomont[75a,75b], Y. Chou[103], E. Y. S. Chow[114], T. Chowdhury[33g], K. L. Chu[169], M. C. Chu[64a], X. Chu[14a,14e], J. Chudoba[131], J. J. Chwastowski[87], D. Cieri[110], K. M. Ciesla[86a], V. Cindro[93], A. Ciocio[17a], F. Cirotto[72a,72b], Z. H. Citron[169,k], M. Citterio[71a], D. A. Ciubotaru[27b], B. M. Ciungu[155], A. Clark[56], P. J. Clark[52], J. M. Clavijo Columbie[48], S. E. Clawson[48], C. Clement[47a,47b], J. Clercx[48], L. Clissa[23a,23b], Y. Coadou[102], M. Cobal[69a,69c], A. Coccaro[57b], R. F. Coelho Barrue[130a], R. Coelho Lopes De Sa[103], S. Coelli[71a], H. Cohen[151], A. E. C. Coimbra[71a,71b], B. Cole[41], J. Collot[60], P. Conde Muiño[130a,130g], M. P. Connell[33c], S. H. Connell[33c], I. A. Connelly[59], E. I. Conroy[126], F. Conventi[72a,ah], H. G. Cooke[20], A. M. Cooper-Sarkar[126], A. Cordeiro Oudot Choi[127], F. Cormier[164], L. D. Corpe[40], M. Corradi[75a,75b], F. Corriveau[104,w], A. Cortes-Gonzalez[18], M. J. Costa[163], F. Costanza[4], D. Costanzo[139], B. M. Cote[119], G. Cowan[95], K. Cranmer[170], D. Cremonini[23a,23b], S. Crépé-Renaudin[60], F. Crescioli[127], M. Cristinziani[141], M. Cristoforetti[78a,78b], V. Croft[114], J. E. Crosby[121], G. Crosetti[43a,43b], A. Cueto[99], T. Cuhadar Donszelmann[160], H. Cui[14a,14e], Z. Cui[7], W. R. Cunningham[59], F. Curcio[43a,43b], P. Czodrowski[36], M. M. Czurylo[63b], M. J. Da Cunha Sargedas De Sousa[57a,57b], J. V. Da Fonseca Pinto[83b], C. Da Via[101], W. Dabrowski[86a], T. Dado[49], S. Dahbi[33g], T. Dai[106], D. Dal Santo[19], C. Dallapiccola[103], M. Dam[42], G. D'amen[29], V. D'Amico[109], J. Damp[100], J. R. Dandoy[128], M. F. Daneri[30], M. Danninger[142], V. Dao[36], G. Darbo[57b], S. Darmora[6], S. J. Das[29,aj], S. D'Auria[71a,71b], C. David[156b], T. Davidek[133], B. Davis-Purcell[34], I. Dawson[94], H. A. Day-hall[132], K. De[8], R. De Asmundis[72a], N. De Biase[48], S. De Castro[23a,23b], N. De Groot[113], P. de Jong[114], H. De la Torre[115], A. De Maria[14c], A. De Salvo[75a], U. De Sanctis[76a,76b], A. De Santo[146], J. B. De Vivie De Regie[60], D. V. Dedovich[38], J. Degens[114], A. M. Deiana[44], F. Del Corso[23a,23b], J. Del Peso[99], F. Del Rio[63a], F. Deliot[135], C. M. Delitzsch[49], M. Della Pietra[72a,72b], D. Della Volpe[56], A. Dell'Acqua[36], L. Dell'Asta[71a,71b], M. Delmastro[4], P. A. Delsart[60], S. Demers[172], M. Demichev[38], S. P. Denisov[37], L. D'Eramo[40], D. Derendarz[87], F. Derue[127], P. Dervan[92], K. Desch[24], C. Deutsch[24], F. A. Di Bello[57a,57b], A. Di Ciaccio[76a,76b], L. Di Ciaccio[4], A. Di Domenico[75a,75b], C. Di Donato[72a,72b], A. Di Girolamo[36], G. Di Gregorio[36], A. Di Luca[78a,78b], B. Di Micco[77a,77b], R. Di Nardo[77a,77b], C. Diaconu[102], M. Diamantopoulou[34], F. A. Dias[114], T. Dias Do Vale[142], M. A. Diaz[137a,137b], F. G. Diaz Capriles[24], M. Didenko[163], E. B. Diehl[106], L. Diehl[54], S. Díez Cornell[48], C. Diez Pardos[141], C. Dimitriadi[24,161], A. Dimitrievska[17a], J. Dingfelder[24],

I.-M. Dinu[27b], S. J. Dittmeier[63b], F. Dittus[36], F. Djama[102], T. Djobava[149b], J. I. Djuvsland[16], C. Doglioni[98,101], A. Dohnalova[28a], J. Dolejsi[133], Z. Dolezal[133], K. M. Dona[39], M. Donadelli[83c], B. Dong[107], J. Donini[40], A. D'Onofrio[77a,77b], M. D'Onofrio[92], J. Dopke[134], A. Doria[72a], N. Dos Santos Fernandes[130a], P. Dougan[101], M. T. Dova[90], A. T. Doyle[59], M. A. Draguet[126], E. Dreyer[169], I. Drivas-koulouris[10], M. Drnevich[117], A. S. Drobac[158], M. Drozdova[56], D. Du[62a], T. A. du Pree[114], F. Dubinin[37], M. Dubovsky[28a], E. Duchovni[169], G. Duckeck[109], O. A. Ducu[27b], D. Duda[52], A. Dudarev[36], E. R. Duden[26], M. D'uffizi[101], L. Duflot[66], M. Dührssen[36], C. Dülsen[171], A. E. Dumitriu[27b], M. Dunford[63a], S. Dungs[49], K. Dunne[47a,47b], A. Duperrin[102], H. Duran Yildiz[3a], M. Düren[58], A. Durglishvili[149b], B. L. Dwyer[115], G. I. Dyckes[17a], M. Dyndal[86a], S. Dysch[101], B. S. Dziedzic[87], Z. O. Earnshaw[146], G. H. Eberwein[126], B. Eckerova[28a], S. Eggebrecht[55], E. Egidio Purcino De Souza[127], L. F. Ehrke[56], G. Eigen[16], K. Einsweiler[17a], T. Ekelof[161], P. A. Ekman[98], S. El Farkh[35b], Y. El Ghazali[35b], H. El Jarrari[35e,148], A. El Moussaouy[108], V. Ellajosyula[161], M. Ellert[161], F. Ellinghaus[171], A. A. Elliot[94], N. Ellis[36], J. Elmsheuser[29], M. Elsing[36], D. Emeliyanov[134], Y. Enari[153], I. Ene[17a], S. Epari[13], J. Erdmann[49], P. A. Erland[87], M. Errenst[171], M. Escalier[66], C. Escobar[163], E. Etzion[151], G. Evans[130a], H. Evans[68], L. S. Evans[95], M. O. Evans[146], A. Ezhilov[37], S. Ezzarqtouni[35a], F. Fabbri[59], L. Fabbri[23a,23b], G. Facini[96], V. Fadeyev[136], R. M. Fakhrutdinov[37], S. Falciano[75a], L. F. Falda Ulhoa Coelho[36], P. J. Falke[24], J. Faltova[133], C. Fan[162], Y. Fan[14a], Y. Fang[14a,14e], M. Fanti[71a,71b], M. Faraj[69a,69b], Z. Farazpay[97], A. Farbin[8], A. Farilla[77a], T. Farooque[107], S. M. Farrington[52], F. Fassi[35e], D. Fassouliotis[9], M. Faucci Giannelli[76a,76b], W. J. Fawcett[32], L. Fayard[66], P. Federic[133], P. Federicova[131], O. L. Fedin[37,a], G. Fedotov[37], M. Feickert[170], L. Feligioni[102], D. E. Fellers[123], C. Feng[62b], M. Feng[14b], Z. Feng[114], M. J. Fenton[160], A. B. Fenyuk[37], L. Ferencz[48], R. A. M. Ferguson[91], S. I. Fernandez Luengo[137f], P. Fernandez Martinez[13], M. J. V. Fernoux[102], J. Ferrando[48], A. Ferrari[161], P. Ferrari[113,114], R. Ferrari[73a], D. Ferrere[56], C. Ferretti[106], F. Fiedler[100], P. Fiedler[132], A. Filipčič[93], E. K. Filmer[1], F. Filthaut[113], M. C. N. Fiolhais[130a,130c,c], L. Fiorini[163], W. C. Fisher[107], T. Fitschen[101], P. M. Fitzhugh[135], I. Fleck[141], P. Fleischmann[106], T. Flick[171], M. Flores[33d,ac], L. R. Flores Castillo[64a], L. Flores Sanz De Acedo[36], F. M. Follega[78a,78b], N. Fomin[16], J. H. Foo[155], B. C. Forland[68], A. Formica[135], A. C. Forti[101], E. Fortin[36], A. W. Fortman[61], M. G. Foti[17a], L. Fountas[9,j], D. Fournier[66], H. Fox[91], P. Francavilla[74a,74b], S. Francescato[61], S. Franchellucci[56], M. Franchini[23a,23b], S. Franchino[63a], D. Francis[36], L. Franco[113], V. Franco Lima[36], L. Franconi[48], M. Franklin[61], G. Frattari[26], A. C. Freegard[94], W. S. Freund[83b], Y. Y. Frid[151], J. Friend[59], N. Fritzsche[50], A. Froch[54], D. Froidevaux[36], J. A. Frost[126], Y. Fu[62a], M. Fujimoto[118,ad], E. Fullana Torregrosa[163,*], K. Y. Fung[64a], E. Furtado De Simas Filho[83b], M. Furukawa[153], J. Fuster[163], A. Gabrielli[23a,23b], A. Gabrielli[155], P. Gadow[36], G. Gagliardi[57a,57b], L. G. Gagnon[17a], E. J. Gallas[126], B. J. Gallop[134], K. K. Gan[119], S. Ganguly[153], J. Gao[62a], Y. Gao[52], F. M. Garay Walls[137a,137b], B. Garcia[29,aj], C. García[163], A. Garcia Alonso[114], A. G. Garcia Caffaro[172], J. E. García Navarro[163], M. Garcia-Sciveres[17a], G. L. Gardner[128], R. W. Gardner[39], N. Garelli[158], D. Garg[80], R. B. Garg[143,n], J. M. Gargan[52], C. A. Garner[155], C. M. Garvey[33a], S. J. Gasiorowski[138], P. Gaspar[83b], G. Gaudio[73a], V. Gautam[13], P. Gauzzi[75a,75b], I. L. Gavrilenko[37], A. Gavrilyuk[37], C. Gay[164], G. Gaycken[48], E. N. Gazis[10], A. A. Geanta[27b], C. M. Gee[136], C. Gemme[57b], M. H. Genest[60], S. Gentile[75a,75b], A. D. Gentry[112], S. George[95], W. F. George[20], T. Geralis[46], P. Gessinger-Befurt[36], M. E. Geyik[171], M. Ghani[167], M. Ghneimat[141], K. Ghorbanian[94], A. Ghosal[141], A. Ghosh[160], A. Ghosh[7], B. Giacobbe[23b], S. Giagu[75a,75b], T. Giani[114], P. Giannetti[74a], A. Giannini[62a], S. M. Gibson[95], M. Gignac[136], D. T. Gil[86b], A. K. Gilbert[86a], B. J. Gilbert[41], D. Gillberg[34], G. Gilles[114], N. E. K. Gillwald[48], L. Ginabat[127], D. M. Gingrich[2,ag], M. P. Giordani[69a,69c], P. F. Giraud[135], G. Giugliarelli[69a,69c], D. Giugni[71a], F. Giuli[36], I. Gkialas[9,j], L. K. Gladilin[37], C. Glasman[99], G. R. Gledhill[123], G. Glemža[48], M. Glisic[123], I. Gnesi[43b,f], Y. Go[29,aj], M. Goblirsch-Kolb[36], B. Gocke[49], D. Godin[108], B. Gokturk[21a], S. Goldfarb[105], T. Golling[56], M. G. D. Gololo[33g], D. Golubkov[37], J. P. Gombas[107], A. Gomes[130a,130b], G. Gomes Da Silva[141], A. J. Gomez Delegido[163], R. Gonçalo[130a,130c], G. Gonella[123], L. Gonella[20], A. Gongadze[149c], F. Gonnella[20], J. L. Gonski[41], R. Y. González Andana[52], S. González de la Hoz[163], S. Gonzalez Fernandez[13], R. Gonzalez Lopez[92], C. Gonzalez Renteria[17a], M. V. Gonzalez Rodrigues[48], R. Gonzalez Suarez[161], S. Gonzalez-Sevilla[56], G. R. Gonzalvo Rodriguez[163], L. Goossens[36], B. Gorini[36], E. Gorini[70a,70b], A. Gorišek[93], T. C. Gosart[128], A. T. Goshaw[51], M. I. Gostkin[38], S. Goswami[121], C. A. Gottardo[36], S. A. Gotz[109], M. Gouighri[35b], V. Goumarre[48], A. G. Goussiou[138], N. Govender[33c], I. Grabowska-Bold[86a], K. Graham[34], E. Gramstad[125], S. Grancagnolo[70a,70b], M. Grandi[146], C. M. Grant[1,135],

P. M. Gravila[27f], F. G. Gravili[70a,70b], H. M. Gray[17a], M. Greco[70a,70b], C. Grefe[24], I. M. Gregor[48], P. Grenier[143], S. G. Grewe[110], C. Grieco[13], A. A. Grillo[136], K. Grimm[31], S. Grinstein[13,s], J.-F. Grivaz[66], E. Gross[169], J. Grosse-Knetter[55], C. Grud[106], J. C. Grundy[126], L. Guan[106], W. Guan[29], C. Gubbels[164], J. G. R. Guerrero Rojas[163], G. Guerrieri[69a,69c], F. Guescini[110], R. Gugel[100], J. A. M. Guhit[106], A. Guida[18], T. Guillemin[4], E. Guilloton[167,134], S. Guindon[36], F. Guo[14a,14e], J. Guo[62c], L. Guo[48], Y. Guo[106], R. Gupta[48], S. Gurbuz[24], S. S. Gurdasani[54], G. Gustavino[36], M. Guth[56], P. Gutierrez[120], L. F. Gutierrez Zagazeta[128], C. Gutschow[96], C. Gwenlan[126], C. B. Gwilliam[92], E. S. Haaland[125], A. Haas[117], M. Habedank[48], C. Haber[17a], H. K. Hadavand[8], A. Hadef[100], S. Hadzic[110], J. J. Hahn[141], E. H. Haines[96], M. Haleem[166], J. Haley[121], J. J. Hall[139], G. D. Hallewell[102], L. Halser[19], K. Hamano[165], M. Hamer[24], G. N. Hamity[52], E. J. Hampshire[95], J. Han[62b], K. Han[62a], L. Han[14c], L. Han[62a], S. Han[17a], Y. F. Han[155], K. Hanagaki[84], M. Hance[136], D. A. Hangal[41,ab], H. Hanif[142], M. D. Hank[128], R. Hankache[101], J. B. Hansen[42], J. D. Hansen[42], P. H. Hansen[42], K. Hara[157], D. Harada[56], T. Harenberg[171], S. Harkusha[37], M. L. Harris[103], Y. T. Harris[126], J. Harrison[13], N. M. Harrison[119], P. F. Harrison[167], N. M. Hartman[110], N. M. Hartmann[109], Y. Hasegawa[140], R. Hauser[107], C. M. Hawkes[20], R. J. Hawkings[36], Y. Hayashi[153], S. Hayashida[111], D. Hayden[107], C. Hayes[106], R. L. Hayes[114], C. P. Hays[126], J. M. Hays[94], H. S. Hayward[92], F. He[62a], M. He[14a,14e], Y. He[154], Y. He[48], N. B. Heatley[94], V. Hedberg[98], A. L. Heggelund[125], N. D. Hehir[94], C. Heidegger[54], K. K. Heidegger[54], W. D. Heidorn[81], J. Heilman[34], S. Heim[48], T. Heim[17a], J. G. Heinlein[128], J. J. Heinrich[123], L. Heinrich[110,ae], J. Hejbal[131], L. Helary[48], A. Held[170], S. Hellesund[16], C. M. Helling[164], S. Hellman[47a,47b], R. C. W. Henderson[91], L. Henkelmann[32], A. M. Henriques Correia[36], H. Herde[98], Y. Hernández Jiménez[145], L. M. Herrmann[24], T. Herrmann[50], G. Herten[54], R. Hertenberger[109], L. Hervas[36], M. E. Hesping[100], N. P. Hessey[156a], H. Hibi[85], E. Hill[155], S. J. Hillier[20], J. R. Hinds[107], F. Hinterkeuser[24], M. Hirose[124], S. Hirose[157], D. Hirschbuehl[171], T. G. Hitchings[101], B. Hiti[93], J. Hobbs[145], R. Hobincu[27e], N. Hod[169], M. C. Hodgkinson[139], B. H. Hodkinson[32], A. Hoecker[36], J. Hofer[48], T. Holm[24], M. Holzbock[110], L. B. A. H. Hommels[32], B. P. Honan[101], J. Hong[62c], T. M. Hong[129], B. H. Hooberman[162], W. H. Hopkins[6], Y. Horii[111], S. Hou[148], A. S. Howard[93], J. Howarth[59], J. Hoya[6], M. Hrabovsky[122], A. Hrynevich[48], T. Hryn'ova[4], P. J. Hsu[65], S.-C. Hsu[138], Q. Hu[62a], Y. F. Hu[14a,14e], S. Huang[64b], X. Huang[14c], Y. Huang[139], Y. Huang[14a], Z. Huang[101], Z. Hubacek[132], M. Huebner[24], F. Huegging[24], T. B. Huffman[126], C. A. Hugli[48], M. Huhtinen[36], S. K. Huiberts[16], R. Hulsken[104], N. Huseynov[12,a], J. Huston[107], J. Huth[61], R. Hyneman[143], G. Iacobucci[56], G. Iakovidis[29], I. Ibragimov[141], L. Iconomidou-Fayard[66], P. Iengo[72a,72b], R. Iguchi[153], T. Iizawa[126], Y. Ikegami[84], N. Ilic[155], H. Imam[35a], M. Ince Lezki[56], T. Ingebretsen Carlson[47a,47b], G. Introzzi[73a,73b], M. Iodice[77a], V. Ippolito[75a,75b], R. K. Irwin[92], M. Ishino[153], W. Islam[170], C. Issever[18,48], S. Istin[21a,al], H. Ito[168], J. M. Iturbe Ponce[64a], R. Iuppa[78a,78b], A. Ivina[169], J. M. Izen[45], V. Izzo[72a], P. Jacka[131,132], P. Jackson[1], R. M. Jacobs[48], B. P. Jaeger[142], C. S. Jagfeld[109], G. Jain[156a], P. Jain[54], G. Jäkel[171], K. Jakobs[54], T. Jakoubek[169], J. Jamieson[59], K. W. Janas[86a], M. Javurkova[103], F. Jeanneau[135], L. Jeanty[123], J. Jejelava[149a,z], P. Jenni[54,g], C. E. Jessiman[34], S. Jézéquel[4], C. Jia[62b], J. Jia[145], X. Jia[61], X. Jia[14a,14e], Z. Jia[14c], Y. Jiang[62a], S. Jiggins[48], J. Jimenez Pena[13], S. Jin[14c], A. Jinaru[27b], O. Jinnouchi[154], P. Johansson[139], K. A. Johns[7], J. W. Johnson[136], D. M. Jones[32], E. Jones[48], P. Jones[32], R. W. L. Jones[91], T. J. Jones[92], H. L. Joos[36,55], R. Joshi[119], J. Jovicevic[15], X. Ju[17a], J. J. Junggeburth[103], T. Junkermann[63a], A. Juste Rozas[13,s], M. K. Juzek[87], S. Kabana[137e], A. Kaczmarska[87], M. Kado[110], H. Kagan[119], M. Kagan[143], A. Kahn[41], A. Kahn[128], C. Kahra[100], T. Kaji[153], E. Kajomovitz[150], N. Kakati[169], I. Kalaitzidou[54], C. W. Kalderon[29], A. Kamenshchikov[155], N. J. Kang[136], D. Kar[33g], K. Karava[126], M. J. Kareem[156b], E. Karentzos[54], I. Karkanias[152], O. Karkout[114], S. N. Karpov[38], Z. M. Karpova[38], V. Kartvelishvili[91], A. N. Karyukhin[37], E. Kasimi[152], J. Katzy[48], S. Kaur[34], K. Kawade[140], M. P. Kawale[120], C. Kawamoto[88], T. Kawamoto[135], E. F. Kay[36], F. I. Kaya[158], S. Kazakos[107], V. F. Kazanin[37], Y. Ke[145], J. M. Keaveney[33a], R. Keeler[165], G. V. Kehris[61], J. S. Keller[34], A. S. Kelly[96], J. J. Kempster[146], K. E. Kennedy[41], P. D. Kennedy[100], O. Kepka[131], B. P. Kerridge[167], S. Kersten[171], B. P. Kerševan[93], S. Keshri[66], L. Keszeghova[28a], S. Ketabchi Haghighat[155], M. Khandoga[127], A. Khanov[121], A. G. Kharlamov[37], T. Kharlamova[37], E. E. Khoda[138], M. Kholodenko[37], T. J. Khoo[18], G. Khoriauli[166], J. Khubua[149b], Y. A. R. Khwaira[66], A. Kilgallon[123], D. W. Kim[47a,47b], Y. K. Kim[39], N. Kimura[96], M. K. Kingston[55], A. Kirchhoff[55], C. Kirfel[24], F. Kirfel[24], J. Kirk[134], A. E. Kiryunin[110], C. Kitsaki[10], O. Kivernyk[24], M. Klassen[63a], C. Klein[34], L. Klein[166], M. H. Klein[106], M. Klein[92], S. B. Klein[56], U. Klein[92], P. Klimek[36], A. Klimentov[29], T. Klioutchnikova[36], P. Kluit[114], S. Kluth[110], E. Kneringer[79], T. M. Knight[155], A. Knue[49], R. Kobayashi[88],

D. Kobylianskii[169], S. F. Koch[126], M. Kocian[143], P. Kodyš[133], D. M. Koeck[123], P. T. Koenig[24], T. Koffas[34], M. Kolb[135], I. Koletsou[4], T. Komarek[122], K. Köneke[54], A. X. Y. Kong[1], T. Kono[118], N. Konstantinidis[96], B. Konya[98], R. Kopeliansky[68], S. Koperny[86a], K. Korcyl[87], K. Kordas[152,e], G. Koren[151], A. Korn[96], S. Korn[55], I. Korolkov[13], N. Korotkova[37], B. Kortman[114], O. Kortner[110], S. Kortner[110], W. H. Kostecka[115], V. V. Kostyukhin[141], A. Kotsokechagia[135], A. Kotwal[51], A. Koulouris[36], A. Kourkoumeli-Charalampidi[73a,73b], C. Kourkoumelis[9], E. Kourlitis[110,ae], O. Kovanda[146], R. Kowalewski[165], W. Kozanecki[135], A. S. Kozhin[37], V. A. Kramarenko[37], G. Kramberger[93], P. Kramer[100], M. W. Krasny[127], A. Krasznahorkay[36], J. W. Kraus[171], J. A. Kremer[48], T. Kresse[50], J. Kretzschmar[92], K. Kreul[18], P. Krieger[155], S. Krishnamurthy[103], M. Krivos[133], K. Krizka[20], K. Kroeninger[49], H. Kroha[110], J. Kroll[131], J. Kroll[128], K. S. Krowpman[107], U. Kruchonak[38], H. Krüger[24], N. Krumnack[81], M. C. Kruse[51], J. A. Krzysiak[87], O. Kuchinskaia[37], S. Kuday[3a], S. Kuehn[36], R. Kuesters[54], T. Kuhl[48], V. Kukhtin[38], Y. Kulchitsky[37,a], S. Kuleshov[137b,137d], M. Kumar[33g], N. Kumari[48], A. Kupco[131], T. Kupfer[49], A. Kupich[37], O. Kuprash[54], H. Kurashige[85], L. L. Kurchaninov[156a], O. Kurdysh[66], Y. A. Kurochkin[37], A. Kurova[37], M. Kuze[154], A. K. Kvam[103], J. Kvita[122], T. Kwan[104], N. G. Kyriacou[106], L. A. O. Laatu[102], C. Lacasta[163], F. Lacava[75a,75b], H. Lacker[18], D. Lacour[127], N. N. Lad[96], E. Ladygin[38], B. Laforge[127], T. Lagouri[137e], F. Z. Lahbabi[35a], S. Lai[55], I. K. Lakomiec[86a], N. Lalloue[60], J. E. Lambert[165], S. Lammers[68], W. Lampl[7], C. Lampoudis[152,e], A. N. Lancaster[115], E. Lançon[29], U. Landgraf[54], M. P. J. Landon[94], V. S. Lang[54], R. J. Langenberg[103], O. K. B. Langrekken[125], A. J. Lankford[160], F. Lanni[36], K. Lantzsch[24], A. Lanza[73a], A. Lapertosa[57a,57b], J. F. Laporte[135], T. Lari[71a], F. Lasagni Manghi[23b], M. Lassnig[36], V. Latonova[131], A. Laudrain[100], A. Laurier[150], S. D. Lawlor[139], Z. Lawrence[101], M. Lazzaroni[71a,71b], B. Le[101], E. M. Le Boulicaut[51], B. Leban[93], A. Lebedev[81], M. LeBlanc[101], F. Ledroit-Guillon[60], A. C. A. Lee[96], S. C. Lee[148], S. Lee[47a,47b], T. F. Lee[92], L. L. Leeuw[33c], H. P. Lefebvre[95], M. Lefebvre[165], C. Leggett[17a], G. Lehmann Miotto[36], M. Leigh[56], W. A. Leight[103], W. Leinonen[113], A. Leisos[152,r], M. A. L. Leite[83c], C. E. Leitgeb[48], R. Leitner[133], K. J. C. Leney[44], T. Lenz[24], S. Leone[74a], C. Leonidopoulos[52], A. Leopold[144], C. Leroy[108], R. Les[107], C. G. Lester[32], M. Levchenko[37], J. Levêque[4], D. Levin[106], L. J. Levinson[169], M. P. Lewicki[87], D. J. Lewis[4], A. Li[5], B. Li[62b], C. Li[62a], C.-Q. Li[62c], H. Li[62a], H. Li[62b], H. Li[14c], H. Li[14b], H. Li[62b], K. Li[138], L. Li[62c], M. Li[14a,14e], Q. Y. Li[62a], S. Li[14a,14e], S. Li[62c,62d,d], T. Li[5], X. Li[104], Z. Li[126], Z. Li[104], Z. Li[92], Z. Li[14a,14e], S. Liang[14a,14e], Z. Liang[14a], M. Liberatore[135], B. Liberti[76a], K. Lie[64c], J. Lieber Marin[83b], H. Lien[68], K. Lin[107], R. E. Lindley[7], J. H. Lindon[2], E. Lipeles[128], A. Lipniacka[16], A. Lister[164], J. D. Little[4], B. Liu[14a], B. X. Liu[142], D. Liu[62c,62d], J. B. Liu[62a], J. K. K. Liu[32], K. Liu[62c,62d], M. Liu[62a], M. Y. Liu[62a], P. Liu[14a], Q. Liu[62c,62d,138], X. Liu[62a], Y. Liu[14d,14e], Y. L. Liu[62b], Y. W. Liu[62a], J. Llorente Merino[142], S. L. Lloyd[94], E. M. Lobodzinska[48], P. Loch[7], S. Loffredo[76a,76b], T. Lohse[18], K. Lohwasser[139], E. Loiacono[48], M. Lokajicek[131,*], J. D. Lomas[20], J. D. Long[162], I. Longarini[160], L. Longo[70a,70b], R. Longo[162], I. Lopez Paz[67], A. Lopez Solis[48], J. Lorenz[109], N. Lorenzo Martinez[4], A. M. Lory[109], G. Löschcke Centeno[146], O. Loseva[37], X. Lou[47a,47b], X. Lou[14a,14e], A. Lounis[66], J. Love[6], P. A. Love[91], G. Lu[14a,14e], M. Lu[80], S. Lu[128], Y. J. Lu[65], H. J. Lubatti[138], C. Luci[75a,75b], F. L. Lucio Alves[14c], A. Lucotte[60], F. Luehring[68], I. Luise[145], O. Lukianchuk[66], O. Lundberg[144], B. Lund-Jensen[144], N. A. Luongo[123], M. S. Lutz[151], A. B. Lux[25], D. Lynn[29], H. Lyons[92], R. Lysak[131], E. Lytken[98], V. Lyubushkin[38], T. Lyubushkina[38], M. M. Lyukova[145], H. Ma[29], K. Ma[62a], L. L. Ma[62b], Y. Ma[121], D. M. Mac Donell[165], G. Maccarrone[53], J. C. MacDonald[100], P. C. Machado De Abreu Farias[83b], R. Madar[40], W. F. Mader[50], T. Madula[96], J. Maeda[85], T. Maeno[29], H. Maguire[139], V. Maiboroda[135], A. Maio[130a,130b,130d], K. Maj[86a], O. Majersky[48], S. Majewski[123], N. Makovec[66], V. Maksimovic[15], B. Malaescu[127], Pa. Malecki[87], V. P. Maleev[37], F. Malek[60], M. Mali[93], D. Malito[95], U. Mallik[80], S. Maltezos[10], S. Malyukov[38], J. Mamuzic[13], G. Mancini[53], G. Manco[73a,73b], J. P. Mandalia[94], I. Mandić[93], L. Manhaes de Andrade Filho[83a], I. M. Maniatis[169], J. Manjarres Ramos[102,aa], D. C. Mankad[169], A. Mann[109], B. Mansoulie[135], S. Manzoni[36], A. Marantis[152,r], G. Marchiori[5], M. Marcisovsky[131], C. Marcon[71a,71b], M. Marinescu[20], M. Marjanovic[120], E. J. Marshall[91], Z. Marshall[17a], S. Marti-Garcia[163], T. A. Martin[167], V. J. Martin[52], B. Martin dit Latour[16], L. Martinelli[75a,75b], M. Martinez[13,s], P. Martinez Agullo[163], V. I. Martinez Outschoorn[103], P. Martinez Suarez[13], S. Martin-Haugh[134], V. S. Martoiu[27b], A. C. Martyniuk[96], A. Marzin[36], D. Mascione[78a,78b], L. Masetti[100], T. Mashimo[153], J. Masik[101], A. L. Maslennikov[37], L. Massa[23b], P. Massarotti[72a,72b], P. Mastrandrea[74a,74b], A. Mastroberardino[43a,43b], T. Masubuchi[153], T. Mathisen[161], J. Matousek[133], N. Matsuzawa[153], J. Maurer[27b], B. Maček[93], D. A. Maximov[37], R. Mazini[148], I. Maznas[152], M. Mazza[107], S. M. Mazza[136], E. Mazzeo[71a,71b], C. Mc Ginn[29],

J. P. Mc Gowan[104], S. P. Mc Kee[106], E. F. McDonald[105], A. E. McDougall[114], J. A. Mcfayden[146], R. P. McGovern[128], G. Mchedlidze[149b], R. P. Mckenzie[33g], T. C. Mclachlan[48], D. J. Mclaughlin[96], S. J. McMahon[134], C. M. Mcpartland[92], R. A. McPherson[165,w], S. Mehlhase[109], A. Mehta[92], D. Melini[150], B. R. Mellado Garcia[33g], A. H. Melo[55], F. Meloni[48], A. M. Mendes Jacques Da Costa[101], H. Y. Meng[155], L. Meng[91], S. Menke[110], M. Mentink[36], E. Meoni[43a,43b], C. Merlassino[126], L. Merola[72a,72b], C. Meroni[71a,71b], G. Merz[106], O. Meshkov[37], J. Metcalfe[6], A. S. Mete[6], C. Meyer[68], J.-P. Meyer[135], R. P. Middleton[134], L. Mijović[52], G. Mikenberg[169], M. Mikestikova[131], M. Mikuž[93], H. Mildner[100], A. Milic[36], C. D. Milke[44], D. W. Miller[39], L. S. Miller[34], A. Milov[169], D. A. Milstead[47a,47b], T. Min[14c], A. A. Minaenko[37], I. A. Minashvili[149b], L. Mince[59], A. I. Mincer[117], B. Mindur[86a], M. Mineev[38], Y. Mino[88], L. M. Mir[13], M. Miralles Lopez[163], M. Mironova[17a], A. Mishima[153], M. C. Missio[113], A. Mitra[167], V. A. Mitsou[163], Y. Mitsumori[111], O. Miu[155], P. S. Miyagawa[94], T. Mkrtchyan[63a], M. Mlinarevic[96], T. Mlinarevic[96], M. Mlynarikova[36], S. Mobius[19], P. Moder[48], P. Mogg[109], A. F. Mohammed[14a,14e], S. Mohapatra[41], G. Mokgatitswane[33g], L. Moleri[169], B. Mondal[141], S. Mondal[132], K. Mönig[48], E. Monnier[102], L. Monsonis Romero[163], J. Montejo Berlingen[13], M. Montella[119], F. Montereali[77a,77b], F. Monticelli[90], S. Monzani[69a,69c], N. Morange[66], A. L. Moreira De Carvalho[130a], M. Moreno Llácer[163], C. Moreno Martinez[56], P. Morettini[57b], S. Morgenstern[36], M. Morii[61], M. Morinaga[153], A. K. Morley[36], F. Morodei[75a,75b], L. Morvaj[36], P. Moschovakos[36], B. Moser[36], M. Mosidze[149b], T. Moskalets[54], P. Moskvitina[113], J. Moss[31,l], E. J. W. Moyse[103], O. Mtintsilana[33g], S. Muanza[102], J. Mueller[129], D. Muenstermann[91], R. Müller[19], G. A. Mullier[161], A. J. Mullin[32], J. J. Mullin[128], D. P. Mungo[155], D. Munoz Perez[163], F. J. Munoz Sanchez[101], M. Murin[101], W. J. Murray[134,167], A. Murrone[71a,71b], J. M. Muse[120], M. Muškinja[17a], C. Mwewa[29], A. G. Myagkov[37,a], A. J. Myers[8], A. A. Myers[129], G. Myers[68], M. Myska[132], B. P. Nachman[17a], O. Nackenhorst[49], A. Nag[50], K. Nagai[126], K. Nagano[84], J. L. Nagle[29,aj], E. Nagy[102], A. M. Nairz[36], Y. Nakahama[84], K. Nakamura[84], K. Nakkalil[5], H. Nanjo[124], R. Narayan[44], E. A. Narayanan[112], I. Naryshkin[37], M. Naseri[34], S. Nasri[159], C. Nass[24], G. Navarro[22a], J. Navarro-Gonzalez[163], R. Nayak[151], A. Nayaz[18], P. Y. Nechaeva[37], F. Nechansky[48], L. Nedic[126], T. J. Neep[20], A. Negri[73a,73b], M. Negrini[23b], C. Nellist[114], C. Nelson[104], K. Nelson[106], S. Nemecek[131], M. Nessi[36,h], M. S. Neubauer[162], F. Neuhaus[100], J. Neundorf[48], R. Newhouse[164], P. R. Newman[20], C. W. Ng[129], Y. W. Y. Ng[48], B. Ngair[35e], H. D. N. Nguyen[108], R. B. Nickerson[126], R. Nicolaidou[135], J. Nielsen[136], M. Niemeyer[55], J. Niermann[36,55], N. Nikiforou[36], V. Nikolaenko[37,a], I. Nikolic-Audit[127], K. Nikolopoulos[20], P. Nilsson[29], I. Ninca[48], H. R. Nindhito[56], G. Ninio[151], A. Nisati[75a], N. Nishu[2], R. Nisius[110], J.-E. Nitschke[50], E. K. Nkadimeng[33g], T. Nobe[153], D. L. Noel[32], T. Nommensen[147], M. B. Norfolk[139], R. R. B. Norisam[96], B. J. Norman[34], J. Novak[93], T. Novak[48], L. Novotny[132], R. Novotny[112], L. Nozka[122], K. Ntekas[160], N. M. J. Nunes De Moura Junior[83b], E. Nurse[96], J. Ocariz[127], A. Ochi[85], I. Ochoa[130a], S. Oerdek[48], J. T. Offermann[39], A. Ogrodnik[133], A. Oh[101], C. C. Ohm[144], H. Oide[84], R. Oishi[153], M. L. Ojeda[48], M. W. O'Keefe[92], Y. Okumura[153], L. F. Oleiro Seabra[130a], S. A. Olivares Pino[137d], D. Oliveira Damazio[29], D. Oliveira Goncalves[83a], J. L. Oliver[160], A. Olszewski[87], Ö. O. Öncel[54], A. P. O'Neill[19], A. Onofre[130a,130e], P. U. E. Onyisi[11], M. J. Oreglia[39], G. E. Orellana[90], D. Orestano[77a,77b], N. Orlando[13], R. S. Orr[155], V. O'Shea[59], L. M. Osojnak[128], R. Ospanov[62a], G. Otero y Garzon[30], H. Otono[89], P. S. Ott[63a], G. J. Ottino[17a], M. Ouchrif[35d], J. Ouellette[29], F. Ould-Saada[125], M. Owen[59], R. E. Owen[134], K. Y. Oyulmaz[21a], V. E. Ozcan[21a], N. Ozturk[8], S. Ozturk[82], H. A. Pacey[126], A. Pacheco Pages[13], C. Padilla Aranda[13], G. Padovano[75a,75b], S. Pagan Griso[17a], G. Palacino[68], A. Palazzo[70a,70b], S. Palestini[36], J. Pan[172], T. Pan[64a], D. K. Panchal[11], C. E. Pandini[114], J. G. Panduro Vazquez[95], H. D. Pandya[1], H. Pang[14b], P. Pani[48], G. Panizzo[69a,69c], L. Paolozzi[56], C. Papadatos[108], S. Parajuli[44], A. Paramonov[6], C. Paraskevopoulos[10], D. Paredes Hernandez[64b], T. H. Park[155], M. A. Parker[32], F. Parodi[57a,57b], E. W. Parrish[115], V. A. Parrish[52], J. A. Parsons[41], U. Parzefall[54], B. Pascual Dias[108], L. Pascual Dominguez[151], E. Pasqualucci[75a], S. Passaggio[57b], F. Pastore[95], P. Pasuwan[47a,47b], P. Patel[87], U. M. Patel[51], J. R. Pater[101], T. Pauly[36], J. Pearkes[143], M. Pedersen[125], R. Pedro[130a], S. V. Peleganchuk[37], O. Penc[36], E. A. Pender[52], H. Peng[62a], K. E. Penski[109], M. Penzin[37], B. S. Peralva[83d], A. P. Pereira Peixoto[60], L. Pereira Sanchez[47a,47b], D. V. Perepelitsa[29,aj], E. Perez Codina[156a], M. Perganti[10], L. Perini[71a,71b,*], H. Pernegger[36], O. Perrin[40], K. Peters[48], R. F. Y. Peters[101], B. A. Petersen[36], T. C. Petersen[42], E. Petit[102], V. Petousis[132], C. Petridou[152,e], A. Petrukhin[141], M. Pettee[17a], N. E. Pettersson[36], A. Petukhov[37], K. Petukhova[133], R. Pezoa[137f], L. Pezzotti[36], G. Pezzullo[172], T. M. Pham[170], T. Pham[105], P. W. Phillips[134], G. Piacquadio[145],

E. Pianori[17a], F. Piazza[71a,71b], R. Piegaia[30], D. Pietreanu[27b], A. D. Pilkington[101], M. Pinamonti[69a,69c], J. L. Pinfold[2], B. C. Pinheiro Pereira[130a], A. E. Pinto Pinoargote[100,135], L. Pintucci[69a,69c], K. M. Piper[146], A. Pirttikoski[56], D. A. Pizzi[34], L. Pizzimento[64b], A. Pizzini[114], M.-A. Pleier[29], V. Plesanovs[54], V. Pleskot[133], E. Plotnikova[38], G. Poddar[4], R. Poettgen[98], L. Poggioli[127], I. Pokharel[55], S. Polacek[133], G. Polesello[73a], A. Poley[142,156a], R. Polifka[132], A. Polini[23b], C. S. Pollard[167], Z. B. Pollock[119], V. Polychronakos[29], E. Pompa Pacchi[75a,75b], D. Ponomarenko[113], L. Pontecorvo[36], S. Popa[27a], G. A. Popeneciu[27d], A. Poreba[36], D. M. Portillo Quintero[156a], S. Pospisil[132], M. A. Postill[139], P. Postolache[27c], K. Potamianos[167], P. A. Potepa[86a], I. N. Potrap[38], C. J. Potter[32], H. Potti[1], T. Poulsen[48], J. Poveda[163], M. E. Pozo Astigarraga[36], A. Prades Ibanez[163], J. Pretel[54], D. Price[101], M. Primavera[70a], M. A. Principe Martin[99], R. Privara[122], T. Procter[59], M. L. Proffitt[138], N. Proklova[128], K. Prokofiev[64c], G. Proto[110], S. Protopopescu[29], J. Proudfoot[6], M. Przybycien[86a], W. W. Przygoda[86b], J. E. Puddefoot[139], D. Pudzha[37], D. Pyatiizbyantseva[37], J. Qian[106], D. Qichen[101], Y. Qin[101], T. Qiu[52], A. Quadt[55], M. Queitsch-Maitland[101], G. Quetant[56], R. P. Quinn[164], G. Rabanal Bolanos[61], D. Rafanoharana[54], F. Ragusa[71a,71b], J. L. Rainbolt[39], J. A. Raine[56], S. Rajagopalan[29], E. Ramakoti[37], K. Ran[14e,48], N. P. Rapheeha[33g], H. Rasheed[27b], V. Raskina[127], D. F. Rassloff[63a], S. Rave[100], B. Ravina[55], I. Ravinovich[169], M. Raymond[36], A. L. Read[125], N. P. Readioff[139], D. M. Rebuzzi[73a,73b], G. Redlinger[29], A. S. Reed[110], K. Reeves[26], J. A. Reidelsturz[171], D. Reikher[151], A. Rej[141], C. Rembser[36], A. Renardi[48], M. Renda[27b], M. B. Rendel[110], F. Renner[48], A. G. Rennie[160], A. L. Rescia[48], S. Resconi[71a], M. Ressegotti[57a,57b], S. Rettie[36], J. G. Reyes Rivera[107], E. Reynolds[17a], O. L. Rezanova[37], P. Reznicek[133], N. Ribaric[91], E. Ricci[78a,78b], R. Richter[110], S. Richter[47a,47b], E. Richter-Was[86b], M. Ridel[127], S. Ridouani[35d], P. Rieck[117], P. Riedler[36], E. M. Riefel[47a,47b], M. Rijssenbeek[145], A. Rimoldi[73a,73b], M. Rimoldi[48], L. Rinaldi[23a,23b], T. T. Rinn[29], M. P. Rinnagel[109], G. Ripellino[161], I. Riu[13], P. Rivadeneira[48], J. C. Rivera Vergara[165], F. Rizatdinova[121], E. Rizvi[94], B. A. Roberts[167], B. R. Roberts[17a], S. H. Robertson[104,w], D. Robinson[32], C. M. Robles Gajardo[137f], M. Robles Manzano[100], A. Robson[59], A. Rocchi[76a,76b], C. Roda[74a,74b], S. Rodriguez Bosca[63a], Y. Rodriguez Garcia[22a], A. Rodriguez Rodriguez[54], A. M. Rodríguez Vera[156b], S. Roe[36], J. T. Roemer[160], A. R. Roepe-Gier[136], J. Roggel[171], O. Røhne[125], R. A. Rojas[103], C. P. A. Roland[68], J. Roloff[29], A. Romaniouk[37], E. Romano[73a,73b], M. Romano[23b], A. C. Romero Hernandez[162], N. Rompotis[92], L. Roos[127], S. Rosati[75a], B. J. Rosser[39], E. Rossi[126], E. Rossi[72a,72b], L. P. Rossi[57b], L. Rossini[54], R. Rosten[119], M. Rotaru[27b], B. Rottler[54], C. Rougier[102,aa], D. Rousseau[66], D. Rousso[32], A. Roy[162], S. Roy-Garand[155], A. Rozanov[102], Y. Rozen[150], X. Ruan[33g], A. Rubio Jimenez[163], A. J. Ruby[92], V. H. Ruelas Rivera[18], T. A. Ruggeri[1], A. Ruggiero[126], A. Ruiz-Martinez[163], A. Rummler[36], Z. Rurikova[54], N. A. Rusakovich[38], H. L. Russell[165], G. Russo[75a,75b], J. P. Rutherfoord[7], S. Rutherford Colmenares[32], K. Rybacki[91], M. Rybar[133], E. B. Rye[125], A. Ryzhov[44], J. A. Sabater Iglesias[56], P. Sabatini[163], L. Sabetta[75a,75b], H.F.-W. Sadrozinski[136], F. Safai Tehrani[75a], B. Safarzadeh Samani[134], M. Safdari[143], S. Saha[165], M. Sahinsoy[110], M. Saimpert[135], M. Saito[153], T. Saito[153], D. Salamani[36], A. Salnikov[143], J. Salt[163], A. Salvador Salas[13], D. Salvatore[43a,43b], F. Salvatore[146], A. Salzburger[36], D. Sammel[54], D. Sampsonidis[152,e], D. Sampsonidou[123], J. Sánchez[163], A. Sanchez Pineda[4], V. Sanchez Sebastian[163], H. Sandaker[125], C. O. Sander[48], J. A. Sandesara[103], M. Sandhoff[171], C. Sandoval[22b], D. P. C. Sankey[134], T. Sano[88], A. Sansoni[53], L. Santi[75a,75b], C. Santoni[40], H. Santos[130a,130b], S. N. Santpur[17a], A. Santra[169], K. A. Saoucha[116b], J. G. Saraiva[130a,130d], J. Sardain[7], O. Sasaki[84], K. Sato[157], C. Sauer[63b], F. Sauerburger[54], E. Sauvan[4], P. Savard[155,ag], R. Sawada[153], C. Sawyer[134], L. Sawyer[97], I. Sayago Galvan[163], C. Sbarra[23b], A. Sbrizzi[23a,23b], T. Scanlon[96], J. Schaarschmidt[138], P. Schacht[110], U. Schäfer[100], A. C. Schaffer[66,44], D. Schaile[109], R. D. Schamberger[145], C. Scharf[18], M. M. Schefer[19], V. A. Schegelsky[37], D. Scheirich[133], F. Schenck[18], M. Schernau[160], C. Scheulen[55], C. Schiavi[57a,57b], E. J. Schioppa[70a,70b], M. Schioppa[43a,43b], B. Schlag[143,n], K. E. Schleicher[54], S. Schlenker[36], J. Schmeing[171], M. A. Schmidt[171], K. Schmieden[100], C. Schmitt[100], S. Schmitt[48], L. Schoeffel[135], A. Schoening[63b], P. G. Scholer[54], E. Schopf[126], M. Schott[100], J. Schovancova[36], S. Schramm[56], F. Schroeder[171], T. Schroer[56], H.-C. Schultz-Coulon[63a], M. Schumacher[54], B. A. Schumm[136], Ph. Schune[135], A. J. Schuy[138], H. R. Schwartz[136], A. Schwartzman[143], T. A. Schwarz[106], Ph. Schwemling[135], R. Schwienhorst[107], A. Sciandra[136], G. Sciolla[26], F. Scuri[74a], C. D. Sebastiani[92], K. Sedlaczek[115], P. Seema[18], S. C. Seidel[112], A. Seiden[136], B. D. Seidlitz[41], C. Seitz[48], J. M. Seixas[83b], G. Sekhniaidze[72a], S. J. Sekula[44], L. Selem[60], N. Semprini-Cesari[23a,23b], D. Sengupta[56], V. Senthilkumar[163], L. Serin[66], L. Serkin[69a,69b], M. Sessa[76a,76b], H. Severini[120],

F. Sforza[57a,57b], A. Sfyrla[56], E. Shabalina[55], R. Shaheen[144], J. D. Shahinian[128], D. Shaked Renous[169], L. Y. Shan[14a], M. Shapiro[17a], A. Sharma[36], A. S. Sharma[164], P. Sharma[80], S. Sharma[48], P. B. Shatalov[37], K. Shaw[146], S. M. Shaw[101], A. Shcherbakova[37], Q. Shen[62c,5], P. Sherwood[96], L. Shi[96], X. Shi[14a], C. O. Shimmin[172], J. D. Shinner[95], I. P. J. Shipsey[126], S. Shirabe[56,h], M. Shiyakova[38,u], J. Shlomi[169], M. J. Shochet[39], J. Shojaii[105], D. R. Shope[125], B. Shrestha[120], S. Shrestha[119,ak], E. M. Shrif[33g], M. J. Shroff[165], P. Sicho[131], A. M. Sickles[162], E. Sideras Haddad[33g], A. Sidoti[23b], F. Siegert[50], Dj. Sijacki[15], R. Sikora[86a], F. Sili[90], J. M. Silva[20], M. V. Silva Oliveira[29], S. B. Silverstein[47a], S. Simion[66], R. Simoniello[36], E. L. Simpson[59], H. Simpson[146], L. R. Simpson[106], N. D. Simpson[98], S. Simsek[82], S. Sindhu[55], P. Sinervo[155], S. Singh[155], S. Sinha[48], S. Sinha[101], M. Sioli[23a,23b], I. Siral[36], E. Sitnikova[48], S.Yu. Sivoklokov[37,*], J. Sjölin[47a,47b], A. Skaf[55], E. Skorda[20], P. Skubic[120], M. Slawinska[87], V. Smakhtin[169], B. H. Smart[134], J. Smiesko[36], S.Yu. Smirnov[37], Y. Smirnov[37], L. N. Smirnova[37,a], O. Smirnova[98], A. C. Smith[41], E. A. Smith[39], H. A. Smith[126], J. L. Smith[92], R. Smith[143], M. Smizanska[91], K. Smolek[132], A. A. Snesarev[37], S. R. Snider[155], H. L. Snoek[114], S. Snyder[29], R. Sobie[165,w], A. Soffer[151], C. A. Solans Sanchez[36], E.Yu. Soldatov[37], U. Soldevila[163], A. A. Solodkov[37], S. Solomon[26], A. Soloshenko[38], K. Solovieva[54], O. V. Solovyanov[40], V. Solovyev[37], P. Sommer[36], A. Sonay[13], W. Y. Song[156b], J. M. Sonneveld[114], A. Sopczak[132], A. L. Sopio[96], F. Sopkova[28b], I. R. Sotarriva Alvarez[154], V. Sothilingam[63a], S. Sottocornola[68], R. Soualah[116b], Z. Soumaimi[35e], D. South[48], N. Soybelman[169], S. Spagnolo[70a,70b], M. Spalla[110], D. Sperlich[54], G. Spigo[36], S. Spinali[91], D. P. Spiteri[59], M. Spousta[133], E. J. Staats[34], A. Stabile[71a,71b], R. Stamen[63a], A. Stampekis[20], M. Standke[24], E. Stanecka[87], M. V. Stange[50], B. Stanislaus[17a], M. M. Stanitzki[48], B. Stapf[48], E. A. Starchenko[37], G. H. Stark[136], J. Stark[102,aa], D. M. Starko[156b], P. Staroba[131], P. Starovoitov[63a], S. Stärz[104], R. Staszewski[87], G. Stavropoulos[46], J. Steentoft[161], P. Steinberg[29], B. Stelzer[142,156a], H. J. Stelzer[129], O. Stelzer-Chilton[156a], H. Stenzel[58], T. J. Stevenson[146], G. A. Stewart[36], J. R. Stewart[121], M. C. Stockton[36], G. Stoicea[27b], M. Stolarski[130a], S. Stonjek[110], A. Straessner[50], J. Strandberg[144], S. Strandberg[47a,47b], M. Stratmann[171], M. Strauss[120], T. Strebler[102], P. Strizenec[28b], R. Ströhmer[166], D. M. Strom[123], L. R. Strom[48], R. Stroynowski[44], A. Strubig[47a,47b], S. A. Stucci[29], B. Stugu[16], J. Stupak[120], N. A. Styles[48], D. Su[143], S. Su[62a], W. Su[62d], X. Su[62a,66], K. Sugizaki[153], V. V. Sulin[37], M. J. Sullivan[92], D. M. S. Sultan[78a,78b], L. Sultanaliyeva[37], S. Sultansoy[3b], T. Sumida[88], S. Sun[106], S. Sun[170], O. Sunneborn Gudnadottir[161], N. Sur[102], M. R. Sutton[146], H. Suzuki[157], M. Svatos[131], M. Swiatlowski[156a], T. Swirski[166], I. Sykora[28a], M. Sykora[133], T. Sykora[133], D. Ta[100], K. Tackmann[48,t], A. Taffard[160], R. Tafirout[156a], J. S. Tafoya Vargas[66], E. P. Takeva[52], Y. Takubo[84], M. Talby[102], A. A. Talyshev[37], K. C. Tam[64b], N. M. Tamir[151], A. Tanaka[153], J. Tanaka[153], R. Tanaka[66], M. Tanasini[57a,57b], Z. Tao[164], S. Tapia Araya[137f], S. Tapprogge[100], A. Tarek Abouelfadl Mohamed[107], S. Tarem[150], K. Tariq[14a], G. Tarna[27b,102], G. F. Tartarelli[71a], P. Tas[133], M. Tasevsky[131], E. Tassi[43a,43b], A. C. Tate[162], G. Tateno[153], Y. Tayalati[35e,v], G. N. Taylor[105], W. Taylor[156b], H. Teagle[92], A. S. Tee[170], R. Teixeira De Lima[143], P. Teixeira-Dias[95], J. J. Teoh[155], K. Terashi[153], J. Terron[99], S. Terzo[13], M. Testa[53], R. J. Teuscher[155,w], A. Thaler[79], O. Theiner[56], N. Themistokleous[52], T. Theveneaux-Pelzer[102], O. Thielmann[171], D. W. Thomas[95], J. P. Thomas[20], E. A. Thompson[17a], P. D. Thompson[20], E. Thomson[128], C. Tian[62a], Y. Tian[55], V. Tikhomirov[37,a], Yu.A. Tikhonov[37], S. Timoshenko[37], D. Timoshyn[133], E. X. L. Ting[1], P. Tipton[172], S. H. Tlou[33g], A. Tnourji[40], K. Todome[154], S. Todorova-Nova[133], S. Todt[50], M. Togawa[84], J. Tojo[89], S. Tokár[28a], K. Tokushuku[84], O. Toldaiev[68], R. Tombs[32], M. Tomoto[84,111], L. Tompkins[143,n], K. W. Topolnicki[86b], E. Torrence[123], H. Torres[102,aa], E. Torró Pastor[163], M. Toscani[30], C. Tosciri[39], M. Tost[11], D. R. Tovey[139], A. Traeet[16], I. S. Trandafir[27b], T. Trefzger[166], A. Tricoli[29], I. M. Trigger[156a], S. Trincaz-Duvoid[127], D. A. Trischuk[26], B. Trocmé[60], C. Troncon[71a], L. Truong[33c], M. Trzebinski[87], A. Trzupek[87], F. Tsai[145], M. Tsai[106], A. Tsiamis[152,e], P. V. Tsiareshka[37], S. Tsigaridas[156a], A. Tsirigotis[152,r], V. Tsiskaridze[155], E. G. Tskhadadze[149a], M. Tsopoulou[152,e], Y. Tsujikawa[88], I. I. Tsukerman[37], V. Tsulaia[17a], S. Tsuno[84], O. Tsur[150], K. Tsuri[118], D. Tsybychev[145], Y. Tu[64b], A. Tudorache[27b], V. Tudorache[27b], A. N. Tuna[36], S. Turchikhin[57a,57b], I. Turk Cakir[3a], R. Turra[71a], T. Turtuvshin[38,x], P. M. Tuts[41], S. Tzamarias[152,e], P. Tzanis[10], E. Tzovara[100], F. Ukegawa[157], P. A. Ulloa Poblete[137c,137b], E. N. Umaka[29], G. Unal[36], M. Unal[11], A. Undrus[29], G. Unel[160], J. Urban[28b], P. Urquijo[105], G. Usai[8], R. Ushioda[154], M. Usman[108], Z. Uysal[21b], L. Vacavant[102], V. Vacek[132], B. Vachon[104], K. O. H. Vadla[125], T. Vafeiadis[36], A. Vaitkus[96], C. Valderanis[109], E. Valdes Santurio[47a,47b], M. Valente[156a], S. Valentinetti[23a,23b], A. Valero[163], E. Valiente Moreno[163], A. Vallier[102,aa], J. A. Valls Ferrer[163], D. R. Van Arneman[114], T. R. Van Daalen[138], A. Van Der Graaf[49], P. Van Gemmeren[6], M. Van Rijnbach[36,125], S. Van Stroud[96],

I. Van Vulpen[114], M. Vanadia[76a,76b], W. Vandelli[36], M. Vandenbroucke[135], E. R. Vandewall[121], D. Vannicola[151], L. Vannoli[57a,57b], R. Vari[75a], E. W. Varnes[7], C. Varni[17b], T. Varol[148], D. Varouchas[66], L. Varriale[163], K. E. Varvell[147], M. E. Vasile[27b], L. Vaslin[40], G. A. Vasquez[165], A. Vasyukov[38], F. Vazeille[40], T. Vazquez Schroeder[36], J. Veatch[31], V. Vecchio[101], M. J. Veen[103], I. Veliscek[126], L. M. Veloce[155], F. Veloso[130a,130c], S. Veneziano[75a], A. Ventura[70a,70b], S. Ventura Gonzalez[135], A. Verbytskyi[110], M. Verducci[74a,74b], C. Vergis[24], M. Verissimo De Araujo[83b], W. Verkerke[114], J. C. Vermeulen[114], C. Vernieri[143], M. Vessella[103], M. C. Vetterli[142,ag], A. Vgenopoulos[152,e], N. Viaux Maira[137f], T. Vickey[139], O. E. Vickey Boeriu[139], G. H. A. Viehhauser[126], L. Vigani[63b], M. Villa[23a,23b], M. Villaplana Perez[163], E. M. Villhauer[52], E. Vilucchi[53], M. G. Vincter[34], G. S. Virdee[20], A. Vishwakarma[52], A. Visibile[114], C. Vittori[36], I. Vivarelli[146], E. Voevodina[110], F. Vogel[109], P. Vokac[132], Yu. Volkotrub[86a], J. Von Ahnen[48], E. Von Toerne[24], B. Vormwald[36], V. Vorobel[133], K. Vorobev[37], M. Vos[163], K. Voss[141], J. H. Vossebeld[92], M. Vozak[114], L. Vozdecky[94], N. Vranjes[15], M. Vranjes Milosavljevic[15], M. Vreeswijk[114], R. Vuillermet[36], O. Vujinovic[100], I. Vukotic[39], S. Wada[157], C. Wagner[103], J. M. Wagner[17a], W. Wagner[171], S. Wahdan[171], H. Wahlberg[90], M. Wakida[111], J. Walder[134], R. Walker[109], W. Walkowiak[141], A. Wall[128], T. Wamorkar[6], A. Z. Wang[170], C. Wang[100], C. Wang[62c], H. Wang[17a], J. Wang[64a], R.-J. Wang[100], R. Wang[61], R. Wang[6], S. M. Wang[148], S. Wang[62b], T. Wang[62a], W. T. Wang[80], W. Wang[14a], X. Wang[14c], X. Wang[162], X. Wang[62c], Y. Wang[62d], Y. Wang[14c], Z. Wang[106], Z. Wang[51,62c,62d], Z. Wang[106], A. Warburton[104], R. J. Ward[20], N. Warrack[59], A. T. Watson[20], H. Watson[59], M. F. Watson[20], E. Watton[59,134], G. Watts[138], B. M. Waugh[96], C. Weber[29], H. A. Weber[18], M. S. Weber[19], S. M. Weber[63a], C. Wei[62a], Y. Wei[126], A. R. Weidberg[126], E. J. Weik[117], J. Weingarten[49], M. Weirich[100], C. Weiser[54], C. J. Wells[48], T. Wenaus[29], B. Wendland[49], T. Wengler[36], N. S. Wenke[110], N. Wermes[24], M. Wessels[63a], A. M. Wharton[91], A. S. White[61], A. White[8], M. J. White[1], D. Whiteson[160], L. Wickremasinghe[124], W. Wiedenmann[170], C. Wiel[50], M. Wielers[134], C. Wiglesworth[42], D. J. Wilbern[120], H. G. Wilkens[36], D. M. Williams[41], H. H. Williams[128], S. Williams[32], S. Willocq[103], B. J. Wilson[101], P. J. Windischhofer[39], F. I. Winkel[30], F. Winklmeier[123], B. T. Winter[54], J. K. Winter[101], M. Wittgen[143], M. Wobisch[97], Z. Wolffs[114], J. Wollrath[160], M. W. Wolter[87], H. Wolters[130a,130c], A. F. Wongel[48], S. D. Worm[48], B. K. Wosiek[87], K. W. Woźniak[87], S. Wozniewski[55], K. Wraight[59], C. Wu[20], J. Wu[14a,14e], M. Wu[64a], M. Wu[113], S. L. Wu[170], X. Wu[56], Y. Wu[62a], Z. Wu[135], J. Wuerzinger[110,ae], T. R. Wyatt[101], B. M. Wynne[52], S. Xella[42], L. Xia[14c], M. Xia[14b], J. Xiang[64c], M. Xie[62a], X. Xie[62a], S. Xin[14a,14e], A. Xiong[123], J. Xiong[17a], D. Xu[14a], H. Xu[62a], L. Xu[62a], R. Xu[128], T. Xu[106], Y. Xu[14b], Z. Xu[52], Z. Xu[14a], Z. Xu[14c], B. Yabsley[147], S. Yacoob[33a], Y. Yamaguchi[154], E. Yamashita[153], H. Yamauchi[157], T. Yamazaki[17a], Y. Yamazaki[85], J. Yan[62c], S. Yan[126], Z. Yan[25], H. J. Yang[62c,62d], H. T. Yang[62a], S. Yang[62a], T. Yang[64c], X. Yang[62a], X. Yang[14a], Y. Yang[44], Y. Yang[62a], Z. Yang[62a], W.-M. Yao[17a], Y. C. Yap[48], H. Ye[14c], H. Ye[55], J. Ye[14a], S. Ye[29], X. Ye[62a], Y. Yeh[96], I. Yeletskikh[38], B. K. Yeo[17b], M. R. Yexley[96], P. Yin[41], K. Yorita[168], S. Younas[27b], C. J. S. Young[36], C. Young[143], C. Yu[14a,14e,ai], Y. Yu[62a], M. Yuan[106], R. Yuan[62b], L. Yue[96], M. Zaazoua[62a], B. Zabinski[87], E. Zaid[52], T. Zakareishvili[149b], N. Zakharchuk[34], S. Zambito[56], J. A. Zamora Saa[137b,137d], J. Zang[153], D. Zanzi[54], O. Zaplatilek[132], C. Zeitnitz[171], H. Zeng[14a], J. C. Zeng[162], D. T. Zenger Jr[26], O. Zenin[37], T. Ženiš[28a], S. Zenz[94], S. Zerradi[35a], D. Zerwas[66], M. Zhai[14a,14e], B. Zhang[14c], D. F. Zhang[139], J. Zhang[62b], J. Zhang[6], K. Zhang[14a,14e], L. Zhang[14c], P. Zhang[14a,14e], R. Zhang[170], S. Zhang[106], T. Zhang[153], X. Zhang[62c], X. Zhang[62b], Y. Zhang[5,62c], Y. Zhang[96], Z. Zhang[17a], Z. Zhang[66], H. Zhao[138], P. Zhao[51], T. Zhao[62b], Y. Zhao[136], Z. Zhao[62a], A. Zhemchugov[38], J. Zheng[14c], K. Zheng[162], X. Zheng[62a], Z. Zheng[143], D. Zhong[162], B. Zhou[106], H. Zhou[7], N. Zhou[62c], Y. Zhou[7], C. G. Zhu[62b], J. Zhu[106], Y. Zhu[62c], Y. Zhu[62a], X. Zhuang[14a], K. Zhukov[37], V. Zhulanov[37], N. I. Zimine[38], J. Zinsser[63b], M. Ziolkowski[141], L. Živković[15], A. Zoccoli[23a,23b], K. Zoch[61], T. G. Zorbas[139], O. Zormpa[46], W. Zou[41], L. Zwalinski[36]

[1] Department of Physics, University of Adelaide, Adelaide, Australia
[2] Department of Physics, University of Alberta, Edmonton, AB, Canada
[3] [(a)]Department of Physics, Ankara University, Ankara, Türkiye; [(b)]Division of Physics, TOBB University of Economics and Technology, Ankara, Türkiye
[4] LAPP, Université Savoie Mont Blanc, CNRS/IN2P3, Annecy, France
[5] APC, Université Paris Cité, CNRS/IN2P3, Paris, France
[6] High Energy Physics Division, Argonne National Laboratory, Argonne, IL, USA
[7] Department of Physics, University of Arizona, Tucson, AZ, USA

[8] Department of Physics, University of Texas at Arlington, Arlington, TX, USA
[9] Physics Department, National and Kapodistrian University of Athens, Athens, Greece
[10] Physics Department, National Technical University of Athens, Zografou, Greece
[11] Department of Physics, University of Texas at Austin, Austin, TX, USA
[12] Institute of Physics, Azerbaijan Academy of Sciences, Baku, Azerbaijan
[13] Institut de Física d'Altes Energies (IFAE), Barcelona Institute of Science and Technology, Barcelona, Spain
[14] [(a)]Institute of High Energy Physics, Chinese Academy of Sciences, Beijing, China; [(b)]Physics Department, Tsinghua University, Beijing, China; [(c)]Department of Physics, Nanjing University, Nanjing, China; [(d)]School of Science, Shenzhen Campus of Sun Yat-sen University, Shenzhen, China; [(e)]University of Chinese Academy of Science (UCAS), Beijing, China
[15] Institute of Physics, University of Belgrade, Belgrade, Serbia
[16] Department for Physics and Technology, University of Bergen, Bergen, Norway
[17] [(a)]Physics Division, Lawrence Berkeley National Laboratory, Berkeley, CA, USA; [(b)]University of California, Berkeley, CA, USA
[18] Institut für Physik, Humboldt Universität zu Berlin, Berlin, Germany
[19] Albert Einstein Center for Fundamental Physics and Laboratory for High Energy Physics, University of Bern, Bern, Switzerland
[20] School of Physics and Astronomy, University of Birmingham, Birmingham, UK
[21] [(a)]Department of Physics, Bogazici University, Istanbul, Türkiye; [(b)]Department of Physics Engineering, Gaziantep University, Gaziantep, Türkiye; [(c)]Department of Physics, Istanbul University, Istanbul, Türkiye
[22] [(a)]Facultad de Ciencias y Centro de Investigaciónes, Universidad Antonio Nariño, Bogotá, Colombia; [(b)]Departamento de Física, Universidad Nacional de Colombia, Bogotá, Colombia
[23] [(a)]Dipartimento di Fisica e Astronomia A. Righi, Università di Bologna, Bologna, Italy; [(b)]INFN Sezione di Bologna, Bologna, Italy
[24] Physikalisches Institut, Universität Bonn, Bonn, Germany
[25] Department of Physics, Boston University, Boston, MA, USA
[26] Department of Physics, Brandeis University, Waltham, MA, USA
[27] [(a)]Transilvania University of Brasov, Brasov, Romania; [(b)]Horia Hulubei National Institute of Physics and Nuclear Engineering, Bucharest, Romania; [(c)]Department of Physics, Alexandru Ioan Cuza University of Iasi, Iasi, Romania; [(d)]Physics Department, National Institute for Research and Development of Isotopic and Molecular Technologies, Cluj-Napoca, Romania; [(e)]University Politehnica Bucharest, Bucharest, Romania; [(f)]West University in Timisoara, Timisoara, Romania; [(g)]Faculty of Physics, University of Bucharest, Bucharest, Romania
[28] [(a)]Faculty of Mathematics, Physics and Informatics, Comenius University, Bratislava, Slovak Republic; [(b)]Department of Subnuclear Physics, Institute of Experimental Physics of the Slovak Academy of Sciences, Kosice, Slovak Republic
[29] Physics Department, Brookhaven National Laboratory, Upton, NY, USA
[30] Facultad de Ciencias Exactas y Naturales, Departamento de Física, y CONICET, Instituto de Física de Buenos Aires (IFIBA), Universidad de Buenos Aires, Buenos Aires, Argentina
[31] California State University, Fresno, CA, USA
[32] Cavendish Laboratory, University of Cambridge, Cambridge, UK
[33] [(a)]Department of Physics, University of Cape Town, Cape Town, South Africa; [(b)]iThemba Labs, Western Cape, South Africa; [(c)]Department of Mechanical Engineering Science, University of Johannesburg, Johannesburg, South Africa; [(d)]National Institute of Physics, University of the Philippines, Diliman, Philippines; [(e)]University of South Africa, Department of Physics, Pretoria, South Africa; [(f)]University of Zululand, KwaDlangezwa, South Africa ; [(g)]School of Physics, University of the Witwatersrand, Johannesburg, South Africa
[34] Department of Physics, Carleton University, Ottawa, ON, Canada
[35] [(a)]Faculté des Sciences Ain Chock, Réseau Universitaire de Physique des Hautes Energies-Université Hassan II, Casablanca, Morocco; [(b)]Faculté des Sciences, Université Ibn-Tofail, Kénitra, Morocco; [(c)]Faculté des Sciences Semlalia, Université Cadi Ayyad, LPHEA-Marrakech, Marrakech, Morocco; [(d)]LPMR, Faculté des Sciences, Université Mohamed Premier, Oujda, Morocco; [(e)]Faculté des sciences, Université Mohammed V, Rabat, Morocco; [(f)]Institute of Applied Physics, Mohammed VI Polytechnic University, Ben Guerir, Morocco
[36] CERN, Geneva, Switzerland
[37] Affiliated with an institute covered by a cooperation agreement with CERN, Geneva, Switzerland
[38] Affiliated with an international laboratory covered by a cooperation agreement with CERN, Geneva, Switzerland

[39] Enrico Fermi Institute, University of Chicago, Chicago, IL, USA
[40] LPC, Université Clermont Auvergne, CNRS/IN2P3, Clermont-Ferrand, France
[41] Nevis Laboratory, Columbia University, Irvington, NY, USA
[42] Niels Bohr Institute, University of Copenhagen, Copenhagen, Denmark
[43] [(a)]Dipartimento di Fisica, Università della Calabria, Rende, Italy; [(b)]INFN Gruppo Collegato di Cosenza, Laboratori Nazionali di Frascati, Frascati, Italy
[44] Physics Department, Southern Methodist University, Dallas, TX, USA
[45] Physics Department, University of Texas at Dallas, Richardson, TX, USA
[46] National Centre for Scientific Research "Demokritos", Agia Paraskevi, Greece
[47] [(a)]Department of Physics, Stockholm University, Stockholm, Sweden; [(b)]Oskar Klein Centre, Stockholm, Sweden
[48] Deutsches Elektronen-Synchrotron DESY, Hamburg and Zeuthen, Germany
[49] Fakultät Physik , Technische Universität Dortmund, Dortmund, Germany
[50] Institut für Kern- und Teilchenphysik, Technische Universität Dresden, Dresden, Germany
[51] Department of Physics, Duke University, Durham, NC, USA
[52] SUPA-School of Physics and Astronomy, University of Edinburgh, Edinburgh, UK
[53] INFN e Laboratori Nazionali di Frascati, Frascati, Italy
[54] Physikalisches Institut, Albert-Ludwigs-Universität Freiburg, Freiburg, Germany
[55] II. Physikalisches Institut, Georg-August-Universität Göttingen, Göttingen, Germany
[56] Département de Physique Nucléaire et Corpusculaire, Université de Genève, Geneva, Switzerland
[57] [(a)]Dipartimento di Fisica, Università di Genova, Genoa, Italy; [(b)]INFN Sezione di Genova, Genoa, Italy
[58] II. Physikalisches Institut, Justus-Liebig-Universität Giessen, Giessen, Germany
[59] SUPA-School of Physics and Astronomy, University of Glasgow, Glasgow, UK
[60] LPSC, Université Grenoble Alpes, CNRS/IN2P3, Grenoble INP, Grenoble, France
[61] Laboratory for Particle Physics and Cosmology, Harvard University, Cambridge, MA, USA
[62] [(a)]Department of Modern Physics and State Key Laboratory of Particle Detection and Electronics, University of Science and Technology of China, Hefei, China; [(b)]Institute of Frontier and Interdisciplinary Science and Key Laboratory of Particle Physics and Particle Irradiation (MOE), Shandong University, Qingdao, China; [(c)]School of Physics and Astronomy, Shanghai Jiao Tong University, Key Laboratory for Particle Astrophysics and Cosmology (MOE), SKLPPC, Shanghai, China; [(d)]Tsung-Dao Lee Institute, Shanghai, China
[63] [(a)]Kirchhoff-Institut für Physik, Ruprecht-Karls-Universität Heidelberg, Heidelberg, Germany; [(b)]Physikalisches Institut, Ruprecht-Karls-Universität Heidelberg, Heidelberg, Germany
[64] [(a)]Department of Physics, Chinese University of Hong Kong, Shatin, N.T., Hong Kong, China; [(b)]Department of Physics, University of Hong Kong, Hong Kong, China; [(c)]Department of Physics and Institute for Advanced Study, Hong Kong University of Science and Technology, Clear Water Bay, Kowloon, Hong Kong, China
[65] Department of Physics, National Tsing Hua University, Hsinchu, Taiwan
[66] IJCLab, Université Paris-Saclay, CNRS/IN2P3, 91405 Orsay, France
[67] Centro Nacional de Microelectrónica (IMB-CNM-CSIC), Barcelona, Spain
[68] Department of Physics, Indiana University, Bloomington, IN, USA
[69] [(a)]INFN Gruppo Collegato di Udine, Sezione di Trieste, Udine, Italy; [(b)]ICTP, Trieste, Italy; [(c)]Dipartimento Politecnico di Ingegneria e Architettura, Università di Udine, Udine, Italy
[70] [(a)]INFN Sezione di Lecce, Lecce, Italy; [(b)]Dipartimento di Matematica e Fisica, Università del Salento, Lecce, Italy
[71] [(a)]INFN Sezione di Milano, Milan, Italy; [(b)]Dipartimento di Fisica, Università di Milano, Milan, Italy
[72] [(a)]INFN Sezione di Napoli, Naples, Italy; [(b)]Dipartimento di Fisica, Università di Napoli, Naples, Italy
[73] [(a)]INFN Sezione di Pavia, Pavia, Italy; [(b)]Dipartimento di Fisica, Università di Pavia, Pavia, Italy
[74] [(a)]INFN Sezione di Pisa, Pisa, Italy; [(b)]Dipartimento di Fisica E. Fermi, Università di Pisa, Pisa, Italy
[75] [(a)]INFN Sezione di Roma, Rome, Italy; [(b)]Dipartimento di Fisica, Sapienza Università di Roma, Rome, Italy
[76] [(a)]INFN Sezione di Roma Tor Vergata, Rome, Italy; [(b)]Dipartimento di Fisica, Università di Roma Tor Vergata, Rome, Italy
[77] [(a)]INFN Sezione di Roma Tre, Rome, Italy; [(b)]Dipartimento di Matematica e Fisica, Università Roma Tre, Rome, Italy
[78] [(a)]INFN-TIFPA, Povo, Italy; [(b)]Università degli Studi di Trento, Trento, Italy
[79] Department of Astro and Particle Physics, Universität Innsbruck, Innsbruck, Austria
[80] University of Iowa, Iowa City, IA, USA
[81] Department of Physics and Astronomy, Iowa State University, Ames, IA, USA

[82] Istinye University, Sariyer, Istanbul, Türkiye
[83] [(a)]Departamento de Engenharia Elétrica, Universidade Federal de Juiz de Fora (UFJF), Juiz de Fora, Brazil; [(b)]Universidade Federal do Rio De Janeiro COPPE/EE/IF, Rio de Janeiro, Brazil; [(c)]Instituto de Física, Universidade de São Paulo, São Paulo, Brazil; [(d)]Rio de Janeiro State University, Rio de Janeiro, Brazil
[84] KEK, High Energy Accelerator Research Organization, Tsukuba, Japan
[85] Graduate School of Science, Kobe University, Kobe, Japan
[86] [(a)]Faculty of Physics and Applied Computer Science, AGH University of Krakow, Kraków, Poland; [(b)]Marian Smoluchowski Institute of Physics, Jagiellonian University, Kraków, Poland
[87] Institute of Nuclear Physics Polish Academy of Sciences, Kraków, Poland
[88] Faculty of Science, Kyoto University, Kyoto, Japan
[89] Research Center for Advanced Particle Physics and Department of Physics, Kyushu University, Fukuoka, Japan
[90] Instituto de Física La Plata, Universidad Nacional de La Plata and CONICET, La Plata, Argentina
[91] Physics Department, Lancaster University, Lancaster, UK
[92] Oliver Lodge Laboratory, University of Liverpool, Liverpool, UK
[93] Department of Experimental Particle Physics, Jožef Stefan Institute and Department of Physics, University of Ljubljana, Ljubljana, Slovenia
[94] School of Physics and Astronomy, Queen Mary University of London, London, UK
[95] Department of Physics, Royal Holloway University of London, Egham, UK
[96] Department of Physics and Astronomy, University College London, London, UK
[97] Louisiana Tech University, Ruston, LA, USA
[98] Fysiska institutionen, Lunds universitet, Lund, Sweden
[99] Departamento de Física Teorica C-15 and CIAFF, Universidad Autónoma de Madrid, Madrid, Spain
[100] Institut für Physik, Universität Mainz, Mainz, Germany
[101] School of Physics and Astronomy, University of Manchester, Manchester, UK
[102] CPPM, Aix-Marseille Université, CNRS/IN2P3, Marseille, France
[103] Department of Physics, University of Massachusetts, Amherst, MA, USA
[104] Department of Physics, McGill University, Montreal, QC, Canada
[105] School of Physics, University of Melbourne, Melbourne, VIC, Australia
[106] Department of Physics, University of Michigan, Ann Arbor, MI, USA
[107] Department of Physics and Astronomy, Michigan State University, East Lansing, MI, USA
[108] Group of Particle Physics, University of Montreal, Montreal, QC, Canada
[109] Fakultät für Physik, Ludwig-Maximilians-Universität München, Munich, Germany
[110] Max-Planck-Institut für Physik (Werner-Heisenberg-Institut), Munich, Germany
[111] Graduate School of Science and Kobayashi-Maskawa Institute, Nagoya University, Nagoya, Japan
[112] Department of Physics and Astronomy, University of New Mexico, Albuquerque, NM, USA
[113] Institute for Mathematics, Astrophysics and Particle Physics, Radboud University/Nikhef, Nijmegen, The Netherlands
[114] Nikhef National Institute for Subatomic Physics and University of Amsterdam, Amsterdam, The Netherlands
[115] Department of Physics, Northern Illinois University, DeKalb, IL, USA
[116] [(a)]New York University Abu Dhabi, Abu Dhabi, United Arab Emirates; [(b)]University of Sharjah, Sharjah, United Arab Emirates
[117] Department of Physics, New York University, New York, NY, USA
[118] Ochanomizu University, Otsuka, Bunkyo-ku, Tokyo, Japan
[119] Ohio State University, Columbus, OH, USA
[120] Homer L. Dodge Department of Physics and Astronomy, University of Oklahoma, Norman, OK, USA
[121] Department of Physics, Oklahoma State University, Stillwater, OK, USA
[122] Joint Laboratory of Optics, Palacký University, Olomouc, Czech Republic
[123] Institute for Fundamental Science, University of Oregon, Eugene, OR, USA
[124] Graduate School of Science, Osaka University, Osaka, Japan
[125] Department of Physics, University of Oslo, Oslo, Norway
[126] Department of Physics, Oxford University, Oxford, UK
[127] LPNHE, Sorbonne Université, Université Paris Cité, CNRS/IN2P3, Paris, France
[128] Department of Physics, University of Pennsylvania, Philadelphia, PA, USA
[129] Department of Physics and Astronomy, University of Pittsburgh, Pittsburgh, PA, USA

[130] [(a)]Laboratório de Instrumentação e Física Experimental de Partículas - LIP, Lisbon, Portugal; [(b)]Departamento de Física, Faculdade de Ciências, Universidade de Lisboa, Lisbon, Portugal; [(c)]Departamento de Física, Universidade de Coimbra, Coimbra, Portugal; [(d)]Centro de Física Nuclear da Universidade de Lisboa, Lisbon, Portugal; [(e)]Departamento de Física, Universidade do Minho, Braga, Portugal; [(f)]Departamento de Física Teórica y del Cosmos, Universidad de Granada, Granada, Spain; [(g)]Departamento de Física, Instituto Superior Técnico, Universidade de Lisboa, Lisbon, Portugal
[131] Institute of Physics of the Czech Academy of Sciences, Prague, Czech Republic
[132] Czech Technical University in Prague, Prague, Czech Republic
[133] Faculty of Mathematics and Physics, Charles University, Prague, Czech Republic
[134] Particle Physics Department, Rutherford Appleton Laboratory, Didcot, UK
[135] IRFU, CEA, Université Paris-Saclay, Gif-sur-Yvette, France
[136] Santa Cruz Institute for Particle Physics, University of California Santa Cruz, Santa Cruz, CA, USA
[137] [(a)]Departamento de Física, Pontificia Universidad Católica de Chile, Santiago, Chile; [(b)]Millennium Institute for Subatomic Physics at High Energy Frontier (SAPHIR), Santiago, Chile; [(c)]Instituto de Investigación Multidisciplinario en Ciencia y Tecnología, y Departamento de Física, Universidad de La Serena, La Serena, Chile; [(d)]Department of Physics, Universidad Andres Bello, Santiago, Chile; [(e)]Instituto de Alta Investigación, Universidad de Tarapacá, Arica, Chile; [(f)]Departamento de Física, Universidad Técnica Federico Santa María, Valparaíso, Chile
[138] Department of Physics, University of Washington, Seattle, WA, USA
[139] Department of Physics and Astronomy, University of Sheffield, Sheffield, UK
[140] Department of Physics, Shinshu University, Nagano, Japan
[141] Department Physik, Universität Siegen, Siegen, Germany
[142] Department of Physics, Simon Fraser University, Burnaby, BC, Canada
[143] SLAC National Accelerator Laboratory, Stanford, CA, USA
[144] Department of Physics, Royal Institute of Technology, Stockholm, Sweden
[145] Departments of Physics and Astronomy, Stony Brook University, Stony Brook, NY, USA
[146] Department of Physics and Astronomy, University of Sussex, Brighton, UK
[147] School of Physics, University of Sydney, Sydney, Australia
[148] Institute of Physics, Academia Sinica, Taipei, Taiwan
[149] [(a)]E. Andronikashvili Institute of Physics, Iv. Javakhishvili Tbilisi State University, Tbilisi, Georgia; [(b)]High Energy Physics Institute, Tbilisi State University, Tbilisi, Georgia; [(c)]University of Georgia, Tbilisi, Georgia
[150] Department of Physics, Technion, Israel Institute of Technology, Haifa, Israel
[151] Raymond and Beverly Sackler School of Physics and Astronomy, Tel Aviv University, Tel Aviv, Israel
[152] Department of Physics, Aristotle University of Thessaloniki, Thessaloniki, Greece
[153] International Center for Elementary Particle Physics and Department of Physics, University of Tokyo, Tokyo, Japan
[154] Department of Physics, Tokyo Institute of Technology, Tokyo, Japan
[155] Department of Physics, University of Toronto, Toronto, ON, Canada
[156] [(a)]TRIUMF, Vancouver, BC, Canada; [(b)]Department of Physics and Astronomy, York University, Toronto, ON, Canada
[157] Division of Physics and Tomonaga Center for the History of the Universe, Faculty of Pure and Applied Sciences, University of Tsukuba, Tsukuba, Japan
[158] Department of Physics and Astronomy, Tufts University, Medford, MA, USA
[159] United Arab Emirates University, Al Ain, United Arab Emirates
[160] Department of Physics and Astronomy, University of California Irvine, Irvine, CA, USA
[161] Department of Physics and Astronomy, University of Uppsala, Uppsala, Sweden
[162] Department of Physics, University of Illinois, Urbana, IL, USA
[163] Instituto de Física Corpuscular (IFIC), Centro Mixto Universidad de Valencia - CSIC, Valencia, Spain
[164] Department of Physics, University of British Columbia, Vancouver, BC, Canada
[165] Department of Physics and Astronomy, University of Victoria, Victoria, BC, Canada
[166] Fakultät für Physik und Astronomie, Julius-Maximilians-Universität Würzburg, Würzburg, Germany
[167] Department of Physics, University of Warwick, Coventry, UK
[168] Waseda University, Tokyo, Japan
[169] Department of Particle Physics and Astrophysics, Weizmann Institute of Science, Rehovot, Israel
[170] Department of Physics, University of Wisconsin, Madison, WI, USA
[171] Fakultät für Mathematik und Naturwissenschaften, Fachgruppe Physik, Bergische Universität Wuppertal, Wuppertal, Germany

[172] Department of Physics, Yale University, New Haven, CT, USA

[a] Also Affiliated with an institute covered by a cooperation agreement with CERN, Geneva, Switzerland
[b] Also at An-Najah National University, Nablus, Palestine
[c] Also at Borough of Manhattan Community College, City University of New York, New York, NY, USA
[d] Also at Center for High Energy Physics, Peking University, China
[e] Also at Center for Interdisciplinary Research and Innovation (CIRI-AUTH), Thessaloniki, Greece
[f] Also at Centro Studi e Ricerche Enrico Fermi, Rome, Italy
[g] Also at CERN, Geneva, Switzerland
[h] Also at Département de Physique Nucléaire et Corpusculaire, Université de Genève, Genève, Switzerland
[i] Also at Departament de Fisica de la Universitat Autonoma de Barcelona, Barcelona, Spain
[j] Also at Department of Financial and Management Engineering, University of the Aegean, Chios, Greece
[k] Also at Department of Physics, Ben Gurion University of the Negev, Beer Sheva, Israel
[l] Also at Department of Physics, California State University, Sacramento, USA
[m] Also at Department of Physics, King's College London, London, UK
[n] Also at Department of Physics, Stanford University, Stanford, CA, USA
[o] Also at Department of Physics, University of Fribourg, Fribourg, Switzerland
[p] Also at Department of Physics, University of Thessaly, Thessaly, Greece
[q] Also at Department of Physics, Westmont College, Santa Barbara, USA
[r] Also at Hellenic Open University, Patras, Greece
[s] Also at Institucio Catalana de Recerca i Estudis Avancats, ICREA, Barcelona, Spain
[t] Also at Institut für Experimentalphysik, Universität Hamburg, Hamburg, Germany
[u] Also at Institute for Nuclear Research and Nuclear Energy (INRNE) of the Bulgarian Academy of Sciences, Sofia, Bulgaria
[v] Also at Institute of Applied Physics, Mohammed VI Polytechnic University, Ben Guerir, Morocco
[w] Also at Institute of Particle Physics (IPP), Canada
[x] Also at Institute of Physics and Technology, Ulaanbaatar, Mongolia
[y] Also at Institute of Physics, Azerbaijan Academy of Sciences, Baku, Azerbaijan
[z] Also at Institute of Theoretical Physics, Ilia State University, Tbilisi, Georgia
[aa] Also at L2IT, Université de Toulouse, CNRS/IN2P3, UPS, Toulouse, France
[ab] Also at Lawrence Livermore National Laboratory, Livermore, USA
[ac] Also at National Institute of Physics, University of the Philippines, Diliman, Philippines
[ad] Also at Ochanomizu University, Otsuka, Bunkyo-ku, Tokyo, Japan
[ae] Also at Technical University of Munich, Munich, Germany
[af] Also at The Collaborative Innovation Center of Quantum Matter (CICQM), Beijing, China
[ag] Also at TRIUMF, Vancouver, BC, Canada
[ah] Also at Università di Napoli Parthenope, Naples, Italy
[ai] Also at University of Chinese Academy of Sciences (UCAS), Beijing, China
[aj] Also at University of Colorado Boulder, Department of Physics, Colorado, USA
[ak] Also at Washington College, Chestertown, MD, USA
[al] Also at Physics Department, Yeditepe University, Istanbul, Türkiye
* Deceased